

# **Optimization of Wind Energy Transfer Using Wind Turbines**

**Gary Duncan Moor**

**Thesis presented in partial fulfilment of the requirements for the degree of  
Master of Engineering at the University of Stellenbosch**



**Supervisor: Dr. HJ Beukes**

**December 2003**

## **Declaration**

I, the undersigned, hereby declare that the work contained in this thesis is my own original work, unless otherwise stated, and has not previously, in its entirety or in part, been submitted at any university for a degree.

GD Moor

September 2003

## Summary

The effect of topography and terrain on wind is examined in order to ensure that the wind turbine positioning will encourage a greater availability of wind energy to it. Maximum power point tracking methods are presented whereby the loading on the wind turbine is controlled to ensure that the maximum available energy from the wind is captured. The wind turbine system is modelled and used in simulations to evaluate the three proposed maximum power point trackers, named *anemometer control*, *calculation control* and *constant step control* for the purpose of this thesis. An additional analog system is also created whereby the complete wind turbine system is able to be simulated. An inverter is used to replicate the generator and the loading is controlled using an active rectifier since this will be used on the practical system. The results from the simulations and analog system are presented whereby one of the trackers is shown to be inadequate and the other two trackers are shown to be close to ideal. The appeal of the calculation method is in the redundancy of an anemometer making it attractive to less expensive, small-scale systems.

## Opsomming

Die invloed van die topografie en die terrein op die dinamika van wind word ondersoek om sodoende te verseker dat die posisionering van wind turbienes 'n beter effektiwiteit van wind energie oordrag sal bewerkstellig. Maksimum drywingspunt volger metodes word bespreek sodat die lading op die wind turbiene beheer kan word om sodoende te verseker dat die maksimum wind energie oorgedra kan word. Die wind turbiene stelsel word gemodeleer en geimplimenteer om die drie voorgestelde maksimum drywingspunt volgers te evalueer, naamlik *windspoed-beheer*, *berekening-beheer* en *konstantestap-beheer* vir die doeleindes van hierdie tesis. 'n Adisionele analog stelsel is ontwerp waarmee die volledige wind turbiene stelsel gesimuleer kan word. 'n Omsetter word gebruik om die generator na te boots en die belading word beheer deur middel van 'n aktiewe gelykrichter soos gebruik 'n praktiese stelsel. Resultate van die simulaties en die analog stelsel is verskaf om te bewys dat een van die volg-metodes onvoldoende volging bewerkstellig, en die ander twee naby aan ideale volging bewerkstellig. Dit is getoon dat die berekening metode meer aantreklik is vir kleinskaal stelsels, aangesien 'n windspoedsensor onnodig is.

## **Acknowledgements**

I would like to acknowledge and thank the following people and institutions:

Dr. Johan Beukes for his leadership, support and for having confidence in me.

Aniel le Roux for his ever present, unselfish support and help.

Geoff Lee for the long, meaningful conversations.

Gous and the guys in the “glas kas” for long nights and good times.

The rest of the students in the Power Electronics Group.

The Electrical Machines Group, particularly Pieter and Rong-Jie.

Telkom for personal financial support and allowing me to further my studies.

My family for the opportunities they have provided for me.

My “Digs Mates” for their encouragement and providing an atmosphere in which to relax.

My Lord and Saviour, Jesus Christ for giving me the ability.

# Table of Contents

<b>CHAPTER 1. INTRODUCTION</b>	<b>1</b>
1.1 Renewable Energy.....	1
1.2 Wind Energy .....	1
1.3 Wind Turbine Positioning .....	2
1.4 Power Point Tracking.....	2
1.5 Wind Turbines.....	4
1.5.1 Wind turbine generation principal.....	4
1.5.2 Wind turbine system overview.....	4
1.5.3 Peripheral control issues.....	8
1.6 Thesis Structure.....	8
<b>CHAPTER 2. WIND DYNAMICS</b>	<b>10</b>
2.1 Wind Effects.....	10
2.1.1 Sea breeze.....	10
2.1.2 Mountain winds.....	10
2.1.3 Surface roughness .....	11
2.1.4 Wind shear.....	12
2.1.5 Obstacles .....	13
2.1.6 Speed up effect.....	13
2.1.7 Hill effect.....	13
2.2 Wind Data .....	14
2.2.1 Wind data inaccuracy .....	14
2.2.2 Site feasibility.....	15
2.3 Summary .....	15
2.3.1 Wind dynamics.....	15

2.3.2	Wind turbine site assessment .....	16
<b>CHAPTER 3. SYSTEM MODEL</b>		<b>17</b>
3.1	Mathematical Modelling of the Wind Turbine .....	17
3.1.1	Rotor profiles.....	17
3.1.2	Generator modelling.....	19
3.2	Active Rectifier Modelling.....	24
3.3	Complete Wind Energy Conversion System Model .....	25
3.4	System Response Modelling via Simulation.....	26
3.4.1	Simulated system parameters .....	27
3.4.2	Wind step response.....	27
3.4.3	Load step response .....	34
3.4.4	System response conclusions .....	35
3.5	Summary .....	36
<b>CHAPTER 4. MAXIMUM POWER POINT TRACKING</b>		<b>37</b>
4.1	Understanding the System.....	37
4.1.1	Introduction to loading on the wind turbine.....	37
4.1.2	The effect of loading on a wind turbine .....	38
4.2	Maximum Power Point Tracking Algorithms.....	41
4.2.1	Constant step control method.....	41
4.2.2	Equation control method .....	46
4.3	Practical System .....	49
4.4	Summary .....	52
<b>CHAPTER 5. SIMULATIONS</b>		<b>54</b>
5.1	Wind Step Response.....	54
5.1.1	Equation method response .....	54
5.1.2	Constant step method response .....	58

5.2	Random Wind Responses.....	59
5.2.1	Anemometer method result.....	60
5.2.2	Calculation method result.....	61
5.2.3	Constant step method result.....	63
5.2.4	Measured results to random wind.....	65
5.3	Summary.....	66
<b>CHAPTER 6. DEVELOPMENT OF AN ANALOG WIND TURBINE SIMULATOR</b>		<b>67</b>
6.1	The Inverter.....	69
6.1.1	Inverter programming structure.....	69
6.1.2	Low-pass filter.....	70
6.2	The Active Rectifier.....	72
6.2.1	Active rectifier programming structure.....	73
6.2.2	Equivalent active rectifier model.....	77
6.2.3	Overall active rectifier description.....	77
6.3	Initial Practical System Results.....	79
6.4	Summary.....	81
<b>CHAPTER 7. EXPERIMENTAL RESULTS</b>		<b>82</b>
7.1	Practical System Parameters.....	82
7.2	Equation Methods Results.....	83
7.2.1	Step Response Results.....	83
7.2.2	Random Wind Results.....	86
7.3	Constant Step Method Results.....	89
7.4	Summary.....	91
<b>CHAPTER 8. CONCLUSIONS</b>		<b>92</b>
8.1	System Conclusions.....	92
8.2	Future Work.....	94

8.2.1	Modifications on current system .....	94
8.2.2	Practical implementation.....	96
<b>CHAPTER 9. REFERENCES</b>		<b>97</b>
<b>APPENDIX A INVERTER CODE</b>		<b>100</b>
<b>APPENDIX B ACTIVE RECTIFIER CODE</b>		<b>106</b>

## List of Figures

Figure 1.1 System outlay.....	4
Figure 2.1 Variance of wind speed with height above ground level.....	12
Figure 2.2 Effect of wind on air pressure on the crest of a hill.....	13
Figure 3.1 Power produced by the rotor at different wind speeds .....	18
Figure 3.2 Rotor power produced versus rotor speed for various wind speeds .....	18
Figure 3.3 Rotor torque produced versus rotor speed for various wind speeds.....	19
Figure 3.4 Per phase circuit diagram of an axial flux machine.....	20
Figure 3.5 Per phase simplified circuit diagram of an electrical machine .....	21
Figure 3.6 Block diagram of the wind turbine mechanical system.....	25
Figure 3.7 Block diagram of the q-axis components in the wind turbine electrical system .....	25
Figure 3.8 Block diagram of the d-axis components in the wind turbine electrical system .....	26
Figure 3.9 Block diagram of a wind turbine .....	26
Figure 3.10 System step response to wind change.....	29
Figure 3.11 Logged power for A and $\alpha$ investigation .....	29
Figure 3.12 Logged power for B and $\beta$ investigation .....	30
Figure 3.13 Power produced from modelling and from simulation.....	31
Figure 3.14 Power output response to load steps .....	34
Figure 3.15 Settling times at various currents for 10 mA increments.....	35
Figure 4.1 Maximum power trace .....	37
Figure 4.2 Current versus voltage produced by the wind turbine at various wind speeds.....	38
Figure 4.3 Current versus voltage at various wind speeds against loading.....	39
Figure 4.4 Wind turbine response for various wind and load changes .....	40
Figure 4.5 Power and current produced by the wind turbine under various loadings.....	41
Figure 4.6 Change in wind speed for stable maximum power tracking.....	43

Figure 4.7 Changes in wind speed during constant loading.....	44
Figure 4.8 Unstable scenario .....	45
Figure 4.9 Optimal power points and fitted equation versus wind speed .....	47
Figure 4.10 1% reduced power region .....	48
Figure 4.11 Calculation method example .....	49
Figure 4.12 System stability regarding current increments.....	50
Figure 4.13 Produced power for 6 m/s input over time .....	51
Figure 4.14 Measured and reference power and current at 6 m/s .....	52
Figure 5.1 Step response of anemometer control method.....	54
Figure 5.2 Step response of calculation control method .....	55
Figure 5.3 Comparison of anemometer and calculation control methods.....	56
Figure 5.4 Anemometer and calculation control routes .....	57
Figure 5.5 Larger step response of anemometer control methods .....	57
Figure 5.6 Step response of constant step method .....	59
Figure 5.7 Power supplied versus reference power for anemometer method .....	60
Figure 5.8 Power supplied versus reference power for calculation method .....	61
Figure 5.9 Anemometer method versus calculation method.....	61
Figure 5.10 Power difference between the calculation and anemometer methods .....	62
Figure 5.11 Calculated wind speed versus real wind speed.....	63
Figure 5.12 Constant step control- lost & regained control .....	64
Figure 5.13 Lost & regained control comparison of current reference.....	65
Figure 6.1 Analog system setup .....	67
Figure 6.2 Inverter.....	68
Figure 6.3 Converter .....	68
Figure 6.4 Inverter programming flow chart.....	70
Figure 6.5 Filter.....	71

Figure 6.6 Bode plot of the filter used .....	72
Figure 6.7 Rectifier programming flow chart .....	76
Figure 6.8 System equivalent circuit.....	77
Figure 6.9 Active rectifier's dynamic model .....	77
Figure 6.10 Block diagram of the active rectifier with the wind turbine .....	78
Figure 6.11 Measured and programmed power profiles for 5 m/s.....	79
Figure 6.12 Measured and programmed power profiles for 6 m/s.....	80
Figure 6.13 Measured and programmed power profiles for 7 m/s.....	80
Figure 7.1 Anemometer method increasing step response.....	83
Figure 7.2 Anemometer method decreasing step response .....	84
Figure 7.3 Calculation method increasing step response .....	84
Figure 7.4 Calculation method decreasing step response .....	85
Figure 7.5 Anemometer method.....	86
Figure 7.6 Calculation method .....	87
Figure 7.7 Comparison of power from anemometer and calculation methods .....	88
Figure 7.8 Wind speed comparisons .....	88
Figure 7.9 Constant step result.....	90
Figure 7.10 Comparison of simulated and measured results .....	90

## List of Tables

Table 2.1	Surface roughness length values .....	11
Table 3.1	Simulated system parameters.....	27
Table 3.2	Transfer functions for stepped wind speeds.....	32
Table 3.3	Settling times for stepped wind speeds .....	33
Table 5.1	Settling times.....	58
Table 5.2	Average simulated power production .....	65
Table 7.1	Analog system parameters .....	82
Table 7.2	Settling times.....	85
Table 7.3	Average power production in the analog system .....	89

## List of Abbreviations and Symbols

$A$	Swept rotor area
$A, B, C$	Coefficients
A/D	Analog to digital
$abc$ plane	Untransformed 3-phase quantities
$C$	Capacitance
$C_p$	Coefficient of performance of rotor blades
D/A	Digital to analog
$dq0$	Direct quadrature frame
DSP	Digital signal processor
$E, e$	Internal excitation voltage
FPGA	Field programmable gate array
$G$	Conductance
$G(s)$	Plant transfer function
$h$	Height above ground level
$i$	Current
$i_a(t)$	Active current component
IGBT	Insulated gate bipolar transistor
$I_s$	Input current amplitude
$J$	Total inertia
$\overline{K}$	Park's transformation matrix
$k_e$	Voltage constant
$L$	Inductance
$L_{line}$	Phase inductance
$m_a$	Modulation index
MFLOPS	Mega-floating point operations per second
MOSFET	Metal oxide semiconductor field effect transistor
$N_g$	Efficiency of the generator and the bearings
$p$	Number of machine poles
$P_{abc}$	Total instantaneous power
$P_b$	Mechanical power produced by the rotor
PEC31	Power electronics controller
$P_{gen}$	Wind turbine generated power

$P_w$	Wind power
$r$	Generator loss
$R$	Load
$r_b$	Blades radius
$R_{copper}$	Copper losses
$R_{eddy}$	Eddy current losses
rms	Root mean square
$\bar{S}$	Arbitrary matrix
$t$	Time
$T_b$	Mechanical torque
$T_e$	Electromagnetic torque
$t_s$	Settling time
$u(t)$	Voltage signal
$v$	Voltage at the terminals of the wind turbine
$V_a$	Rectifier input voltage amplitude
$V_{DC}$	DC bus voltage
$v_{meas}$	Measured voltage
$V_s$	Voltage amplitude
$w_s$	Wind speed
$X_{abc}$	$abc$ plane variable
$X_{dq0}$	$dq0$ plane variable
$X_{ref}$	Reference value
$X_s$	Stationary variable
$y(t)$	Output
$z_o$	Roughness length
$\alpha, \beta, i$	Poles of a function
$\alpha\beta$ plane	Alpha beta plane
$\gamma$	Tip speed ratio
$\theta$	Mechanical angle
$\lambda$	Flux linkage
$\Lambda$	Rotating vector
$\rho$	Air density
$\sigma$	Real component of dominant pole in the s-plane

$\psi$	Angle between the q-axis and a-axis
$\omega_c$	Cut-off frequency
$\omega_e$	Electrical frequency
$\omega_r, \omega_{rpm}$	Mechanical angular velocity

# Chapter 1. Introduction

## 1.1 Renewable Energy

In a world of increasing power demand, alternative energy sources are needed to alleviate the use of fossil fuels and nuclear energy for generation of electrical power. Safer and environmentally cleaner ways of harvesting energy is required to provide electrical power. These natural and “clean” sources of energy need to have no by-products associated with their operation [1]. Governments are under increasing pressure to impose steps against pollution generating mediums like fossil fuels and so restrictive measures like carbon taxes are being proposed, which improve the competitiveness of renewable technologies [2]. Consumers have the choice of purchasing “green” energy from electricity suppliers at a premium in some countries [3] [4].

Renewable energy resources are fast becoming very popular in a world where demands for more power and sustainable development are increasing dramatically. *Solar*, *hydro* and *wind* power are the three most widely available natural resources.

- Solar resources can consist of systems with solar panels, Stirling engines and so forth. Any method whereby the direct use of the sun’s heat or light is utilized for power generation is considered solar powered;
- Hydro resources are systems which make use of the movement of water in order to generate power;
- The kinetic energy in wind can be used for the generation of energy (see below).

This thesis focus’s on wind energy and the effective utilization of wind. Wind energy is gaining momentum in this field of “clean” energy due to its relatively low cost.

## 1.2 Wind Energy

Wind can be seen as a result of solar radiation, as the change in temperatures around the globe lead to winds. Wind harvesting technology has been costly in the early stages of wind generation systems. Technology advances in wind turbines and the mass production of these turbines [2] along with various tax incentives and research grants [5] has made wind generation a more economically and environmentally viable energy source. The cost of harvesting energy from the wind has dropped by 85% during the last 20 years [6]. The difference between costs of

generating power through fossil fuels and generating power through wind is getting smaller as the wind turbine technology becomes more affordable.

Wind generation farms have been in use since the late seventies in the United States of America [2] but Europe's rapidly growing wind capacity has seen Germany become the world leader in installed capacity. The development of wind farms has grown at a rapid rate and now wind farms can be seen covering a larger area of Europe. Novel systems have even seen wind turbines been erected in the sea [7].

In South Africa, more attention is being paid to small scale wind turbines for areas where the national grid supply is too far away to utilize [8]. Small stand-alone systems are now being used in remote areas as an alternative to solar panels. This is due to the huge losses of panels as a result of theft [9]. Wind turbines are unattractive to the common thief due to their electrical complexity and the difficulty in concealment during operation.

Large-scale wind turbines are also being investigated as a generation medium for South Africa's electricity grid [10]. Eskom, the national power network operator, has installed three large scale wind turbines at a site near Cape Town for research and investigational purposes. These turbines are the first of their kind in the sub-Saharan region.

### ***1.3 Wind Turbine Positioning***

Wind dynamics are affected by the surrounding terrain. These effects can be employed to ensure a greater energy harvest. The effects of the surrounding topography of a wind turbine site can also be detrimental to the wind turbine with regards to the quality of the wind arriving at the rotor blades. Physical stresses on the wind turbine can reduce its life span. In order for wind energy to be an attractive alternative, wind turbines need to be very efficient. Wind speeds are not uniform and vary with the terrain and surrounding region's topography. Thus the wind turbine's geographical placement is a determining factor in the speed of the wind striking the blades and thus the energy available. A good understanding of wind dynamics is important in erecting wind turbines.

### ***1.4 Power Point Tracking***

The characteristic of a wind turbine is such that there is a maximum available power that the rotor can produce for different wind speeds. This maximum power point occurs at different rotor speeds for different wind speeds. The way in which the rotor speed can be controlled, is by

changing the electrical loading on the wind turbine. A wind turbine has a unique maximum power for a particular wind speed, and an attempt to try and acquire more power by deviating from the optimal rotor speed will result in an inefficient transfer of power from the wind.

The most common method of energy capture on small scale wind turbine systems in operation is the use of passive rectification of the AC signals from the wind turbine, to a DC bus. A diode bridge is connected directly between the wind turbine and DC bus, and thus generation to the bus is only possible when the wind turbine is able to generate a voltage higher than the bus voltage. As the rotor speed is directly proportional to the voltage produced by the wind turbine, the rotor speed is held constant over varying wind speeds by the voltage (equal to the DC bus voltage). This is an inefficient method of energy capture, as the maximum available power will not be produced for all but one wind speed.

Power point trackers are algorithms that control the loading on a particular source so that the optimal power transfer can be obtained. This can be achieved under various external load conditions by using energy storage for excess or shortage of power.

The large wind turbine system in the 100's of kilowatts range, use pitch control of their blades to extract the maximum available power from the wind [7] [11]. The largest wind turbine systems also incorporate a regenerative slip control system on their induction machines for a more efficient system [7] [12]. The additional price of these methods on small-scale systems far outweighs the cost savings and so a cheap alternative is required.

There are two main power point tracking methods proposed in this thesis. The first one is very rudimentary and is based on the power point trackers used in photovoltaic arrays (solar panels) and has been found to work very well with them. As will be shown in this thesis, this is not necessarily the best method to use with wind generation. The second method requires that the wind turbine characteristics are known prior to implementation. The initial method requires an anemometer to measure the wind speed striking the rotor. This is feasible with larger scale turbines since the cost of the additional anemometer is small as compared to the overall system. An alternative and improved method was created resulting in the removal of the anemometer. This method was found to be similar to methods proposed by [13], [14] and [15].

## 1.5 Wind Turbines

### 1.5.1 Wind turbine generation principal

A wind turbine is a unit consisting of an electrical machine, operating as a generator, and blades. The function of a wind turbine is to convert the kinetic energy from the wind into electrical energy (they are sometimes also used to convert to mechanical energy). The rotor blades operate using the same principle as aircraft wings. They can be seen as wings connected at their bases to a shaft. The different air pressures caused by the wind striking the surface of the blades cause lift. This effect is known as the Bernoulli principle. This lift generated, is perpendicular to the direction of the wind which provides a turning force on the shaft to which the blades are connected. The rotating shaft drives the rotor in the generator, inducing voltages in the windings and generating electricity.

### 1.5.2 Wind turbine system overview

The biggest need for wind generation in South Africa is in deep rural areas with high wind resources, such as the Eastern Cape region. Since the main electricity network does not reach these areas, the configuration will be stand-alone as seen in Figure 1.1.

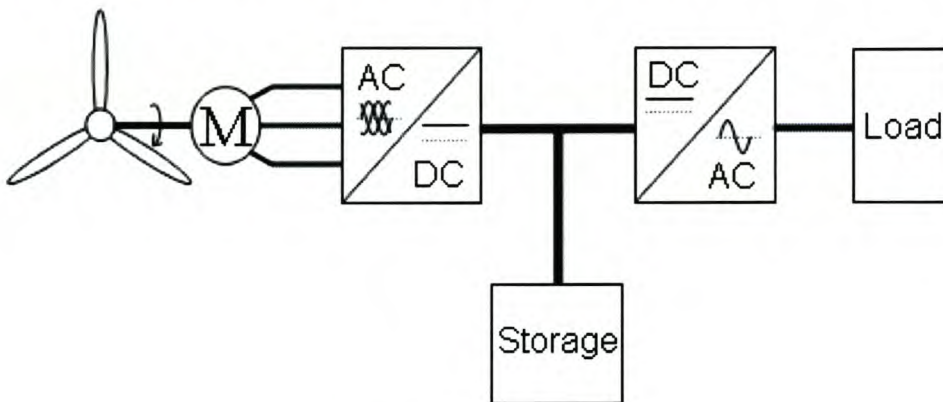


**Figure 1.1 System outlay**

The entire system of a small scale wind turbine plant (typically below 10 kW) under investigation comprises of the following sub-systems:

- A generation unit consisting of a wind turbine;
- An active rectifier connected between the wind turbine and a DC bus;
- A storage unit connected to the DC bus (note, a large scale system connected to a grid does not necessarily need storage);

- An inverter to provide either a DC output at a desired level, or an AC output.

### **1.5.2.1 Rotor**

The rotor typically consists of three blades connected to a common shaft. The blades to be used on the wind turbine system are the AE 1kW blades. These blades were developed by a South African company, Aero Energy, and are therefore specifically designed for South African climate and conditions [16]. Europe has a greater average wind speed than South Africa and their wind turbines typically aim to harvest energy in the 8 m/s to 12 m/s wind speed range. South Africa's target range of operation is between 4 m/s to 8 m/s [17]. This means that the South African designed wind turbines need to operate efficiently at lower wind speeds as compared to European designs. This blade has also been designed to operate much quieter than other blades in its class [16].

Simulations for these blades were done with Propid (Selig, 1998). This computer software was able to optimize and give accurate predictions of the performance expected from these blades [16].

### **1.5.2.2 Generator**

The generator that was used on the original African Wind Power wind turbine was developed by Hugh Piggot in Scotland and was not optimally designed. The new generator to be used on the wind turbine was created by the Machines Group at the University of Stellenbosch. This generator is an axial flux, permanent magnet synchronous machine (AFPMSM). The technology involved with the development on this machine is relatively new and preliminary results have shown it to be very promising in the wind turbine field [18] [19] [20]. Conventional machines used in wind turbines are permanent magnet machines with a laminated stator core, which result in the machine having a "cogging" effect. This is the effect that can be felt when turning a machine by hand and is the result of the magnetic attractions between the windings and the magnets and the effect of the air gaps in between the laminations [19]. The AFPMSM has no cogging effect and so there is little resistance on the rotor at start-up. This makes it easier for the rotor blades to begin turning from stand still and so lower cut-in wind speeds are to be expected (speed at which the wind turbine begins turning). The machine has an efficiency above 90% which is better than the old generator (below 90%) and is also lighter than the old generator. The small line inductance associated with these types of machines also ensures good voltage regulation.

### **1.5.2.3 Storage**

Wind turbines are a source of energy when there is enough movement of air to overcome the internal losses in a wind turbine and to generate electricity. The only source of energy in a stand alone system is energy from the wind generation; there are no other external sources of supply. The wind is not constant and thus cannot always produce the desired amount of energy. It is thus important that there is a buffering system where energy can be stored in times of little or no wind. An ideal system would mean that there is always exactly enough wind energy to supply the demand on the system but as the wind is too erratic to model accurately, the wind turbine must always be able to supply more power than is needed. This will ensure a better probability of perpetual satisfaction of the load demand.

Two main types of storage are attractive for wind turbine storage, namely the common lead acid battery and high-speed flywheels, which are a newer type of technology. Both have advantages and disadvantages associated with them.

#### ***1.5.2.3.1 Lead acid batteries***

Lead acid batteries are the most common type of rechargeable batteries available today due to their good performance against their low cost and also due to their extensive development. Various types are available which are appropriate for different applications. The deep-cycle version is designed to enable many repeated charge and discharge cycles which is favourable to energy storage.

A large proportion of a battery's life expectancy is affected by the charging and discharging of the battery. Quick discharge and charge cycles shorten the lifespan of the battery. There are three states in which battery can be charged [2]:

1. Fast charge (bulk charge) where the 80% to 90% of the capacity of the battery is replaced;
2. Taper charge where the rate of charge is decreased so that the remaining capacity of the battery is gradually filled;
3. Trickle charge where the battery's self discharge is opposed and the battery's capacity is held constant.

These different states of charging will need to be implemented in the loading controller at different stages of charge in the battery.

### **1.5.2.3.2 Flywheels**

Flywheels rely on motion to store energy. This energy is stored in the angular momentum of a spinning rotor. The amount of stored energy in a spinning rotor is measured by the angular momentum of the spinning rotor, which is dependant on the inertia and speed of the rotor. The energy conversion from electrical to mechanical energy and then back again is obtained via an electrical machine. This motor is used to spin up the wheel in times when there is excess electricity and to generate electricity back when demanded. The spinning up state can be referred to as the charging state and the generation back to electrical energy, the discharge state. Flywheels are usually housed in a vacuum in order to reduce mechanical friction on the spinning wheel. Flywheel conversion efficiency can be up to 90% efficient for a complete charge to discharge cycle, which is much greater than batteries.

The advantages of a flywheel over a battery are the following [2]:

- Very deep discharge;
- Long life which is independent of the amount of charge/ discharge cycles;
- Better efficiency;
- Better quality of power;
- Easy power management (speed determines state);
- High peak power delivery can design for specific voltage and current.

Research into flywheels for wind turbine systems have been done previously [21] [22], but the most significant and determining factor in the selection between batteries or flywheels for these practical systems, is the cost. Flywheels are not as simple and widely trusted as batteries and so their manufacturing cost is still much higher. Due to this and their higher level of complexity, batteries are chosen as the storage medium for this project.

### **1.5.2.4 Load**

The load on the wind turbine system can either be a DC or an AC load. The DC load application will typically be used in telecommunication applications and the AC load will supply mini-grid applications i.e. rural housing electrification or water pumping etc.

### **1.5.3 Peripheral control issues**

The control of the power produced by the wind turbine is categorized either due to the loading demand on the wind turbine and/ or due to the winds behaviour.

#### **1.5.3.1 Wind dependencies**

When the wind starts blowing the wind turbine needs to overcome the static friction from standstill and needs to start rotating. There should be no loading on the generator at this stage in order for this to happen.

When the wind is blowing too hard the wind turbine is fitted with a vane that turns the wind turbine out of the oncoming wind at a wind speed known as the *furling speed*, until the wind speed has dropped. This ensures that the mechanical stress on the blades at high wind speeds does not destroy them.

#### **1.5.3.2 Loading dependencies**

When a state is reached when there is not a required loading on the wind turbine due to a fully charged battery and no external load, the wind turbine can be loaded heavily so that it runs into an inefficient mode and the rotor speed drops. These control and system properties enabling this feature will be explained in forthcoming chapters.

If a state is reached where the required loading is less than the maximum available power from the wind, a similar state to the method above is used and the power control system goes into a mode where the power point tracker runs into an inefficient zone until the required power is met.

If the loading required is greater than the maximum available wind power, the maximum available power from the wind must be used and the excess power will be obtained from the storage medium used. It is in this mode where the main interest for this thesis lies. Maximum power point tracking is required to ensure that the maximum available energy in the wind is transferred to the electrical load even while the available power in the wind changes due to the irregular nature of wind.

## **1.6 Thesis Structure**

The initial focus of this thesis will be on the wind dynamics associated with the location of a wind turbine. Wind phenomenon beneficial and unbeneficial to wind turbines will be revealed and discussed.

The dynamics of the wind turbine will be discussed in Chapter 3. A model of the wind turbine is created which is to be used in simulations of the whole wind turbine system. Responses of the system to wind and loading will then be investigated from the simulation model and used for further investigations.

Chapter 4 shows the effect of electrical loading on a wind turbine and methods to try and harvest the maximum available energy from the wind via the control of electrical loading on the wind turbine will be discussed. Different proposals will be explained and examined.

Simulations of the proposed maximum power point tracking methods described in Chapter 4 will be shown in Chapter 5. Assessment of the tracking methods can then be made.

Chapter 6 describes a practical system whereby the wind turbine system can be analogously simulated and the different tracking algorithms tested. The practical setup and the internal processes are explained.

The results of the practical tests done on the analog model are displayed in Chapter 7. The different proposed maximum power point tracking methods are tested and the results discussed.

A final conclusion of the project and the tracking methods are expressed in Chapter 8. Future work and recommendations are also provided in this final chapter.

## Chapter 2. Wind Dynamics

The objective of this project is to harvest the maximum amount of energy from the wind. Chapter 4 deals with the electrical loading on the wind turbine and how it can be adjusted to harvest the maximum energy available from the wind striking the blades. This chapter investigates the wind properties that are determined by the topography and lay of the terrain surrounding the region on which a wind turbine erection is proposed, so that the maximum wind speed can be made available to the wind turbine by calculated positioning and design of the structure. Thus, by a good knowledge of wind dynamics, more energy can be made available to the wind turbine. The majority of the following section is produced from [7]

### 2.1 Wind Effects

Wind is created by the heating of the earth's surface. About 1% to 2% of the sun's energy used by the earth is converted into wind energy. The high winds that are found at altitudes above 1000 m are known as *geostrophic winds* and are a result of the temperature differences between the equator and the poles [23]. These winds are not affected by the surface of the earth and can reach very high speeds. *Surface winds* are the winds that occur at altitudes up to 100 m and are subjective to the terrain. Surface winds are the winds that concern the research of wind turbines. The calculation of the energy content of these winds is required.

#### 2.1.1 Sea breeze

The coastal regions are a source of winds. The land is heated faster during the day than the sea creating a temperature difference. The air pressures around the two mediums change and in turn induce a wind known as a *sea breeze*, which flows in towards the land. As the day becomes night, the temperature difference slowly changes and the wind direction is reversed. This is called a *land breeze*.

#### 2.1.2 Mountain winds

As a lot of the sites in which small scale wind turbine erection is being considered lie in hilly regions, these winds are of significance. When a north-facing slope is heated during the day, the air around it is heated and it rises against the slope towards the crest. This process is reversed during the night and the wind flows back down.

### 2.1.3 Surface roughness

As was mentioned earlier, the surface winds are determined by the topography of the terrain. The roughness of the terrain provides friction against the wind, slowing it down near the earth. As the altitude increases, the effect that the earth has on the wind diminishes. The orography of, and the obstacles on the ground also affect the wind.

With regards to mechanical friction, the rougher the surfaces of two materials, the greater the resistance to movement between them. Friction also exists between wind and the surface of the earth. The courser the surface of the earth, the more the wind is slowed down. Studies have been done and different terrain roughness has been classified into different classes. Dams and lakes barely slow the wind down, whereas forests and built-up areas slow the wind down significantly.

Roughness classes range from 0, which is a smooth surface, to roughness class 4, which are areas with many trees and or buildings. The *roughness length*  $z_0$  is a numerical value used to calculate the roughness of the surface of a particular terrain. The roughness length depends on the cross sectional area of the element facing the wind, the height of the element and the horizontal area the element occupies. The following table represents the most common terrains' roughness lengths.

**Table 2.1 Surface roughness length values**

Type of surface	$z_0$ (cm)
Sand	0.07
Mown Grass	0.5
Short Grass	2
Fallow field	2.5
Long Grass	7
Pine Forest (mean height: 15m)	95
Densely built-up suburbs	100

## 2.1.4 Wind shear

Wind speeds vary with height above ground level as a result of the friction from the earth's surface. Different roughness lengths obviously slow the wind to different degrees. Thus the roughness length of the earth below it determines the wind's variation with height. The equation, which describes the variation of the wind with height, is given below [24].

$$\frac{w_{s1}}{w_{s2}} = \frac{\ln\left(\frac{h_1}{z_0}\right)}{\ln\left(\frac{h_2}{z_0}\right)} \quad (2.1)$$

where  $w_{s1}$  is the wind speed measured at height  $h_1$ ,  $w_{s2}$  is the wind speed at height  $h_2$ , which is under investigation and  $z_0$  is the roughness length. Note that (2.1) is only valid to a height of about 200 m above ground level. This equation is suitable for wind turbines as their hub height is well below 200 m.

The variation with height up to 30 m can be seen in the graph below. The roughness chosen are for sand, long grass and a densely build-up suburbs. We will assume that the wind speed was measured as an average of 3 m/s and was measured at a height of 2 m.

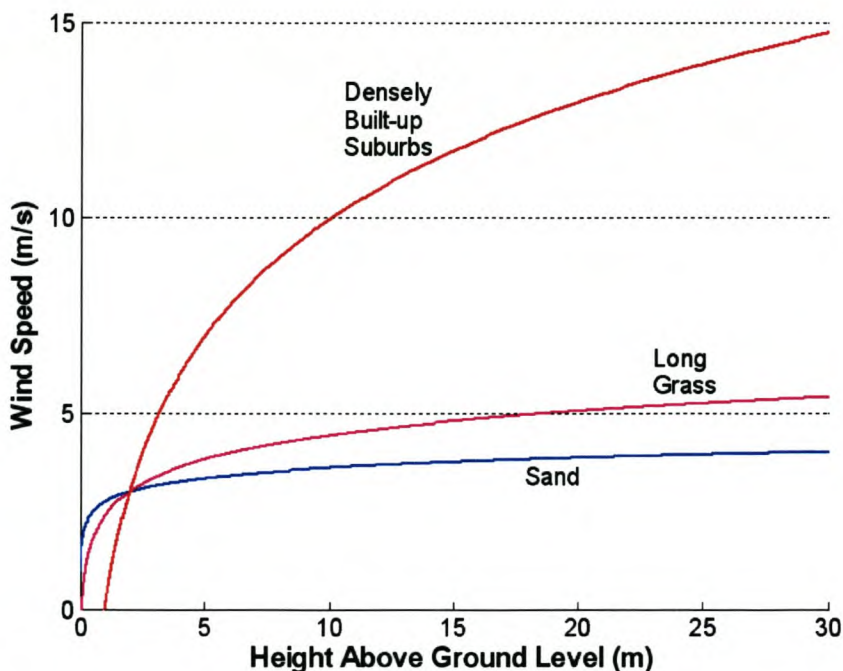


Figure 2.1 Variance of wind speed with height above ground level

These calculations assume that there are no obstacles closer than 1 km, which could affect the wind dynamics at the location of interest. These variations of wind speed with height do not seem very important, but because the power produced by the turbine is a third power to the wind speed as will be explained in (2.2), there is a sharp increase of power produced as height above ground level is raised.

### 2.1.5 Obstacles

Obstacles like trees and buildings can slow the wind downstream of the obstacle by a large factor as they create turbulences. An obstacle can affect the wind dynamics as far as 1 km away.

### 2.1.6 Speed up effect

When wind blows into a constricting area, the speed of the wind passing through that area increases. This is because the volume of air remains the same, but the available cross-sectional area becomes smaller and thus the pressure increases resulting in a higher wind speed. This is known as the *tunnel effect*. This phenomenon can occur between obstacles (e.g. buildings) or natural gullies. This tunnel effect can be beneficial to wind turbines situated in these regions, as they would experience higher wind speeds.

### 2.1.7 Hill effect

The most applicable and beneficial effect for wind turbines is the *hill effect*. This positioning on top of the hill is firstly good as it has fewer obstacles from the surrounding terrain to block the wind. Secondly, wind speeds can be up to 100% higher on the crest of hills [9]. This is because the air pressure builds up as the wind blows against the windward side of the hill. The wind then reaches the crest of the hill and flows into the low-pressure side on the leeward side. The large pressure difference between the windward and leeward side causes a fast rush of air (wind). This wind is additional to the wind striking the face of the hill and thus the resulting wind speed on the crest of the hill is faster than the prevailing wind. This effect can be seen in Figure 2.2.

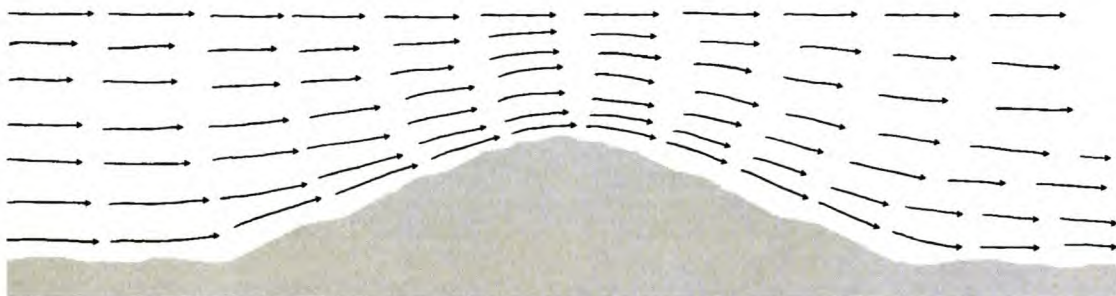


**Figure 2.2 Effect of wind on air pressure on the crest of a hill**

If the hill is steep, the ‘climb’ of the wind up the face of the hill is not gradual and turbulences are created which causes additional wear and tear on the turbine. Wind turbines are generally placed on taller towers to be higher than the turbulences caused by the ground and to also rise above nearby obstacles. The shear effect ensures that there are even greater wind speeds at higher heights above the crest of a hill.

## 2.2 Wind Data

The power available from the wind in the swept area of the rotor can be represented by the following equation [2]:

$$P_w = 0.5 \times \rho \times A \times w_s^3 \quad (2.2)$$

where  $P_w$  is the available power from the wind,  $\rho$  is the air density,  $A$  is the swept area of the rotor exposed to the wind and  $w_s$  is the wind speed. It is impossible to extract all the power from the wind because some wind flow must be maintained through the rotor (else a brick wall would be a 100% efficient wind power extractor). An equation for the power generated by a wind turbine is as follows:

$$P_{gen} = \frac{1}{2} \times C_p \times N_g \times \rho \times A \times w_s^3 \quad (2.3)$$

where  $P_{gen}$  is the generated power,  $C_p$  is the coefficient of performance of the wind turbine blades (0.59 is the theoretical maximum from Betz’s law) and  $N_g$  is the efficiency of the generator and the bearings.

### 2.2.1 Wind data inaccuracy

The wind data that is available for South Africa is available from the *South African Weather Bureau*. This data is obtained from weather stations situated throughout the country. The weather stations are mainly for meteorological measurements, and thus measure temperature, wind, rainfall etc. The stations are not intended to measure data for wind turbine sites and thus there are a few points to reveal.

The anemometers that are used have a large tolerance rating and are quite old. The present anemometers used are rated to a tolerance of 1m/s. This means that an average of 4 m/s wind measurement can result in a 25% error measured. A 10% error reading is considerably large when the wind speed is used to calculate the available power at a particular site. This is because

the power generated by a wind turbine is a third power of the wind speed as shown in (2.2) above. Thus a 10% error reading would result in a 33% error reading at the measured height. If the prospective turbine height is even higher than the actual measured height, conversion calculations must be done and this can increase the magnitude of the error. For example, if the wind speed is measured at a height of 10 m and is measured with an error of 10% and then the conversion is calculated to a height of 50 m, the error in the power computation is 75%. These are substantially large errors to be made, and could seriously affect the site feasibility decisions based on wind power availability made from these measurements.

## **2.2.2 Site feasibility**

The positioning of the anemometers does not always take the roughness and obstacles around the weather station into consideration and this affects the wind measurements drastically as discussed in section 2.1.

### **2.2.2.1 Wind averages**

The average wind speeds of a region alone cannot be used to calculate the power production expected at that region [23]. This is because the power production of a wind turbine varies with the third power of the wind speed. For example, if the wind blows at 4 m/s for 24 hours, the mean wind speed is 4 m/s. The power produced from a wind at 4 m/s for a particular area and air density is 64 W, which generates a mean of  $64 \times 24 = 1.536$  kWh for that day. If the wind blew at 8 m/s for 12 hours, the mean wind speed is still 4m/s but the power produced at 8 m/s is 512 W for that same air density and area under investigation. This means that  $512 \times 12 = 6.144$  kWh was produced for that day. This shows that the wind speed data intervals over which the power is calculated, needs to be as small as possible to get an accurate power production calculation.

## **2.3 Summary**

### **2.3.1 Wind dynamics**

With a better understanding of the dynamics of wind, the correct positioning of wind turbines will increase the amount of energy available to the wind turbine. The landscape surrounding the proposed erection area of a wind turbine, can ensure from the above properties of wind that small positional differences can and will be beneficial. The ideal spot for a wind turbine would be on top of a high mast, which is on top of a hill in a region with no obstacles and a flat surface. Due

to this not always being possible, one of the other effects could be exploited to contribute to an increase of energy available at the wind turbine.

### **2.3.2 Wind turbine site assessment**

The wind data from the weather bureau is revealed to be insufficient for accurate analysis of possible sites for the erection of wind turbines. The best method would be to install anemometers at the proposed site and at the proposed hub height. The wind speeds logged at these sites can be correlated with the nearest weather station to get a relationship between the wind experienced at the proposed site and the wind at the weather station. The average expected wind could then be calculated from the data logged over a few years from the weather station. This would provide a better estimate of the feasibility of a proposed site.

## Chapter 3. System Model

The transfer of wind energy to the final electrical energy is not instantaneous. There is a response time during which the change in wind striking the blades transfers to a change in electrical energy at the output of the wind turbine. This transfer response between the changes in wind to the changes in electrical power needs to be analyzed in order to develop a mathematical model on which to base simulations. It is also important to obtain an indication of the response time to the wind and load variances so that the maximum power point tracking methods, explained later in this thesis, can be calculated for the wind turbine system time constraints.

### 3.1 Mathematical Modelling of the Wind Turbine

The first task is to describe a physical model of the wind turbine system. The wind turbine in its entirety can be broken up into two sections, namely the *rotor blades* and the *generator*.

#### 3.1.1 Rotor profiles

The mechanical power [W] that can be produced by the blades is described by different parameters, namely the wind speed striking the surface of the blades  $w_s$  [m/s], the frontal area of the blades  $A$  [m<sup>2</sup>], the air density  $\rho$  [kg/m<sup>3</sup>] and a function describing the coefficient of performance known as the power coefficient  $C_p$ . The power coefficient is a function of the tip speed ratio  $\gamma$  which is described by:

$$\gamma = \frac{r_b \omega_r}{w_s} \quad (3.1)$$

where  $r_b$  is the radius of the blades [m] and  $\omega_r$  is the mechanical angular velocity of the rotor [rad/s].

The mechanical power  $P_b$  produced by the rotor blades is now described from [2]:

$$P_b = \frac{1}{2} C_p \rho A w_s^3 \quad (3.2)$$

Only the actual rotor power profiles for separate wind speeds, shown in Figure 3.1 and Figure 3.2, were obtained from the manufacturer and not  $C_p$ , but these profiles are sufficient for the purposes of this study and are used in all the simulations regarding the rotor.

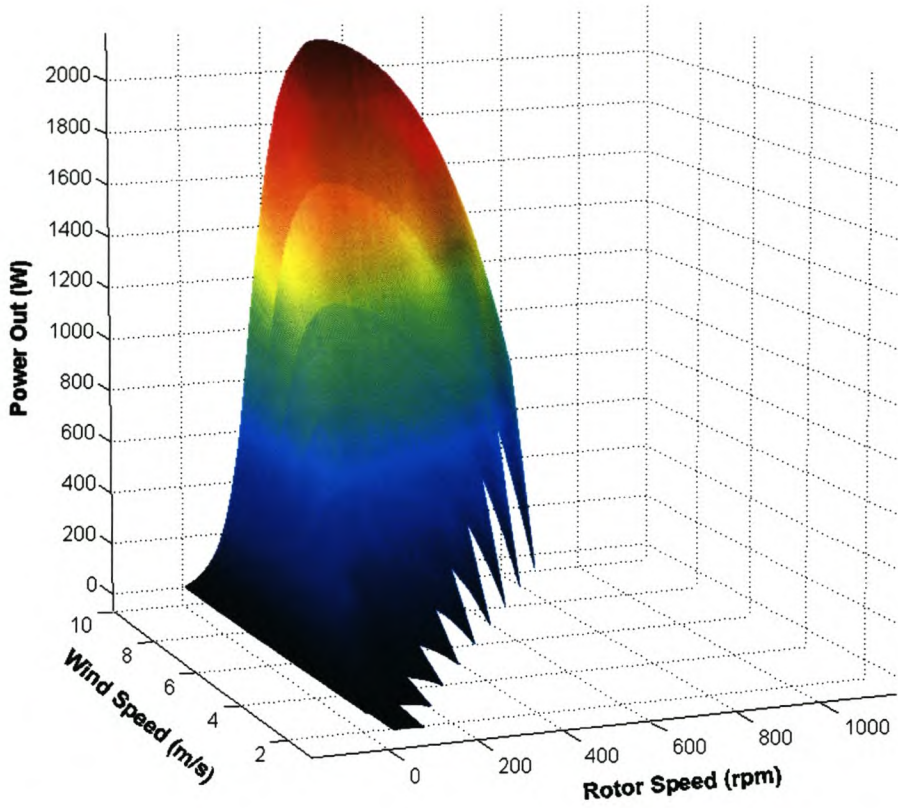


Figure 3.1 Power produced by the rotor at different wind speeds

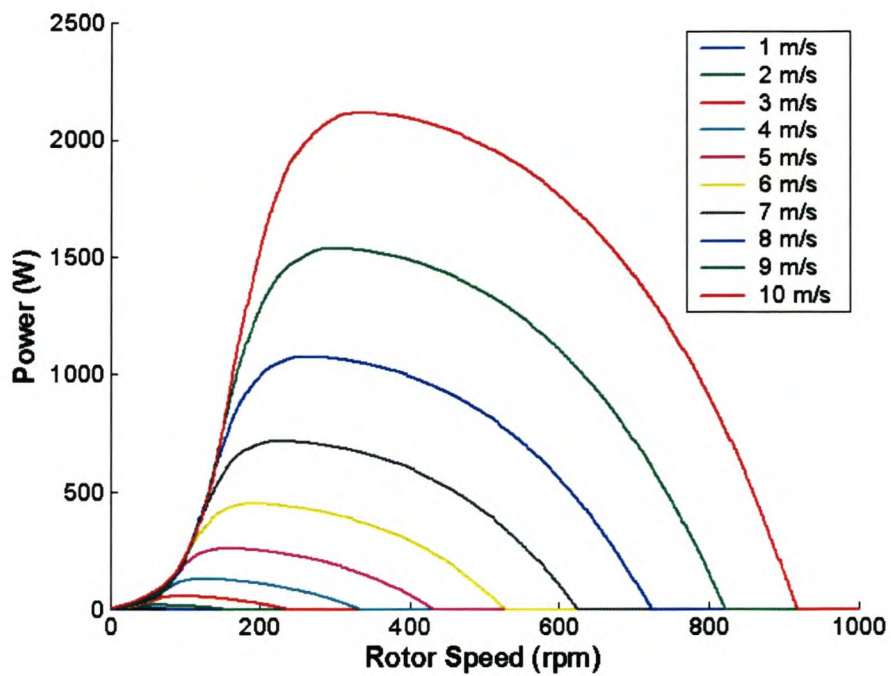
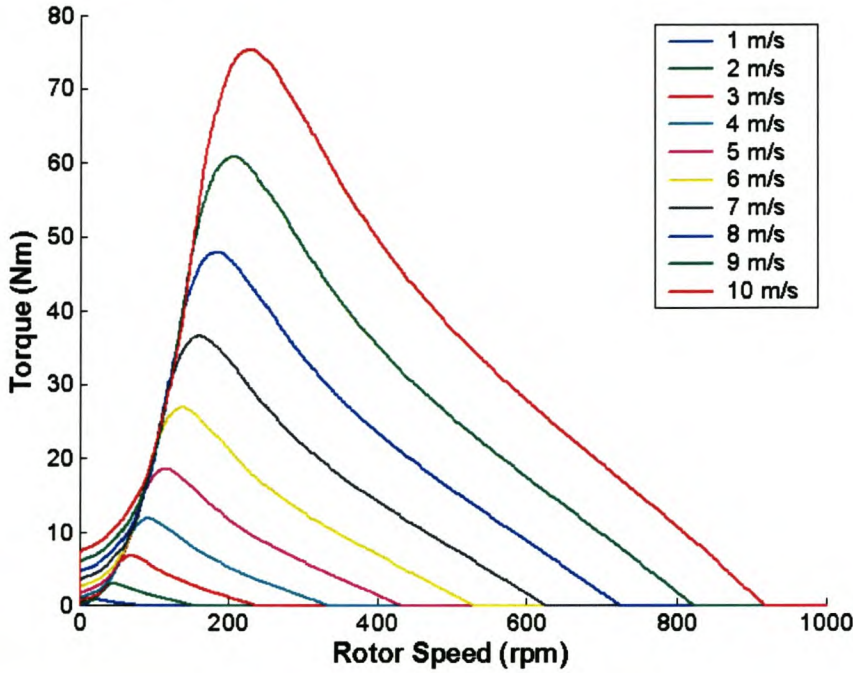


Figure 3.2 Rotor power produced versus rotor speed for various wind speeds

The mechanical torque  $T_b$  [Nm] produced by the blades is calculated from the mechanical power from the following equation:

$$T_b = \frac{P_b}{\omega_r} \quad (3.3)$$

From the power profiles in Figure 3.2, torque profiles for each wind speed can now be plotted.



**Figure 3.3 Rotor torque produced versus rotor speed for various wind speeds**

A function for the power produced and the torque developed as per these graphs is defined as follows.

$$P_b = f(\omega_{rpm}, w_s) \quad (3.4)$$

$$T_b = f(\omega_{rpm}, w_s) \quad (3.5)$$

### 3.1.2 Generator modelling

The generator used is a 3-phase permanent magnet, synchronous axial flux machine. This circuit is analyzed on a per phase basis implying that the system is assumed to be balanced, which is expected in the practical system.

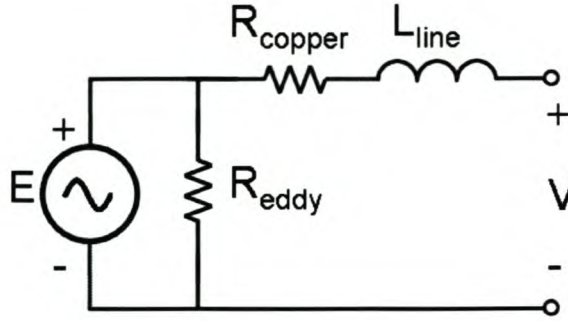


**Figure 3.4 Per phase circuit diagram of an axial flux machine**

The internal excitation voltage  $E$  is induced from the rotating magnetic field and it has a linear relationship  $k_e$  (voltage constant) with the speed of the rotating rotor [25].

$$E = k_e \omega_r \quad (3.6)$$

The term  $R_{eddy}$  is the effective resistance due to Eddy Current losses [ $\Omega$ ],  $R_{copper}$  is the resistance [ $\Omega$ ] from the internal windings and  $L_{line}$  is the phase inductance [H]. The voltages at the terminals of the machine are represented by  $v_a$ ,  $v_b$  and  $v_c$  for the respective phases. The effect of the eddy currents can be ignored in a simplified circuit due to its small effect on the overall system at lower rotational speeds as expected from this system [26].

In order for the modelling of the machine to be simplified, the variables described in the common  $abc$  plane, are transformed to the  $dq0$  rotating reference frame. This eliminates the time varying concerns in the machine equations and enables the DC values of the machine to be realised by continuously measuring the different parameters from a reference time varying concern, namely the rotating rotor. This transformation is achieved using the *Park's Transformation* [27]. The transformation is achieved via the following equation matrix.

$$\overline{S}_{qd0} = \overline{K} \overline{S}_{abc} \quad (3.7)$$

where  $\overline{S}_{qd0}$  and  $\overline{S}_{abc}$  can represent either voltage, current or flux linkage in their respective frames. The S matrixes are expanded below.

$$\overline{S}_{abc} = \begin{bmatrix} S_a \\ S_b \\ S_c \end{bmatrix}; \overline{S}_{qd0} = \begin{bmatrix} S_q \\ S_d \\ S_0 \end{bmatrix}; \quad (3.8)$$

$\overline{K}$  is the transformation matrix given below.

$$\bar{K} = \frac{2}{3} \begin{bmatrix} \cos \psi & \cos(\psi - \frac{2\pi}{3}) & \cos(\psi + \frac{2\pi}{3}) \\ \sin \psi & \sin(\psi - \frac{2\pi}{3}) & \sin(\psi + \frac{2\pi}{3}) \\ \frac{1}{2} & \frac{1}{2} & \frac{1}{2} \end{bmatrix} \quad (3.9)$$

The angle  $\psi$  is the angle between the rotating q-axis and the magnetic a-axis of the stator. Due to the machine under investigation being a synchronous machine, the angle between the q-axis and the magnetic a-axis is equal to the electrical angle  $\theta$  (the word ‘synchronous’ indicates this) and can be calculated by the following [25]:

$$\theta = \int \omega_e(s) ds = \psi \quad (3.10)$$

where  $\omega_e$  is the electrical frequency of the rotor.

The simplified equivalent per phase circuit diagram of a synchronous machine can be drawn from [25] and is depicted in Figure 3.5.

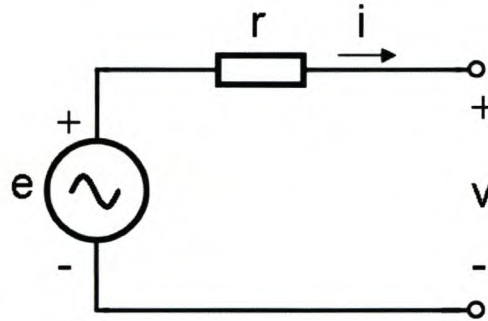


**Figure 3.5 Per phase simplified circuit diagram of an electrical machine**

Summing the 3-phase voltages of this diagram produces the following:

$$\overline{v_{abc}} = -\overline{r_{abc} i_{abc}} + \overline{e_{abc}} \quad (3.11)$$

where  $v_{abc}$  are the voltages seen at the terminals of the generator,  $r_{abc}$  are the losses in the generator and  $e_{abc}$  are the voltages excited by the flux from the rotating rotor. The excited voltage in the system is a function of the rate of flux linkage change where  $\lambda$  is the flux linkage,

hence  $e_{abc}$  can be written as  $\frac{d\lambda_{abc}}{dt}$  which yields:

$$\overline{v_{abc}} = -\overline{r_{abc} i_{abc}} + \frac{d}{dt} \overline{\lambda_{abc}} \quad (3.12)$$

Now using Park's transformation [25], this same relationship expressed in the  $dq0$  plane is

$$\overline{v_{dq0}} = -\overline{r_s i_{qd0}} + \omega_e \overline{\lambda_{dq}} + \frac{d}{dt} \overline{\lambda_{qd0}} \quad (3.13)$$

Because the practical system under investigation is balanced, the  $0$  axis components will be zero. Equation (3.13) can now be split into its  $d$  and  $q$  axis components resulting in the following:

$$v_q = -r_s i_q + \omega_e \lambda_d + \frac{d}{dt} \lambda_q \quad (3.14)$$

$$v_d = -r_s i_d - \omega_e \lambda_q + \frac{d}{dt} \lambda_d \quad (3.15)$$

The flux linkage can be expanded from [25] into the following:

$$\lambda_q = -L_q i_q \quad (3.16)$$

$$\lambda_d = -L_d i_d + \lambda_m \quad (3.17)$$

where  $L_d$  and  $L_q$  represent the equivalent  $d$  and  $q$  axis inductance. Substituting (3.16) and (3.17) into (3.14) and (3.15), leads to the following equation.

$$v_q = -(r_s + \frac{d}{dt} L_q) i_q - \omega_e L_d i_d + \omega_e \lambda_m \quad (3.18)$$

$$v_d = -(r_s + \frac{d}{dt} L_d) i_d + \omega_e L_q i_q \quad (3.19)$$

The expression for the electromagnetic torque  $T_e$  developed in the machine in the  $dq$  plane is obtained from [25] and expressed as the following:

$$T_e = \left(\frac{3}{2}\right) \left(\frac{p}{2}\right) (\lambda_d i_q - \lambda_q i_d) \quad (3.20)$$

where  $p$  is the number of poles in the machine. Substituting (3.16) and (3.17) into (3.20) leads to

$$T_e = \left(\frac{3}{2}\right) \left(\frac{p}{2}\right) [\lambda_m i_q + (L_d - L_q) i_q i_d] \quad (3.21)$$

It is reasonable to assume  $L_d$  and  $L_q$  to be equal to each other due to the manufacturing process [25] and are subsequently denoted by  $L_s$ , thus (3.21) becomes:

$$T_e = \left(\frac{3}{2}\right) \left(\frac{p}{2}\right) \lambda_m i_q \quad (3.22)$$

The relationship between the electrical rotor speed  $\omega_e$  and the mechanical rotor speed  $\omega_r$  is obtained by the following equation.

$$\omega_e = \left(\frac{p}{2}\right) \omega_r \quad (3.23)$$

The external torque applied to a generator, when greater than the counter torque produced by the generator, incites acceleration in the rotor. This acceleration leads to an increase in rotor speed, which increases the voltage in the windings. This causes a larger current to flow in the windings for the same load, which increases the torque contribution from the electrical circuitry (electromagnetic torque), providing a bigger counter torque to the externally supplied torque on the rotor. This feedback loop is maintained until equilibrium is reached when the torques are equal. The torque produced by the electrical circuitry can also be controlled by varying the load, which consequently varies the current in the windings. This is an important point for later in this thesis. The relationship of these torques is found in [28].

$$T_e = -J \left(\frac{2}{p}\right) \frac{d}{dt} (\omega_e) + T_b \quad (3.24)$$

$J$  is the complete machines inertia [ $\text{kg}\cdot\text{m}^2$ ]. Manipulation of (3.24) provides an expression for  $\omega_e$ .

$$\omega_e = \int \frac{p(T_b - T_e)}{2J} dt \quad (3.25)$$

A torque constant  $k_t$  is generally used when dealing with the conversion from the q-axis current to the electromagnetic torque and the relationship is defined in the following form [25].

$$T_e = k_t i_q \quad (3.26)$$

It can be seen from (3.22) that  $k_t$  has the following relationship to  $\lambda_m$ .

$$k_t = \left(\frac{3}{2}\right) \left(\frac{p}{2}\right) \lambda_m \quad (3.27)$$

A voltage constant  $k_e$  is defined in (3.6) as the relationship between the induced voltage and the mechanical rotor speed. The voltage constant  $k_e$  has the following relationship with the flux linkage  $\lambda_m$ .

$$k_e = \left(\frac{p}{2}\right) \lambda_m \quad (3.28)$$

Using (3.27) with (3.28), the following relationship can be deduced.

$$k_t = \left(\frac{3}{2}\right) k_e \quad (3.29)$$

The total instantaneous power between the  $abc$  plane and the  $dq0$  plane can be represented by the following equation from [25]:

$$P_{abc} = \frac{3}{2} (v_q i_q + v_d i_d + 2v_0 i_0) \quad (3.30)$$

As the system is balanced, the  $0$  components are zero. A power relationship between the simulated or calculated  $dq$  plane power and the  $abc$  plane power can be obtained from (3.30).

$$P_{abc} = \frac{3}{2} (v_q i_q + v_d i_d) \quad (3.31)$$

It is consequentially possible to build a dynamic model of the axial flux permanent magnet synchronous generator.

### **3.2 Active Rectifier Modelling**

The power characteristic of the active rectifier is subsequently investigated. The control to be implemented in the active rectifier will make use of the measured input voltage as a reference signal for the required current. A unitary signal is to be generated from instantaneous voltage measurements and then scaled to the required purposes at that present time. As the current is being controlled, and is to be switched from a voltage reference signal, the current and voltage signals will be in phase with each other thus drawing only real power. Thus only balanced real power is expected at the rectifier and the effect of any inductive or capacitive influence is removed. From [29], the current and voltage is related as follows:

$$i_a(t) = Gu(t) \tag{3.32}$$

The term  $i_a(t)$  is the active current component which in this case is the only current component and  $u(t)$  is the voltage signal.  $G$  is the conductance of the system and thus from (3.32), the active rectifier can be modelled as having only a resistive component, and can thus be modelled as a resistor.

### 3.3 Complete Wind Energy Conversion System Model

The results seen in section 3.1 are now used to create a block model of the wind energy conversion system. The block diagram of the mechanical torques on the rotor can be described from (3.25) by the following diagram.

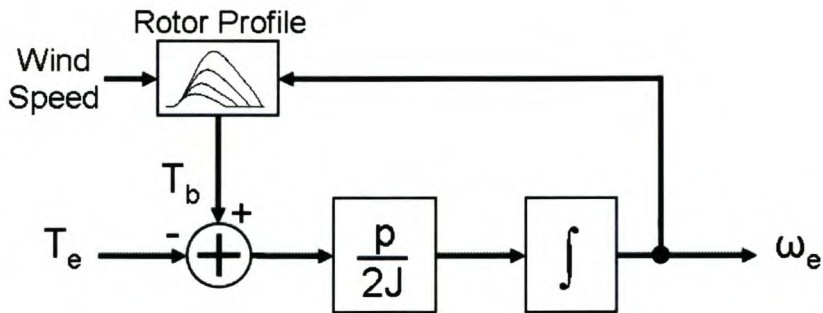


**Figure 3.6 Block diagram of the wind turbine mechanical system**

The q-axis component of the voltage produced by the generator can be modelled from (3.18). The current  $i_q$  is determined by the load over which the voltage  $v_q$  is applied.

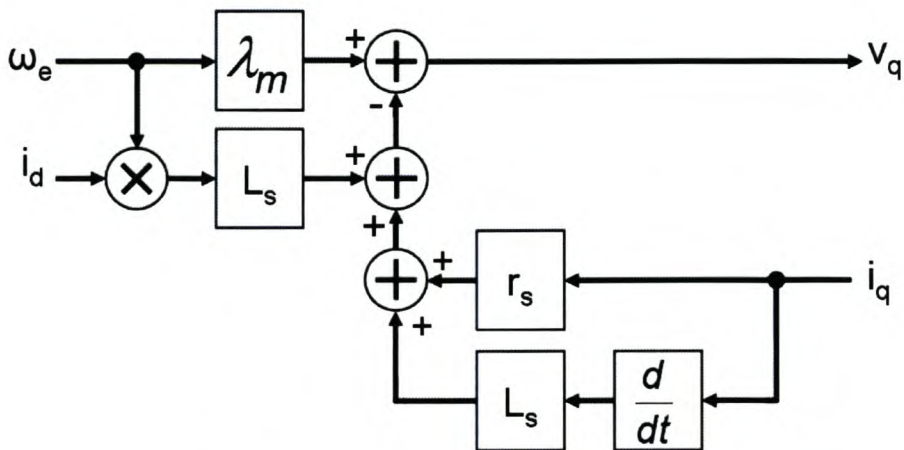


**Figure 3.7 Block diagram of the q-axis components in the wind turbine electrical system**

The d-axis component of the voltage produced by the generator can similarly be modelled from (3.19) where the current  $i_d$  is determined by the load over which the voltage  $v_d$  is applied.

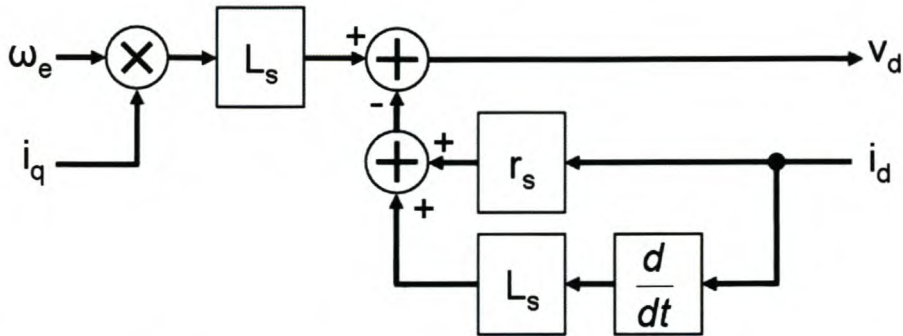


**Figure 3.8** Block diagram of the d-axis components in the wind turbine electrical system

These three models can now be combined to obtain a final model of the wind energy conversion system from the inputted wind speed, to the response of the loading on the generators terminals.

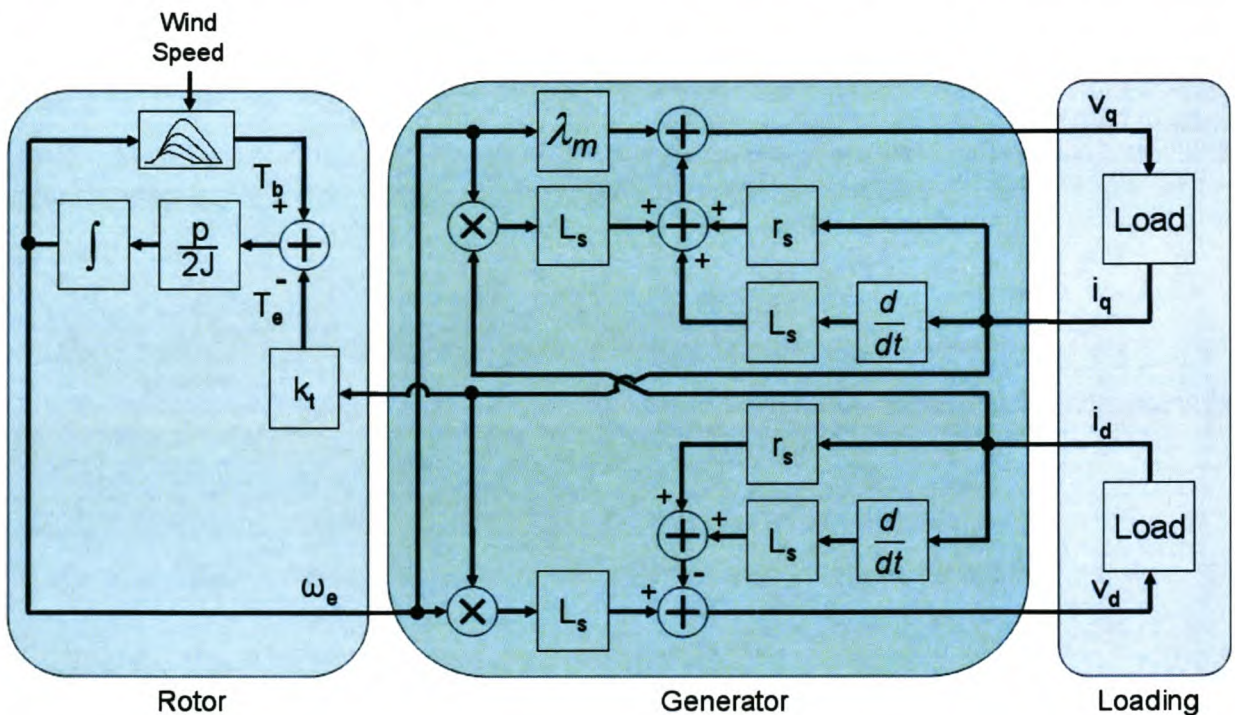


**Figure 3.9** Block diagram of a wind turbine

This model can now be adapted to be simulated in a computer program.

### 3.4 System Response Modelling via Simulation

The system under investigation is non-linear due to the torque profiles generated by the wind turbine blades. As an investigation into non-linear control systems would be complex and out of

the scope of this project, it was decided to linearize the system to significantly reduce the complexity of the dynamic response calculation. A method is proposed to model the wind turbine around strategic wind speeds and at specific loads. Due to the complexity of the mathematical calculations at these various wind speeds and loads, a model of the wind turbine was created in Simplorer™ (version 5.0) of the results adapted from section 3.3.

### 3.4.1 Simulated system parameters

The parameters used in the simulations were required for accurate results. The total inertia of the rotor and generator was unavailable so the inertia of a similar 1.5 kW system was used as presented in [28]. The practically measured parameters of the generator proposed to be used in the practical system were used for the rest of the machine parameters. The torque profiles were implemented directly from the curves produced by the manufacturer. Table 3.1 displays the machine parameters used in the simulations.

**Table 3.1 Simulated system parameters**

Parameter	Value
Total Inertia (J)	1.954 kg·m <sup>2</sup>
Phase Resistance (R <sub>s</sub> )	2.77 Ω
Phase Inductance (L <sub>s</sub> )	2.02 mH
Voltage Constant (k <sub>e</sub> )	0.9707
Poles (p)	32

### 3.4.2 Wind step response

The main objective of this thesis is to allow a wind turbine to harvest the maximum amount of energy from the wind for South African wind conditions. Due to the specific wind conditions in South African lying in the region of 4 m/s to 8 m/s [17], this region is chosen for investigation of the linearization of the wind turbine. The first response to be investigated is the effect of the wind changes. The loading on the wind turbine is held constant at a predetermined optimal loading for a wind speed in the middle of the wind speeds step range and is not updated over the step's interval of transition. The step input on the wind speed is then used to gather information about the dynamic response of the simulated model of the wind turbine to wind variance. The

response is then analysed using MATLAB® (version 6.5) to obtain a transfer function between wind speed and instantaneous power of the system in that stepped region.

Examination of the stepped response indicated that the wind turbine could possibly be modelled as a second order system (gradual decay of the output). Thus a second order system is used to approximate the wind turbine at various wind speeds under the pre-determined optimal loadings at those points. Step inputs from 4 m/s to 8 m/s in 0.5 m/s intervals were used and the step response was used to model a second order transfer function for this region from the transient-response data gathered. The load was held constant at an optimal value for a wind speed half way in between the wind speed step under investigation. The example below shows the extent of the accuracy of the modelled result.

### 3.4.2.1 Response modelling

It is assumed that the response is the sum of exponentials [30].

$$y(t) = y(\infty) + Ae^{-\alpha t} + Be^{-\beta t} + Ce^{-\gamma t} + \dots \quad (3.33)$$

where  $y(t)$  is the output. Due to the system being modelled as a second order transfer function, only the first three terms are used. If it is assumed that  $-\alpha$  is the slowest pole and more dominant than  $-\beta$ ,  $-\beta$  can be ignored and the final output value can be subtracted to reduce (3.33) to the following:

$$y(t) - y(\infty) \cong Ae^{-\alpha t} \quad (3.34)$$

$$\log_{10}[y(t) - y(\infty)] \cong \log_{10} A - \alpha t \log_{10} e \quad (3.35)$$

The result,  $\log_{10} A - \alpha \log_{10}(e)$ , is the equation of a line with a slope  $\alpha$  and an intercept  $A$ . A linear curve is fitted to the trace of  $\log_{10}[y(t) - y(\infty)]$  and the slope and intercept is used to determine these parameters.

When  $A$  and  $\alpha$  have been determined,  $B$  and  $\beta$  can be calculated by similarly using the trace of  $\log_{10}[y(t) - y(\infty) - Ae^{-\alpha t}]$ . This method gives a good fit of the step response data.

The result of step response data of the 5 to 5.5 m/s step is used to provide a better indication of the modelling method used. The step response is depicted in Figure 3.10 below.

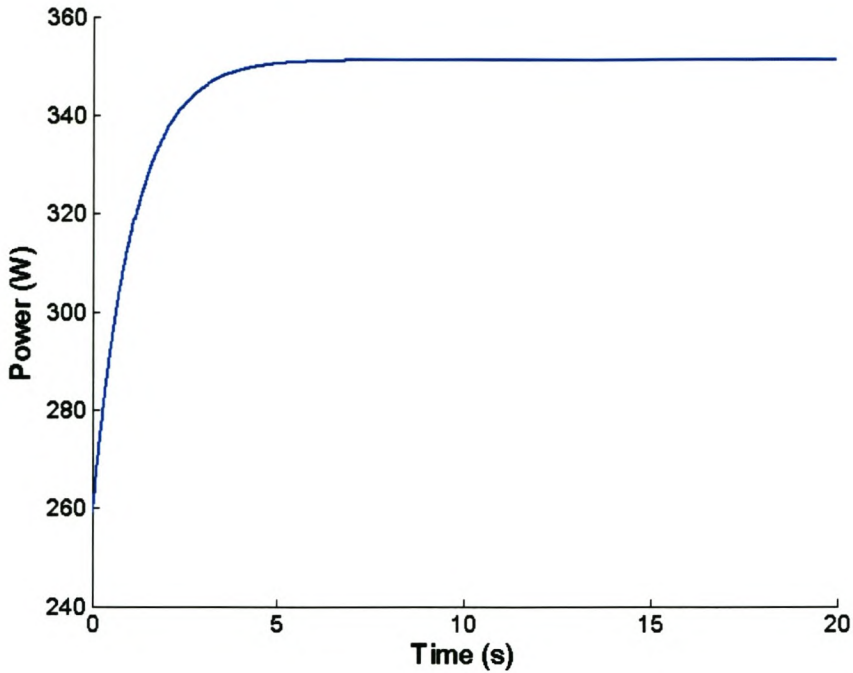


**Figure 3.10 System step response to wind change**

The initial offset was removed in order to evaluate all the responses from a common point. The log of the final steady state power minus the power outputted over time is plotted in Figure 3.11. A linear approximation of the trace is also plotted.

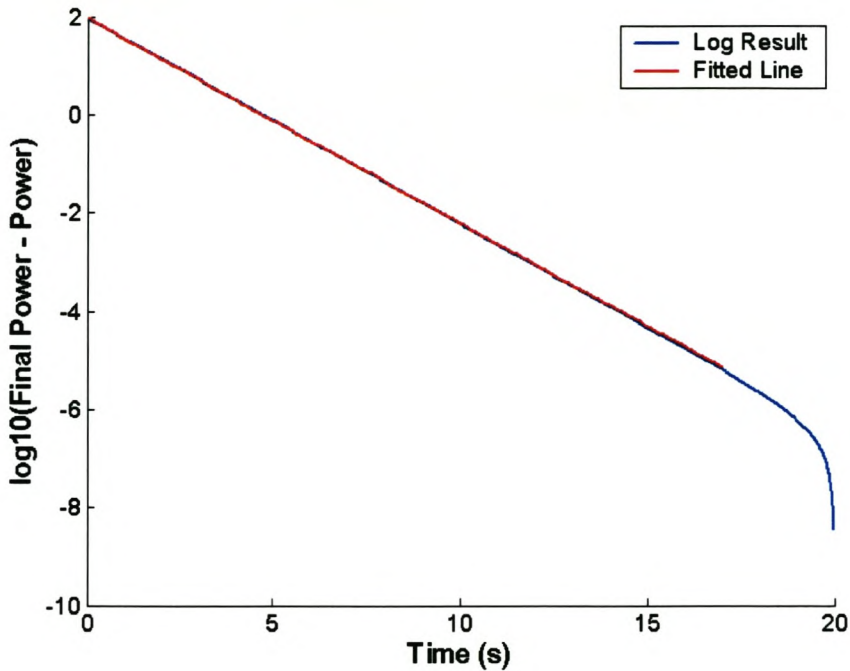


**Figure 3.11 Logged power for A and  $\alpha$  investigation**

The intercept of the line and the gradient are found and used to calculate  $A$  and  $\alpha$  ( $A$  is the y-axis intercept and  $\alpha$  is the gradient).

$$-\alpha t \log_{10} e = \frac{\Delta \text{power}}{\Delta t} \tag{3.36}$$

$$\Rightarrow \alpha = 0.9636 \tag{3.37}$$

$A$  can now be calculated.

$$\log_{10} |A| = 1.9910 \tag{3.38}$$

$A$  is negative because the curve is in the form of  $1 - e^{-t}$  where the negative sign in front of the  $e$  indicates this and the final value of power outputted is larger than the initial power.

$$\Rightarrow A = -97.9517 \tag{3.39}$$

Looking at the third term in (3.33),  $B$  and  $\beta$  are similarly calculated by plotting  $\log_{10}[y(t) - y(\infty) - Ae^{-\alpha t}]$  and evaluating the gradient and intercept at  $t=0$ .

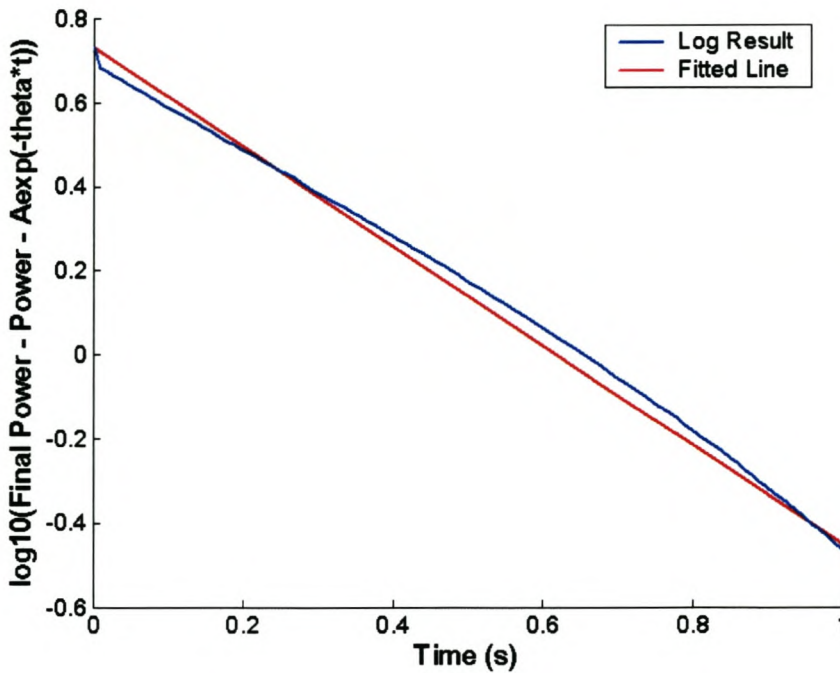


**Figure 3.12** Logged power for  $B$  and  $\beta$  investigation

Similarly from (3.36) and (3.38),

$$\beta = 2.7240 \tag{3.40}$$

$$B = 5.4174 \quad (3.41)$$

Substituting (3.39), (3.37), (3.40) and (3.41) into (3.33), an expression for  $y(t)$  is obtained.

$$y(t) = 92.5343 - 97.9517e^{-0.9636t} + 5.4174e^{-2.7240t} \quad (3.42)$$

The original power output less the initial power and (3.42) is plotted on the same graph in Figure 3.13.

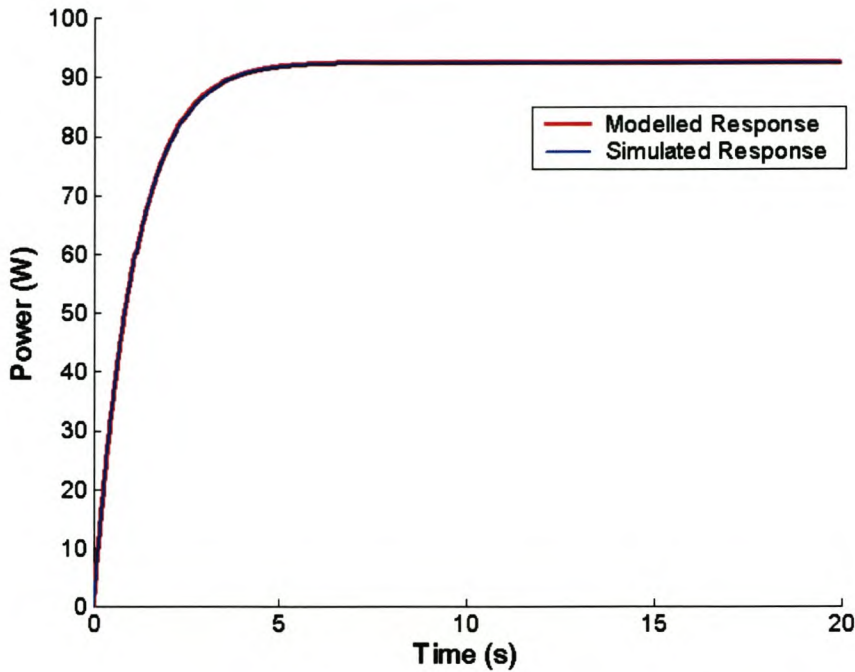


**Figure 3.13 Power produced from modelling and from simulation**

It can be seen that the modelled 2<sup>nd</sup> order response represents the simulated response very well.

To transform (3.42) into the frequency domain, the Laplace transform is used [30].

$$Y(s) = \frac{y(\infty)}{s} + \frac{A}{s + \alpha} + \frac{B}{s + \beta} \quad (3.43)$$

Using the values that have been calculated and simplifying, the output power expressed in the frequency domain (3.43) is reduced to the following.

$$Y(s) = \frac{79.63(s + 3.05)}{s(s^2 + 3.688s + 2.625)} \quad (3.44)$$

It is known that the output,  $y(t)$  is a product of the input step  $u(t)$  and the system  $g(t)$  as shown below.

$$Y(s) = G(s)U(s) \quad (3.45)$$

The input waveform was a step of amplitude of  $\frac{1}{2}$ . The systems transfer function can now be deduced.

$$U(s) = \frac{1}{2} \left( \frac{1}{s} \right) \quad (3.46)$$

$$\Rightarrow G(s) = \frac{159.26(s + 3.05)}{(s^2 + 3.688s + 2.625)} \quad (3.47)$$

The transfer function  $G(s)$  now represents the modelled transfer function of the wind turbine system between the stepped wind speeds of 5 to 5.5 m/s.

The same procedure was used to obtain transfer functions for the intervals from 4 m/s up to 8 m/s. Table 3.2 below represents the transfer functions modelled around the respective wind speeds using the method described above.

**Table 3.2 Transfer functions for stepped wind speeds**

Step in wind speed (m/s)	Transfer function for inputted wind
4 to 4.5	$G_{4 \rightarrow 4.5}(s) = \frac{(-8.882[10^{-16}])s^2 + (85.47)s + 225.5}{s^2 + (3.13)s + 1.846}$
4.5 to 5	$G_{4.5 \rightarrow 5}(s) = \frac{(-1.776[10^{-15}])s^2 + (107.5)s + 316}{s^2 + (3.497)s + 2.38}$
5 to 5.5	$G_{5 \rightarrow 5.5}(s) = \frac{(159.3)s + 485.8}{s^2 + (3.688)s + 2.625}$
5.5 to 6	$G_{5.5 \rightarrow 6}(s) = \frac{(-1.776[10^{-15}])s^2 + (189.5)s + 700.7}{s^2 + (4.295)s + 3.527}$
6 to 6.5	$G_{6 \rightarrow 6.5}(s) = \frac{(1.776[10^{-15}])s^2 + (262.7)s + 1029}{s^2 + (4.59)s + 3.939}$
6.5 to 7	$G_{6.5 \rightarrow 7}(s) = \frac{(-1.776[10^{-15}])s^2 + (324.2)s + 1289}{s^2 + (4.891)s + 4.646}$

$$7 \text{ to } 7.5 \quad G_{7 \rightarrow 7.5}(s) = \frac{(427.8)s + 1534}{s^2 + (4.64)s + 4.369}$$

$$7.5 \text{ to } 8 \quad G_{7.5 \rightarrow 8}(s) = \frac{(-1.776[10^{-15}])s^2 + (478.3)s + 2393}{s^2 + (5.975)s + 6.502}$$

From [30], it is possible to get a good estimate of the settling time  $t_s$  for each of these transfer functions. The settling time is defined as the time taken for the output to decay to within 1% of its final steady state value and is calculated as follows:

$$\begin{aligned} e^{-\sigma t_s} &= 1\% \\ \Rightarrow t_s &\approx \frac{4.6}{\sigma} \end{aligned} \tag{3.48}$$

The term  $\sigma$  is the real component of the position of the most dominant pole in the s-plane. Using the results from Table 3.2, the settling times can be calculated. The settling times from the simulations are measured manually and tabulated alongside the results from (3.45) in Table 3.3.

**Table 3.3 Settling times for stepped wind speeds**

Step in wind speed (m/s)	Power difference (W)	Measured settling time (s)	Calculated settling time (s)
4 to 4.5	61.0951	5.9090	5.8418
4.5 to 5	66.3913	5.0590	4.9770
5 to 5.5	92.5343	4.8390	4.7789
5.5 to 6	99.3302	4.2290	4.1633
6 to 6.5	130.6751	4.0890	4.0312
6.5 to 7	138.7001	3.6190	3.5683
7 to 7.5	175.5504	3.5490	3.5064
7.5 to 8	184.0204	3.2490	3.2182

The power change as a result of the wind change is directly coupled to the wind's direction of change. Thus an increase in the wind will always produce a complete increase in the power.

### 3.4.3 Load step response

The wind speed is one input variable to the wind turbine system; the load also affects the dynamics of the system. The system has a dynamic response to a load change but as in section 3.4.1, the dynamics of the wind turbine system are non-linear and thus practical simulations simulating the effect of varying the loading on the system were carried out. Incremental step changes in the loading were done and the settling time of the output power was measured. These settling times are needed for a proposed algorithm to be explained in Chapter 4. An example of the simulated response of the output power to a step change in the load can be seen in Figure 3.14. The step change is in  $10\Omega$  increments. Notice the time taken for the output power to settle.

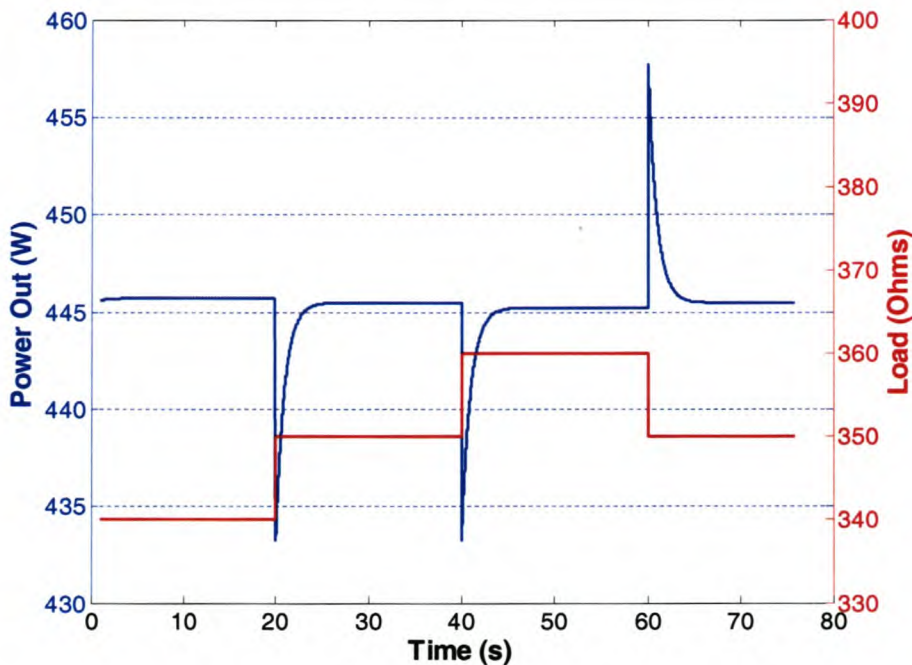


**Figure 3.14 Power output response to load steps**

The system parameters of the real wind turbine were used in the simulation program Simplorer™ and the output power was evaluated. The time taken for the power to settle to within 1% of the difference between the initial and final values of the power was regarded as the settling point of the transient. The simulation was run for constant wind speeds of 4, 6 and 8 m/s and the loading of the system was prepared so that the current increments through the load were in 0.01 A intervals in the  $dq$  plane. A MATLAB® program was written to evaluate the simulated response

data and to obtain the time taken for the power output to settle once a step in the load had been introduced. Figure 3.15 shows the settling times at the different stages of the output current.

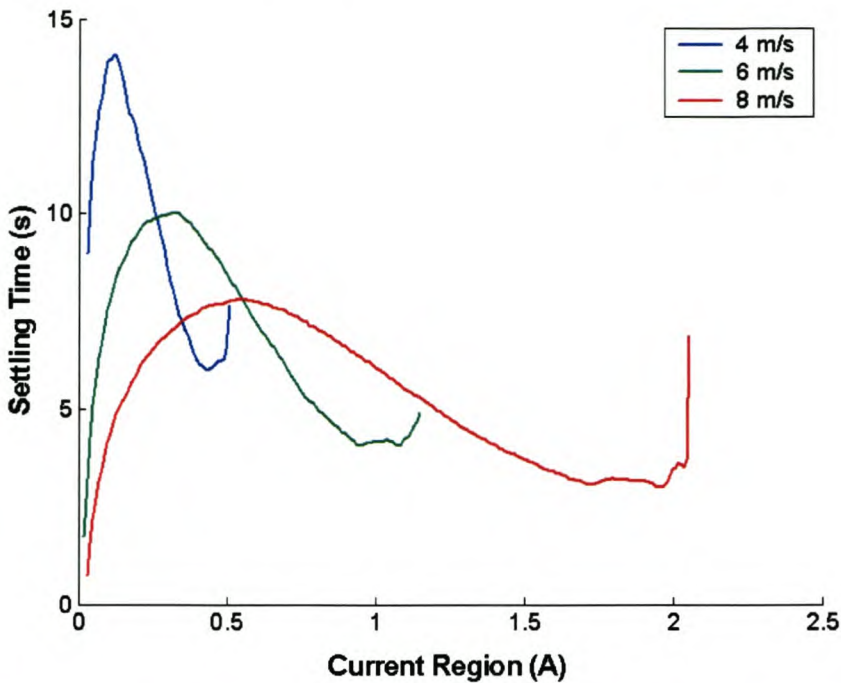


**Figure 3.15 Settling times at various currents for 10 mA increments**

(The curve towards the end of the trace is the region where the current was decreasing as the loading increased). From Figure 3.15, it can be seen that the output power takes a long time to settle. For loading in the 6 m/s scenario to reach the maximum controllable region for this wind speed from an initial 0.02 A (this controllable region will be discussed in Chapter 4), over 100 increments were made at a moderate 0.01 A increments. If the new increment was made after each settling time, the total time taken to traverse the range from a complete standstill under optimal conditions would take more than 10 minutes. Simulations results show that the smaller the increments, the longer the total time taken to traverse the same range as larger increments. It can also be observed that the settling time for constant current increments has no linear relationships.

#### 3.4.4 System response conclusions

Due to the settling times for moderate load changes being even larger than a large wind speed changes, it can be concluded that the load response times are going to be more dominant than the wind transient responses. Step changes in the load will have to be compensated for by controlling algorithms and will be of more concern than the wind transients.

### **3.5 Summary**

A model of the wind turbine system was developed which is used to obtain a better understanding of the system's response to wind and loading changes. The wind turbine system is non-linear due to the non-linear power curves of the blades and thus the system was modelled from simulations to obtain transfer functions at various points. These simulations indicated that the constant step method to be discussed in Chapter 4 could be problematic.

Proposals for maximum power point tracking algorithms are presented in the following chapter.

## Chapter 4. Maximum Power Point Tracking

In order for a wind turbine to harvest the maximum amount of energy available from the wind at any given instant, the electrical loading on the generator needs to be correct to realise the maximum available energy transfer from the rotor. If the load is too large or too small for a particular wind speed, the output power deviates from optimal point and the system efficiency is lower.

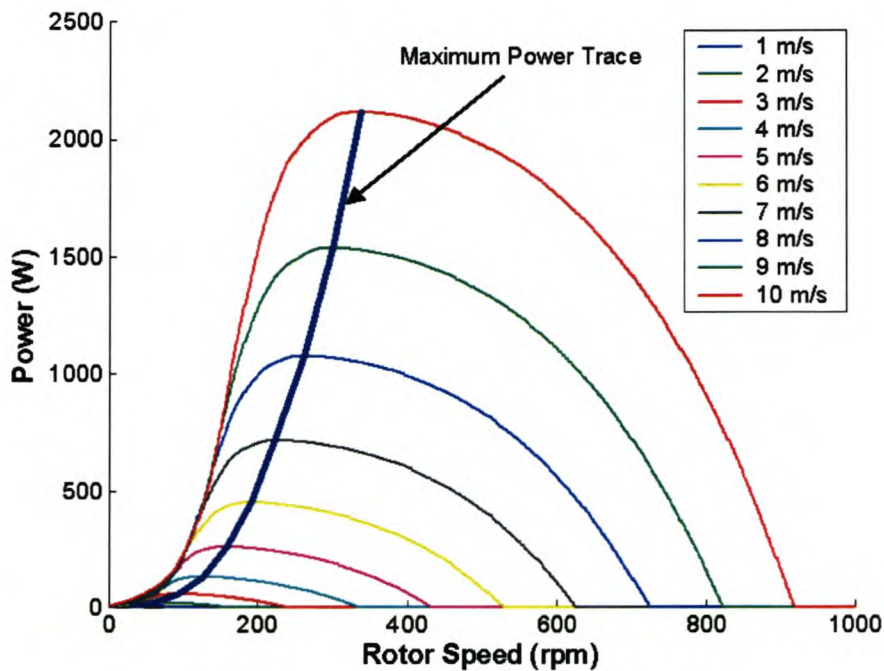


**Figure 4.1 Maximum power trace**

Figure 4.1 displays the maximum available power from the wind turbine over different wind speeds. This section discusses the algorithms proposed to determine the loading on the wind turbine. The generator in the system is assumed to be ideal without any internal impedance.

### 4.1 Understanding the System

#### 4.1.1 Introduction to loading on the wind turbine

A resistor is assumed to be the load on the wind turbine for the purpose of this explanation. When a wind turbine has no load on it, there is no torque from the generator to counter the torque developed from the rotor blades and the system accelerates up until a mechanical or aerodynamic limiter engages which limits the angular velocity or slows the rotor down. This is either due to a stall or mechanical brake or some other feature of that particular wind turbine.

Due to the output voltage being a function of the rotor speed, the voltage at the terminals is largest at this stage (unloaded).

If a resistor of large magnitude is applied between the output terminals, a small current would flow through the machines windings producing a counter torque to the torque developed by the rotor blades. The rotor speed thus drops until the equilibrium point is reached where the difference between the torques is zero.

As the resistance is decreased, more current flows, which produces a larger counter torque. The rotor speed drops and thus the voltage, but the power continues to increase due to the current not having a linear relationship with the rotor speed. A point is reached where the product of the voltage and the current (power) is a maximum and any further increase in the loading causes the output power to decrease. It is this optimal point which a maximum power point tracker endeavours to obtain by means of load control.

#### 4.1.2 The effect of loading on a wind turbine

The relationship between the current and the voltage can be obtained by using the power equation, where  $I = P/V$  and  $P$  is the power profiles provided by the blade manufacturer and  $V$  is the voltage produced which is a function of the rotor speed. The traces of the current produced by the wind turbine as a function of the voltage produced for individual wind speeds are plotted in Figure 4.2.

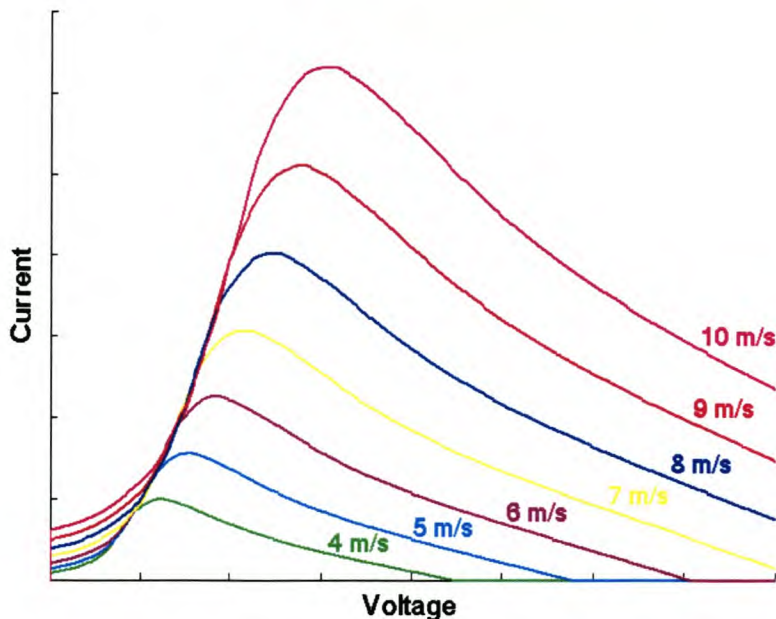


**Figure 4.2** Current versus voltage produced by the wind turbine at various wind speeds

From Ohm's Law, the current flowing through a resistor is a function of the voltage across it.

$$I = \left(\frac{1}{R}\right)V \tag{4.1}$$

Since the active rectifier can be modelled as an active impedance on the wind turbine, traces are plotted in Figure 4.3 for various resistance values over a voltage range on the same set of axis's as the wind turbine's current versus voltage plots. Now from the simple equation of (4.1), the relationship between the current and voltage can be explained by straight traces where  $1/R$  is the gradient.

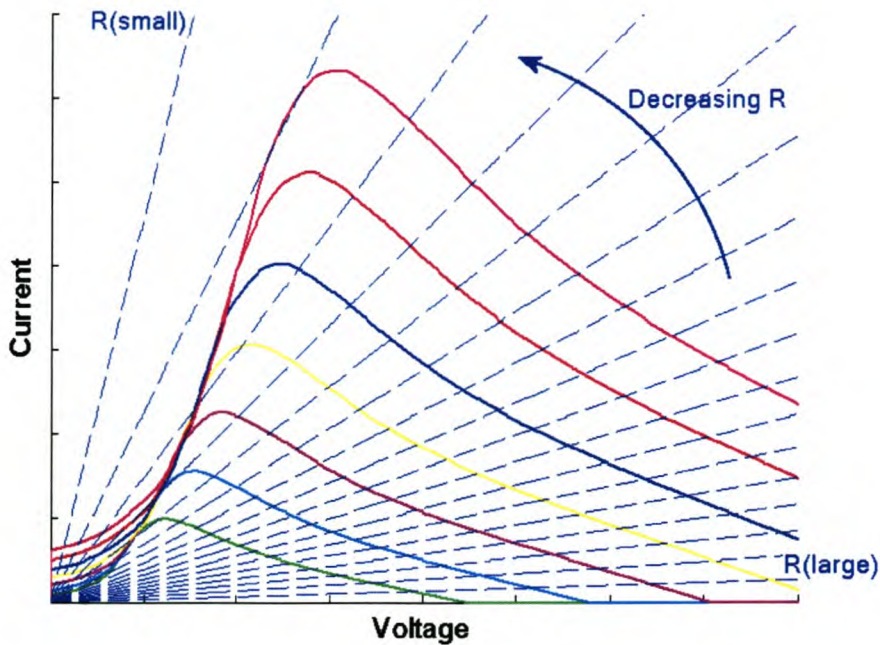


**Figure 4.3 Current versus voltage at various wind speeds against loading**

The traces for the various impedances represent the relationship between the current and voltage for that specific impedance. Because the current versus voltage characteristics from the wind turbine are already known for each wind speed, the intercept of the two traces is the point at which the wind turbine will operate for that particular impedance at that particular wind speed.

An example of load and wind speed changes can be seen in Figure 4.4. If the wind is blowing at  $w_{sa}$  and a load of  $Z_1$  is applied to the wind turbine, the operating point will lie at the point 1.  $I_1$  is the current that will flow through the load and  $V_1$  will be the voltage across it at this point. If the loading was decreased at the same wind speed (resistance increases) to  $Z_2$ , the operating point

would move to point 2 ( $I_2, V_2$ ). An increase in wind speed to  $w_{sb}$  at the same loading will cause the operating point to move to point 3, and if the loading was increased at that wind speed, to point 4.

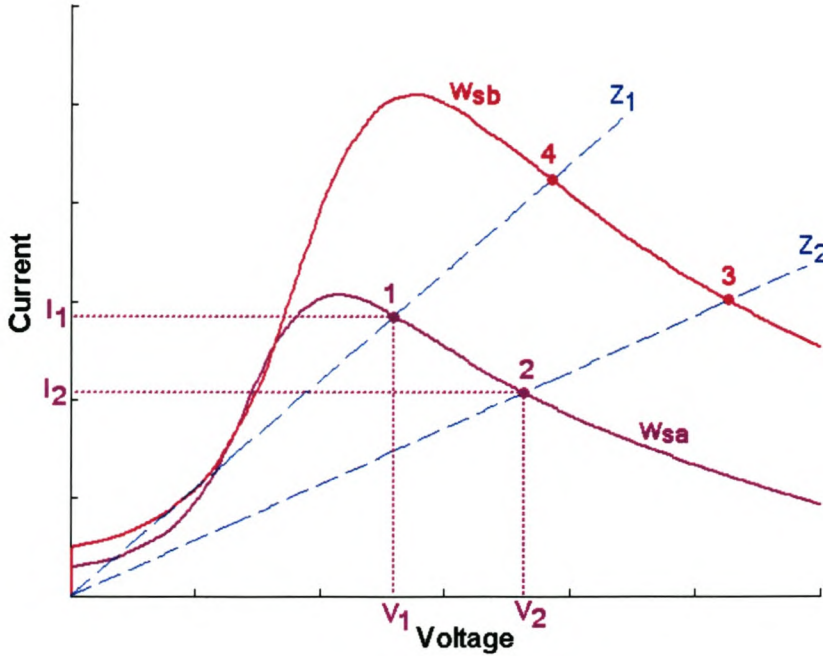


**Figure 4.4 Wind turbine response for various wind and load changes**

The power that the wind turbine delivers is now plotted in Figure 4.5 for a constant wind speed. Each impedance value will sustain a corresponding power over the load, although this is not a unique power as will be seen in section 4.2.1.1. The maximum power point is of interest in this project and it can be seen that it does not correspond to the maximum current.

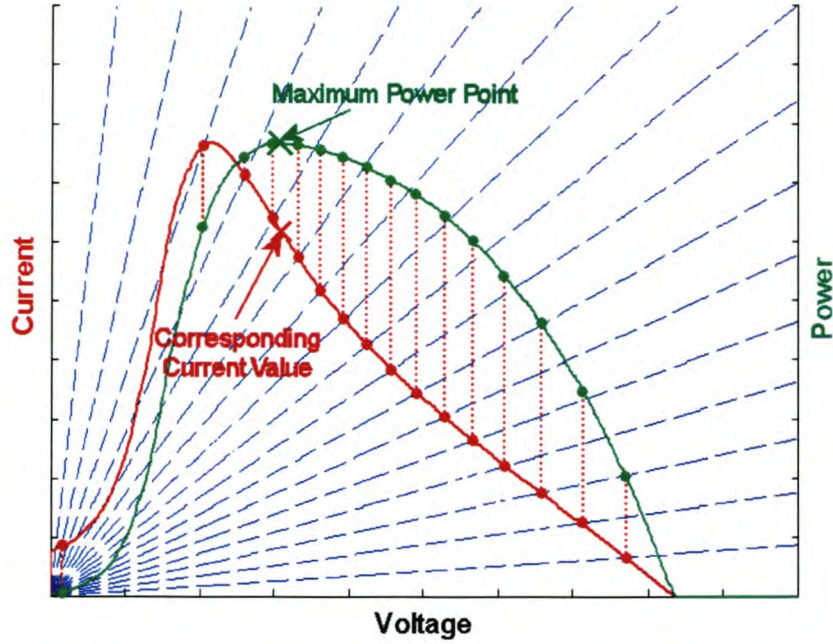


**Figure 4.5 Power and current produced by the wind turbine under various loadings**

## **4.2 Maximum Power Point Tracking Algorithms**

A method to determine the optimal loading on the generator at any specific time is needed to be able to transfer the maximum amount of available energy from the wind. Recall that the maximum available power is determined by the wind speed and thus this method must be able to constantly track the maximum available power throughout wind speed variations.

Two main proposals for maximum power point tracking are considered. The two main methods are referred to as *Constant step control* and *Equation control* for the purposes of this thesis. Equation Control is further divided into two variations namely *Anemometer control* and *Calculation control*.

### **4.2.1 Constant step control method**

As explained in section 4.1, any change in the load is going to generate a change in the output power. An active method is proposed whereby the loading is changed and the effect of that load change on the output power is assessed to make a calculated decision about the next change in the loading.

This method changes the loading in constant steps and the power at a time  $t$  is measured and its value stored. A small step change is then made in the loading, either a positive or negative with

respect to the original load value. The power being produced one sample later is measured and the power change for that sample is used to calculate the direction of the next step change. If the result of the step change produced more power than the original power outputted, the direction of the change (load was increased or decreased) is repeated. If the power change was negative, the direction of the load change was incorrect and the load step direction is reversed.

This method is effectively changing the rotor speed so that the output power ‘climbs up’ the trace of the power curve (increasing the power) for that particular wind speed. When the top of the trace is reached, the algorithm keeps on changing the load and thus the rotor speed and so the power starts moving down the opposite side of the trace. The algorithm reverses the direction of the load change and the output power increases once again. This process continues indefinitely and can be seen as oscillating around the peak of the power curve.

The dynamics of the generator is such that the output power needs time to settle before the new increment or decrement in the load can be made, as displayed in section 3.4. This slow response time and the constant variation in the wind speeds will lead to this power point tracker lagging behind the optimal loading trace for periods of changing wind speeds.

#### **4.2.1.1 Constant step control response to load and wind changes**

The simplified system used for explanation in section 4.1 is used to provide an insight into the response of an ideal system to the step changes instigated by the step control methods.

Considering Figure 4.6, upon initialisation of the step control algorithm, the current will be at a minimum and the voltage at a maximum. The wind speed at this instant in time for this illustration is  $w_{sa}$ . The specific operating point is not illustrated on the figure but lies along the voltage-axis at a point higher than the wind speed’s current profile interception with the axis (exact value determined by the wind turbine’s mechanics). As the step controller begins increasing the loading on the wind turbine, the operating point moves up from the region of initialisation indicated by the digit 1 towards the maximum power point indicated by 2 on the current profile. Once the maximum power point has been reached, the operating point will oscillate around this point. The frequency and the size of these oscillations are determined by the sampling time and step size of the algorithm respectively.

If the wind speed suddenly drops to  $w_{sb}$ , the operating point will move to point 3 where analysis of the power response to an increase or decrease in the loading will reveal that the load needs to be decreased leading to the tracker finding the maximum power at point 4 for that wind speed.

If the wind speed were to increase once more to  $w_{sa}$ , the operating point would move up to point 5 and the tracker would once again ensure that the maximum power point at 2 would be found and maintained for as long as the wind speed remained at  $w_{sa}$ .

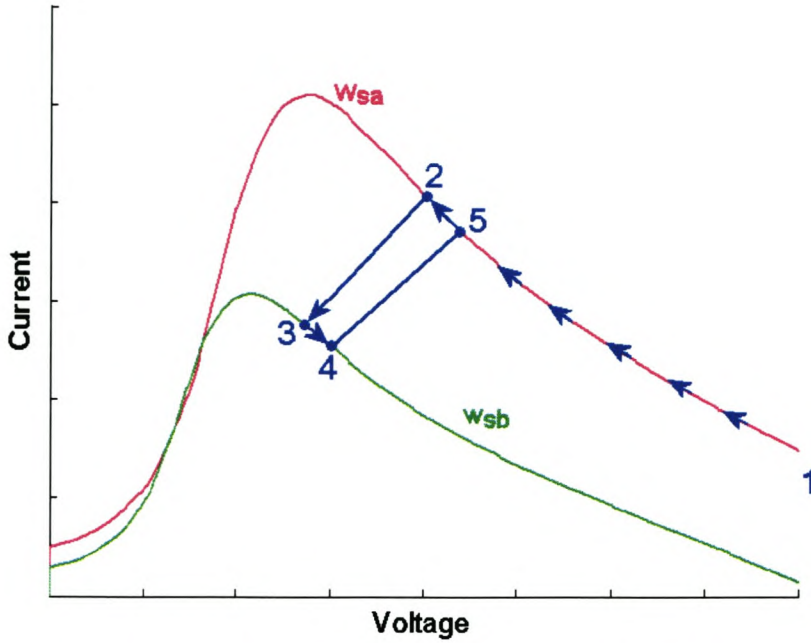


**Figure 4.6 Change in wind speed for stable maximum power tracking**

The system is not always theoretically ‘stable’ with regards to wind speed and loading changes. If the wind drops directly from a high wind speed to a lower wind speed and the loading does not react fast enough, the load can move the operating point onto the left hand side slopes of the current profiles as shown in Figure 4.7.

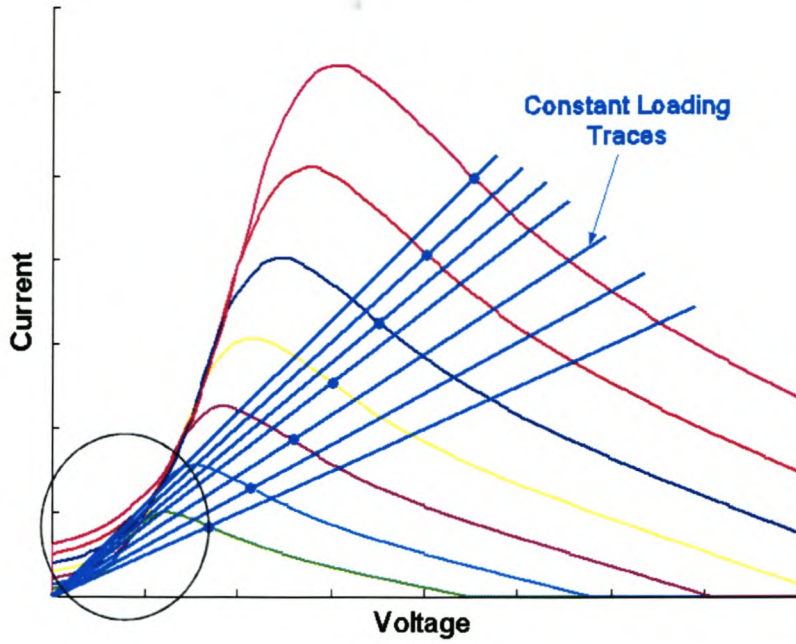


**Figure 4.7 Changes in wind speed during constant loading**

The operating points would move from their maximum power points on the current profiles, down the constant loading traces until the new wind speed's current profile is intercepted. The area circled in Figure 4.7 is of importance as this is where some of the loading traces from the higher maximum power points intercept the lower current profiles on the left hand side or 'unstable' slopes. These slopes are defined as unstable due to the control algorithm implemented in the practical system as is explained in section 4.3.

An example of a scenario where this 'instability' occurs is described in Figure 4.8.

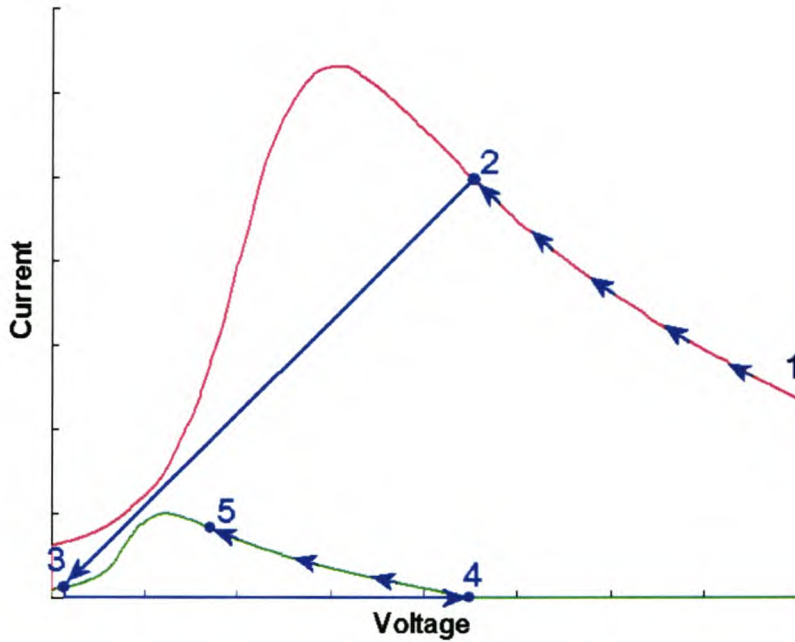


**Figure 4.8 Unstable scenario**

The system's operating point initially lies at a high voltage in region 1. The power point tracker enables the operating point to climb up to the maximum power point at 2 where it is maintained. If the wind speed drops suddenly from the current high wind speed to a much lower one and the loading stays the same for that change, the operating point shifts down to point 3. Due to the nature of the practical controller (to be discussed in section 4.3), the operating point is unable to be moved back over the peak available current point by the conventional tracking system and so another command sequence is activated where the loading is completely removed. As there is no loading on the wind turbine, it speeds up and the operating point moves to point 4. The power point tracker then commences again and the maximum power point at 5 is found.

In order for this scenario to occur, the wind speed change has to be dramatic and/or a combination of a large step on the wrong side of the maximum power point before the wind speed change or small steps with long settling times. Thus this scenario is dependant on a combination of three variables, the size of the loading steps, the length of the sample time and the rate of change in the wind speed.

This scenario is made more likely when factors like measurement errors are considered in the practical system. Errors in the measurement system can sometimes lead to the incorrect power being measured due to the small power difference around the maximum power point and the step change can move the operating point closer to the unstable region. Thus, if the wind speed

decreased, there would be a greater chance of the operating point moving into the unstable region.

## **4.2.2 Equation control method**

Another approach to maximum power point tracking is to make use of a predetermined look-up table or an equation describing the loading required to achieve the maximum power point.

### **4.2.2.1 Anemometer control method**

The maximum power point of a wind turbine is a function of the wind speed. Thus the wind speed must be known at any given instant to be able to calculate the optimal load required for that particular wind speed in this proposed open-loop-type system. The wind speed is measured using an anemometer and the load value required for optimal efficiency is determined and applied.

The optimal loading for various wind speeds needs to be pre-programmed into the control system. These optimal points can either be calculated from the expected power profiles or physically measured during practical testing of the wind turbine. Once the optimal loading for various wind speeds is determined, an equation describing the relationship is deduced.

In Figure 4.9 below, the 'x' markers are the points of the maximum available power from the rotor at individual wind speeds acquired from the rotor's theoretical power profiles. The interlinking trace is of an equation that describes the optimal power at those different wind speeds closest, i.e. a fitted equation for the 'x' markers.

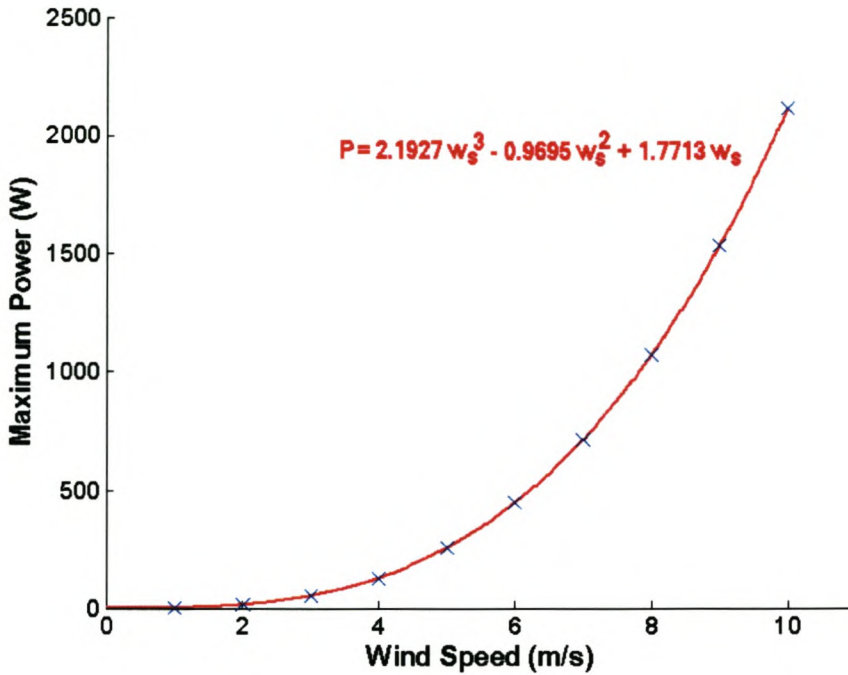


**Figure 4.9 Optimal power points and fitted equation versus wind speed**

When the wind speed is obtained from the anemometer, the optimal load corresponding to that wind speed is calculated from the fitted equation (a look-up table can also be used) and the load is adjusted for maximum power transfer.

Due to the small derivation of power near the maximum available power points of the power profiles, there is a relatively large room for error in the algorithm's accuracy where the power output of the system will not be greatly affected. In other words, if the algorithm is slightly inaccurate in the optimal loading calculation, the reduction in the power produced is minimal. Figure 4.10 represents the deviation region where the reduction in power will be less than 1%.

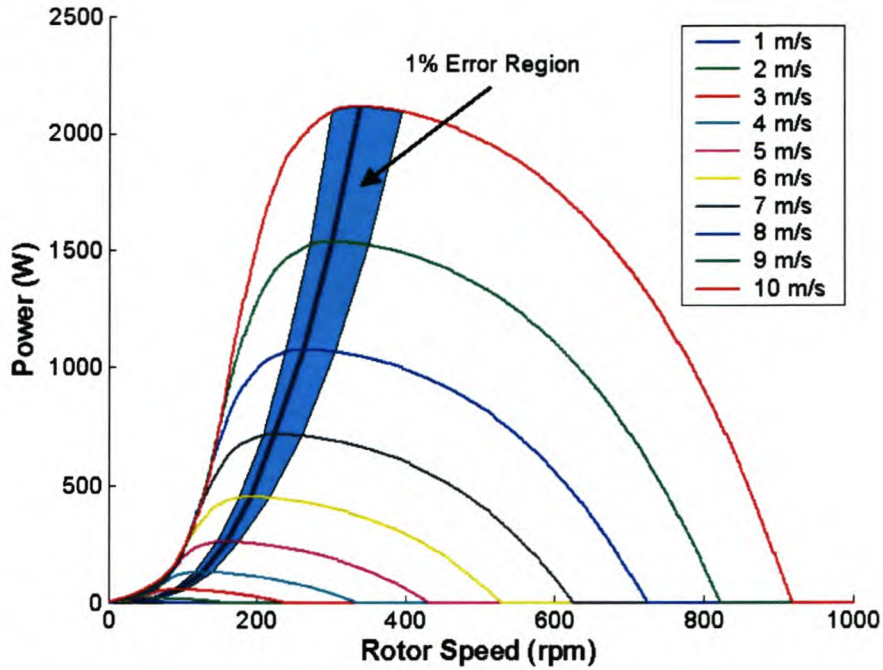


**Figure 4.10 1% reduced power region**

#### 4.2.2.2 Calculation control method

Anemometers are expensive instruments and their inclusion for power point tracking is not financially viable on small scale wind turbines. A method is proposed whereby the anemometer is removed and the wind speeds are calculated from the available electrical parameters at the generator’s output terminals.

Due to the generator on the wind turbine being a synchronous machine, the electrical frequency produced by the generator is directly proportional to the angular acceleration of the rotor. Thus, by measuring the electrical frequency, the rotor speed can be calculated. The power versus rotor speed profiles are unique for each wind speed. This means that for one particular rotor speed, there is a unique power that the rotor blades will deliver for each wind speed.

Because the power delivered by the wind turbine is measurable and the electrical frequency can also be determined, it is possible to calculate the instantaneous wind speed responsible for the system’s power generation at any time. Because the power profiles are only available for a few of the wind speeds, interpolation is used to determine the wind speeds where the measured power does not exactly correspond to a given power profile.

Figure 4.11 is an example of this wind speed calculation method. The power measured from a hypothetical wind turbine system was found to be 1 kW and the frequency of the voltage signals

showed that the rotor was turning at 600 rpm. By plotting these points on the power versus rotor speed curve, it can be seen that the operating point lies in between the 8 m/s and 9 m/s power profiles. The wind speed corresponding to this measurement therefore lies somewhere in between 8 and 9 m/s.

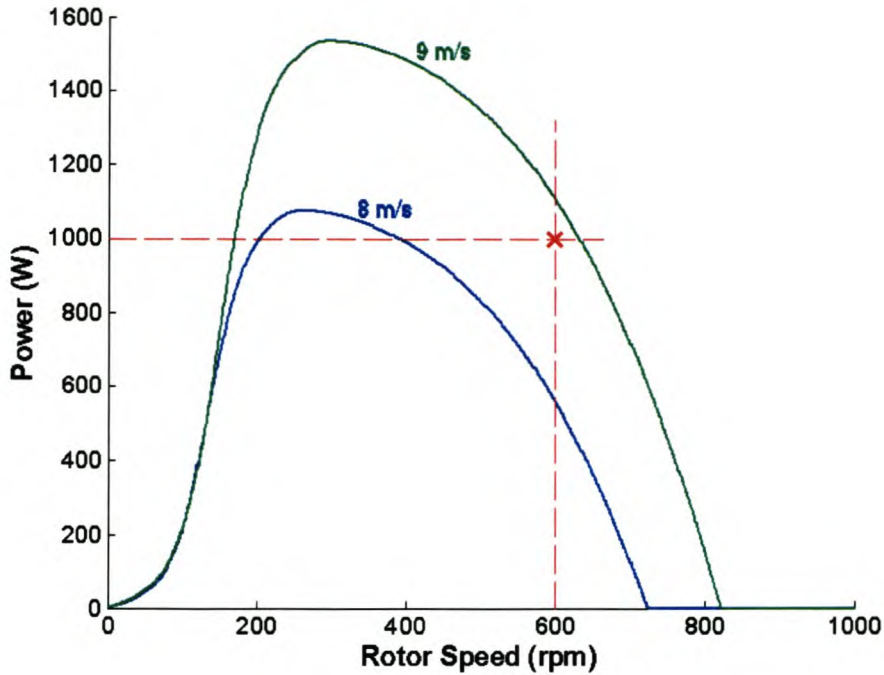


**Figure 4.11 Calculation method example**

Interpolation of this point between the 8 and 9 m/s power profiles shows that the wind speed is 8.8 m/s at this instant.

Once the wind speed is known, the anemometer control method described in section 4.2.2.1 is used to calculate the optimal load. This method effectively removes the need for an anemometer.

### **4.3 Practical System**

When controlling power from the wind turbine system, it is customary for the controller that requests the power by changing the loading to have a feedback system. This ensures that the error between the requested power and the delivered power is minimised. Because of the nature of the power profiles of the wind turbine, there is a peak available power. If a power request is greater than the peak available power, due to the nature of a feedback system, the error in the feedback path will result in the requested power being increased to try and obtain the original requested power. This will result in the wind turbine’s operating point running into an avalanche effect, reducing the rotor speed until the wind turbine stops. This region left of the peak available

power can thus be described as an unstable region and therefore the operating point must try to avoid it.

Because the current deliverable by the wind turbine is not linear to the power deliverable by the wind turbine, the maximum available power is not at the same rotor speed as the rotor speed at which the maximum available current is situated. This can be used to the controller's advantage. This can be seen in Figure 4.5 where the maximum current point lies at a lower rotor speed for the respective maximum power point. All the wind speeds have this same characteristic. The controller can now be designed to use the current to control the wind turbine's power, where the peak of the available current now determines the unstable region of the controller. If only the rotor speeds greater than the rotor speeds at the maximum available currents are used, then the unstable region of the controller lies in the regions where the rotor speeds are lower than the peak currents' rotor speeds. The maximum available power thus lies in the stable region and it can now be found by controlling the current without too much concern about runaway around this point.

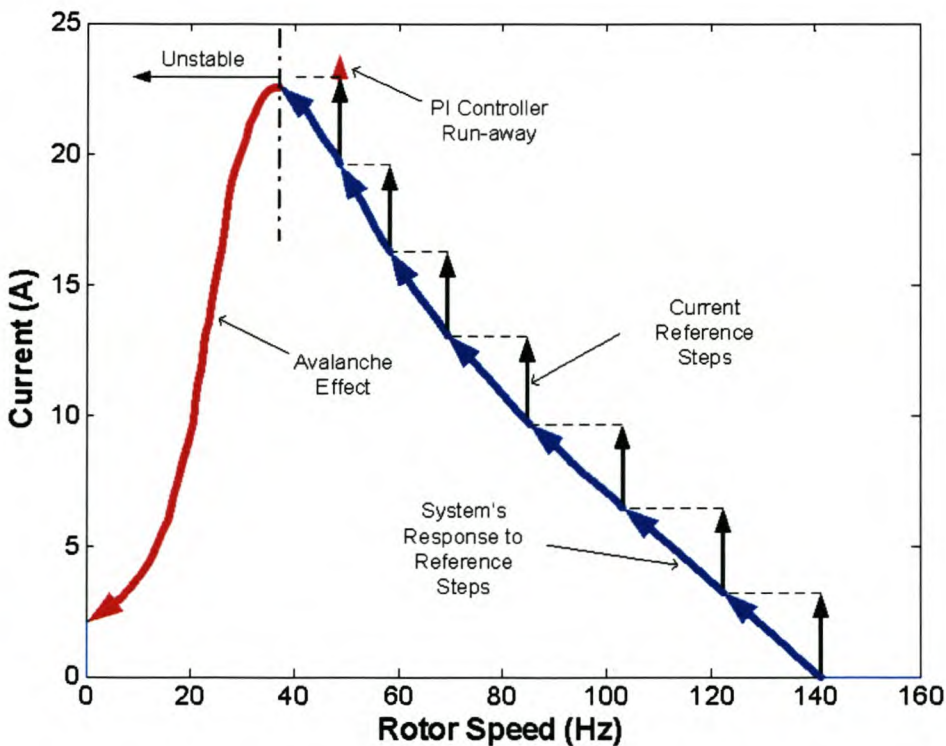


**Figure 4.12 System stability regarding current increments**

The controller can still fall into the unstable region for different scenarios as discussed in section 4.2.1.1. Figure 4.12 shows situation where the step method increases past the maximum power point into the unstable region. Constant incremental current steps are made until the operating

point reaches the peak on the current profile. The requested current is greater than the maximum available current and the system avalanches while the requested current tries to compensate for the incorrectly delivered current.

The analog system explained in Chapter 6 was used to illustrate this point. The current delivered by the wind turbine was the controlled parameter and a current reference was increased slowly over time. Figure 4.13 and Figure 4.14 are the measured results from the experiment. The red '\*' in Figure 4.14 represent the logged power produced and the green trace is the reference power profile for that wind speed. The blue trace is the current profile calculated from the programmed power profile.

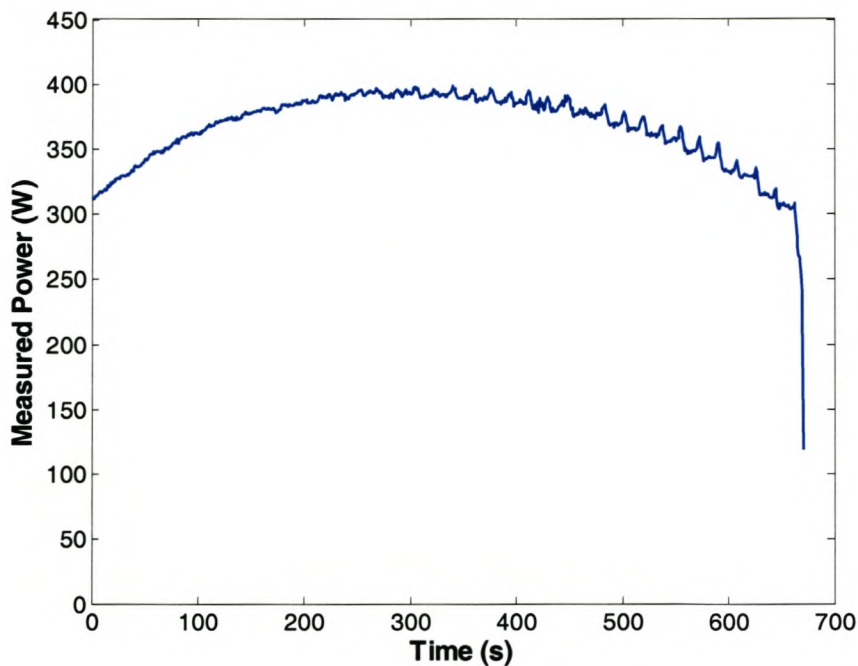


**Figure 4.13 Produced power for 6 m/s input over time**

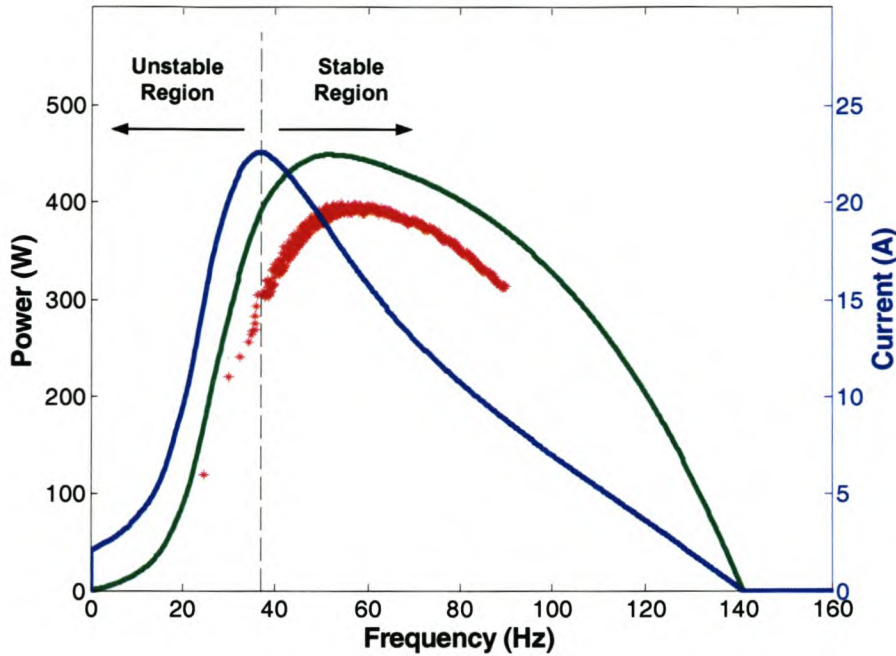


**Figure 4.14 Measured and reference power and current at 6 m/s**

The wind turbine section was programmed to start operating from a higher rotor speed upon initialisation because the stable current operation region lies at the higher rotor speeds. As the current reference signal was increased, the power increased and the rotor speed decreased as expected. A point was reached where the power started decreasing. This indicates that the maximum power for that wind speed was achieved but due to the maximum current point being at a lower rotor speed, the current reference could be increased further. A point was finally reached where the maximum available current was exceeded and as explained above, the control system pulled the wind turbine system into avalanche and the system quickly collapsed. The collapse of the system can be seen in Figure 4.13 and the logged power points left of the maximum available current rotor speed in Figure 4.14. The logged power was logged at constant intervals and the collapse can be seen as the fewer amount of logged points as the system collapsed.

#### **4.4 Summary**

In order to ensure a maximum power harvest from the wind, maximum power point trackers are needed to optimise the loading on the wind turbine. Three algorithms are proposed for this purpose.

The *constant step* method is considered whereby the effect of a load change on the power output is analysed to establish the new loading. Preliminary speculation is that this method will not operate efficiently, as the system response is much slower than the typical fluctuations in wind speed.

An *anemometer method* was proposed where the present wind speed is measured and used in a predetermined optimal loading table or equation to adjust the loading. Slight inaccuracy in the algorithm is not of too much concern as the reduction in power production would be minimal.

A variation on the anemometer method entitled the *calculation method* was created where the wind speed is calculated from the current condition of system's parameters. The anemometer method is then used to calculate the optimal loading for that calculated wind speed. The attractiveness of this method is that it removes the need of an expensive anemometer.

Simulations of the proposed maximum power point tracking algorithms are used to investigate the validity of them. The results are presented in the following chapter.

## Chapter 5. Simulations

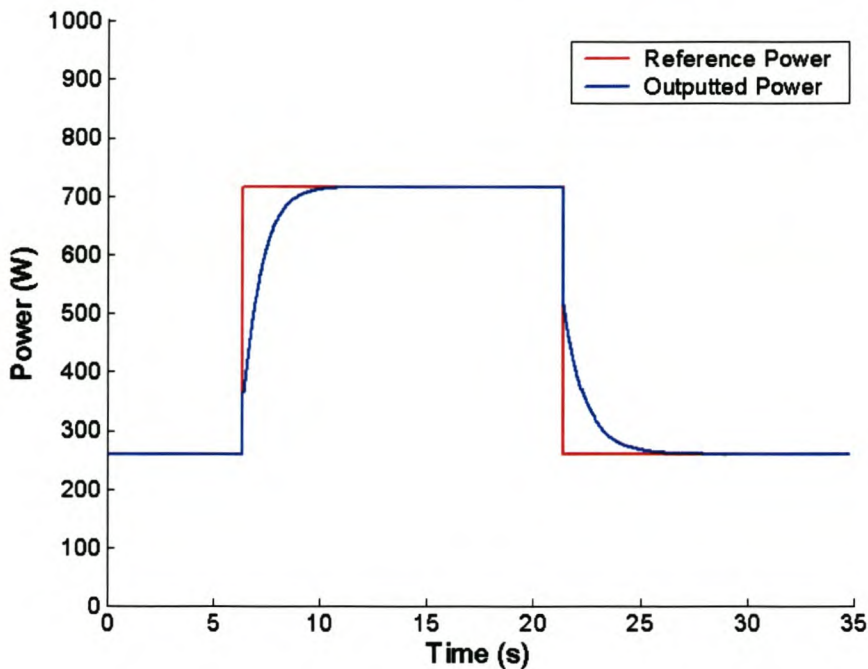
Simulations were required to evaluate the system under certain conditions as explained in the previous chapters, and also to demonstrate the different power point tracking algorithms. Simulations were done in Simplorer™ using the model created from the results generated in section 3.3 and displayed in Figure 3.9.

### 5.1 Wind Step Response

The first simulation conducted was to determine the time in which the power point tracking algorithm could acquire the maximum power point. A step input on the wind speed from 5 m/s to 7 m/s and then back was introduced once the different algorithms were in a steady state.

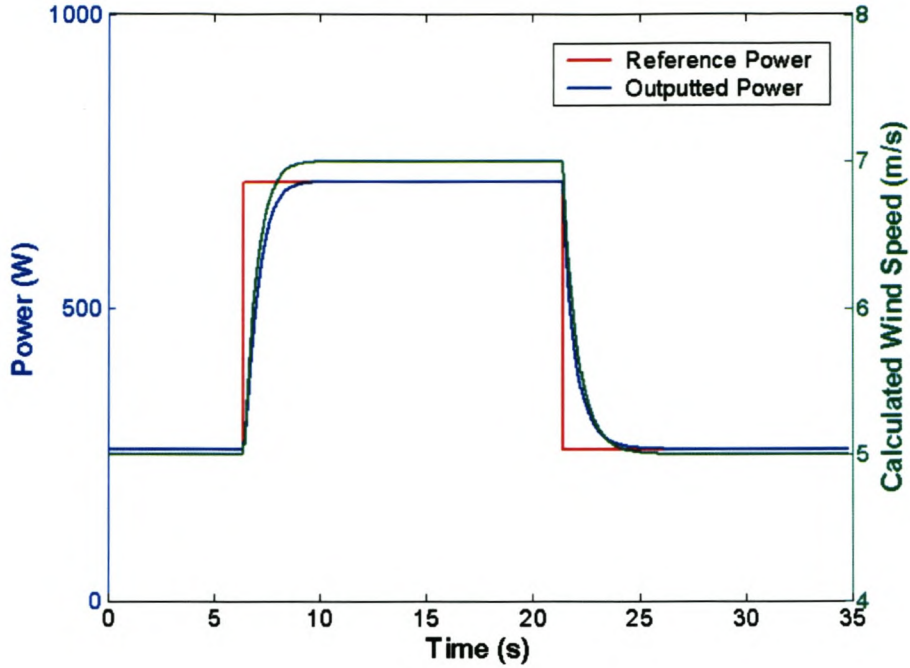
#### 5.1.1 Equation method response

The response of the algorithm using the provided wind speed is shown in Figure 5.1 below. The reference power trace represents the ideal power for the wind step.



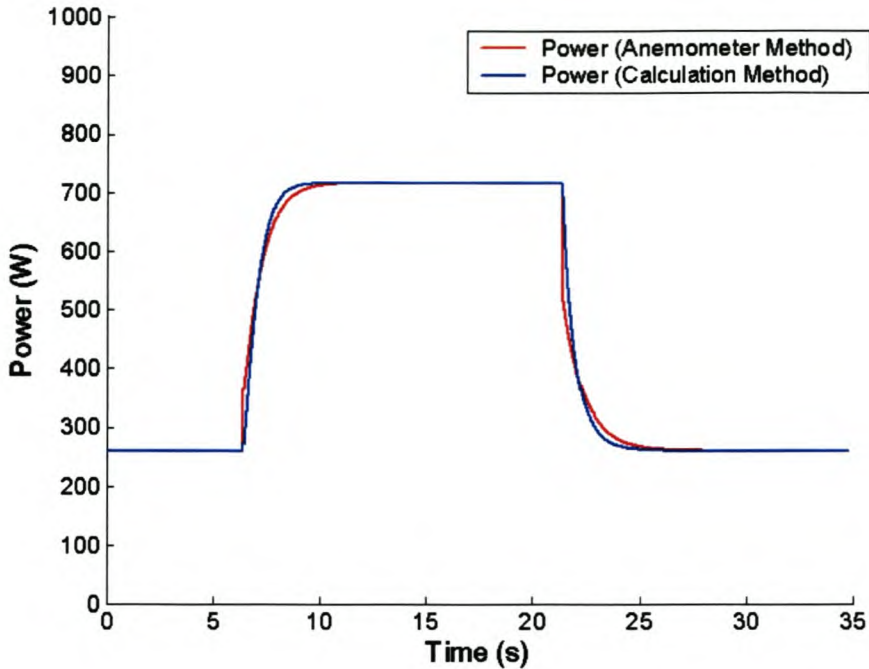
**Figure 5.1 Step response of anemometer control method**

Figure 5.2 is the result from the calculation method. The calculated wind speed is superimposed onto the power curves.



**Figure 5.2 Step response of calculation control method**

The responses in Figure 5.1 and Figure 5.2 show that the algorithms do have a response time but this is expected due to the effect of the inertia of the mechanical system. The steady state values are at the required values and any minor deviations can be contributed to the slight inaccuracies in the calculation of the predetermined optimal loading values. Due to the optimal loading being calculated from the exact system parameters being used in the simulations, no steady state error is expected.



**Figure 5.3 Comparison of anemometer and calculation control methods**

Figure 5.3 shows that the calculation method, where the wind speed is calculated from the system parameters, has an improved response time when compared to the anemometer method, where the wind speed is measured using an external anemometer.

This is in contradiction to the initial assumption that the method using the externally measured wind speed would be ideal. In order to explain this, the systems must be analysed from an instantaneous perspective. The effect of inertia prohibits the mechanical system from changing instantaneously. Time is needed for the rotor speed to increase or decrease to the new maximum power point's respective rotor speed. The anemometer method is not as effective; as it attempts to load the wind turbine at the optimal load for the new wind speed, but this new loading is not optimal for the transition to the new operating point.

This concept is illustrated in Figure 5.4. The operating point before the wind change lies at 1. The wind speed changes and the loading changes to the new optimal loading. The voltage, which is proportional to the rotor speed, is experiencing the effect of inertia and does not change as fast, thus the operating point moves to the new optimal loading depicted by 2, but the voltage did not change much. The slower rotor (voltage) transition then moves the operating point to the maximum power point at 3 where the optimal loading is valid.

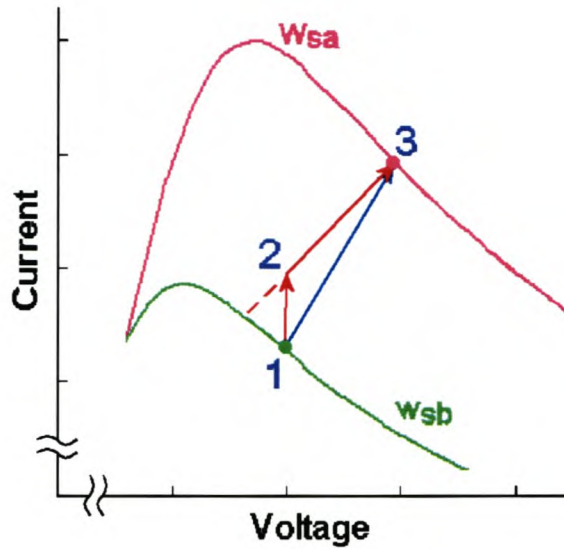


**Figure 5.4 Anemometer and calculation control routes**

The calculation method is more in tune with the actual system and loads the system in accordance with the wind speed that the system is experiencing at that particular moment. The idea can be visualised by drawing a straight line between the two maximum power points. This can be seen as the route from 1 straight through to the new maximum power point at 3 in Figure 5.4. This route is quicker; illustrating that the response time for the calculation method is quicker. Confirmation of the idea that the anemometer method incorporates a hard step change in the loading can be seen in Figure 5.5 where a larger wind step was simulated.

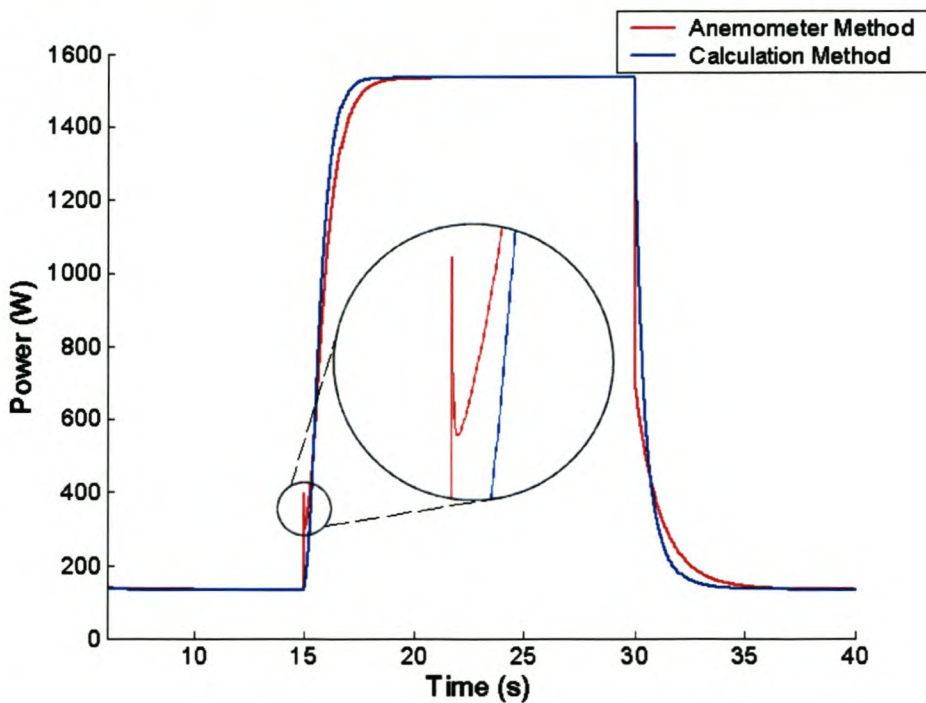


**Figure 5.5 Larger step response of anemometer control methods**

The effect of the anemometer method's overriding load step can be seen in Figure 5.5 whereas the calculation method has a more continuous response. The results of the anemometer method could be improved by using a "running average" of the measured wind speed value from the anemometer. This would low-pass filter the anemometer measurement; artificially introducing "inertia" into the control loop. The operation of the mechanical anemometers does have some inertia, and so the practical implementation of the anemometer method would be better than simulated.

Calculation of the energy transfer for the 5 m/s to 7 m/s steps showed the calculation method providing a greater transfer of energy (25163 J) as apposed to the anemometer method (24946 J).

Table 5.1 below displays the results of the settling times from the equation methods for the wind speed steps of between 5 and 7 m/s. The settling times were calculated as the time taken for the output to decay to within 5% and also 2% of the steady state values.

**Table 5.1 Settling times**

	Anemometer method		Calculation method	
	5%	2%	5%	2%
<b>Rising settling times (s)</b>	2.309	3.019	1.805	2.270
<b>Falling settling times (s)</b>	2.499	3.449	1.909	2.584

The faster transient response of the calculation method is confirmed from the results shown in Table 5.1.

### 5.1.2 Constant step method response

The responses of the step method algorithms in Figure 5.6 can be seen to be extremely slow and can not even be compared to the faster rise times in the equation methods. From the simulation results, the system went into the unstable region during the transition from 7 to 5 m/s and the loading had to be drastically decreased in order to recover control of the system.

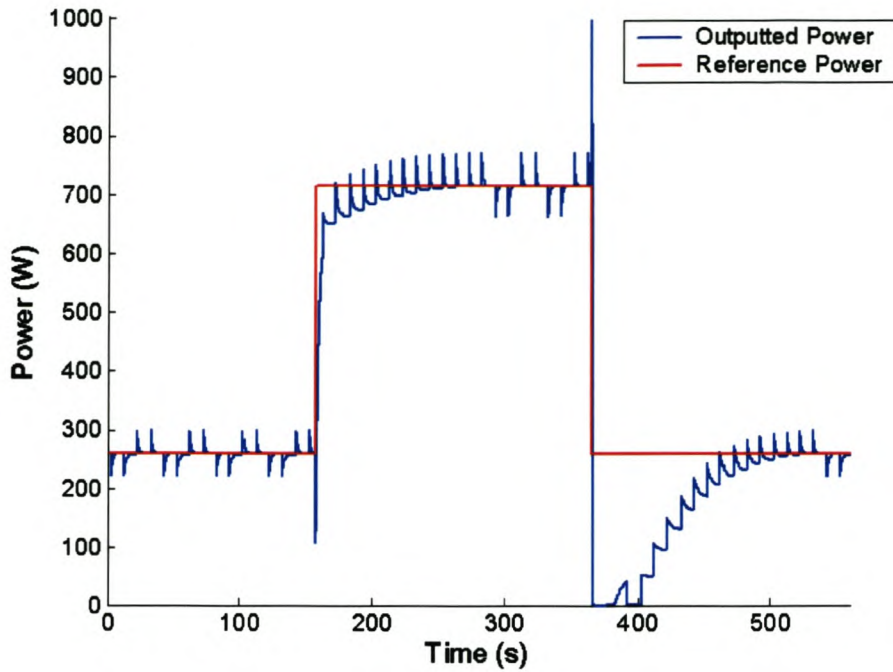


**Figure 5.6 Step response of constant step method**

The rise time is over 100 s and in the practical system, the wind speed would have changed long before the system has found the maximum power point. If the size of the steps is increased too much, the risk of the system running into the unstable region is increased as described in section 4.2.1.1. Therefore this method is unviable, and not recommended.

## **5.2 Random Wind Responses**

The absence of real, high resolution wind speed data has meant that the dynamics of wind could not be investigated for this thesis. A random wind profile was generated from an image of measured wind speed over 180 s in [28]. The same random wind profile was then used on the different algorithms to ascertain which algorithm performed best.

### 5.2.1 Anemometer method result

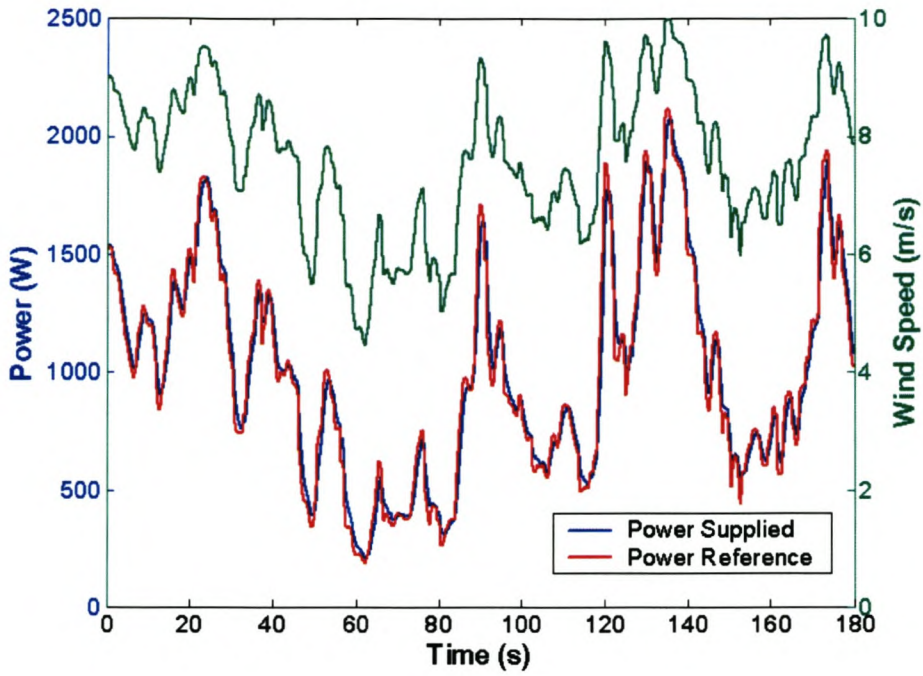


**Figure 5.7 Power supplied versus reference power for anemometer method**

Figure 5.4 is the trace of the response from the anemometer method. It can be seen how well the output power follows the maximum available power reference. This ideal maximum available power reference trace is obtained from instantaneous evaluation of the wind speed and thus does not take the effect of inertia into account.

## 5.2.2 Calculation method result

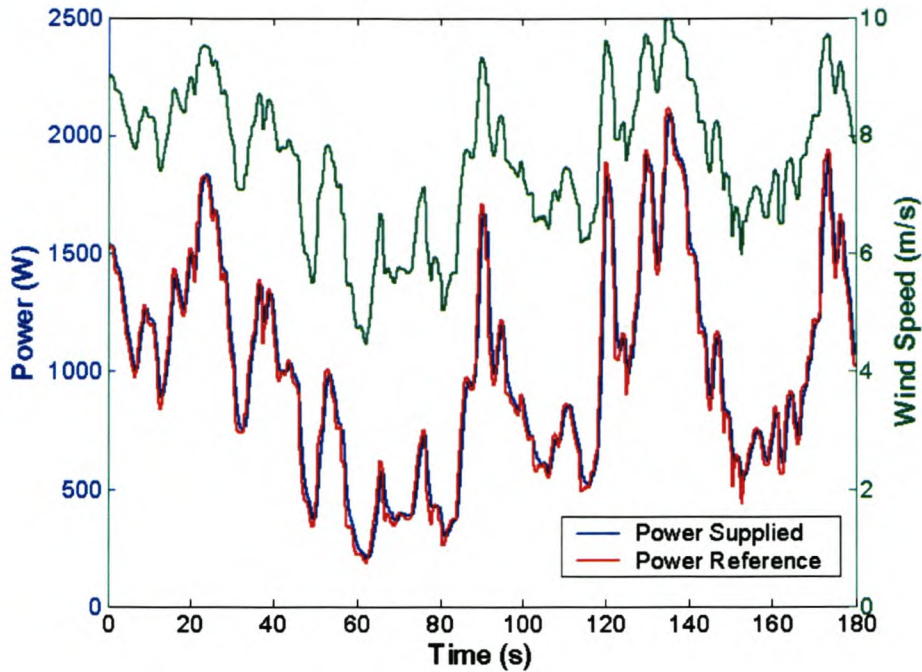


**Figure 5.8 Power supplied versus reference power for calculation method**

The result of the calculation method for the same random wind speed is shown in Figure 5.8. The result looks very similar to the anemometer method but comparison of the two responses in Figure 5.9 shows them to be slightly different.

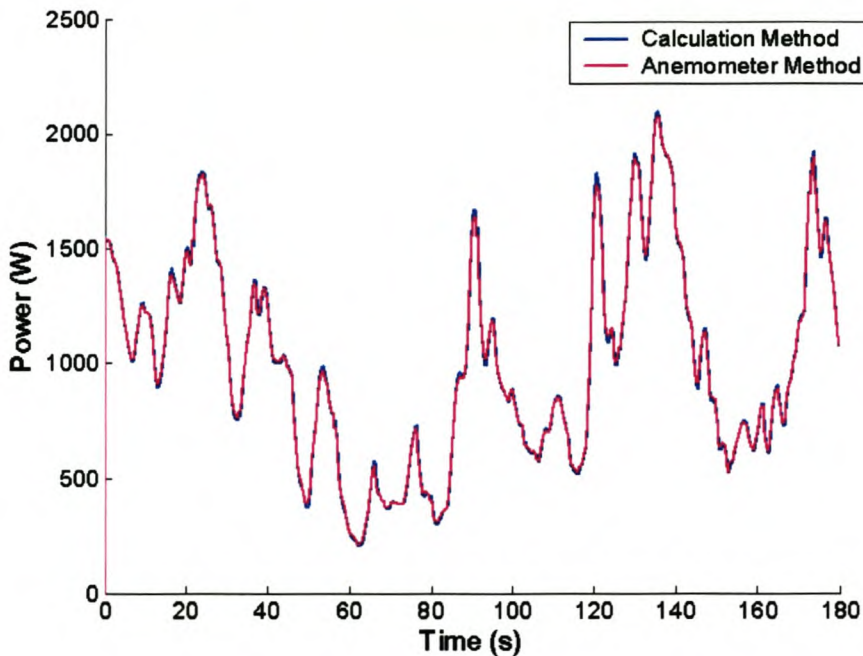


**Figure 5.9 Anemometer method versus calculation method**

The difference is nominal and the average power produced by the algorithms is presented in Table 5.2. The output power difference between the calculation and anemometer methods over time is plotted in Figure 5.10. The sum of the power difference over the time period is positive indicating the superiority of the calculation method.

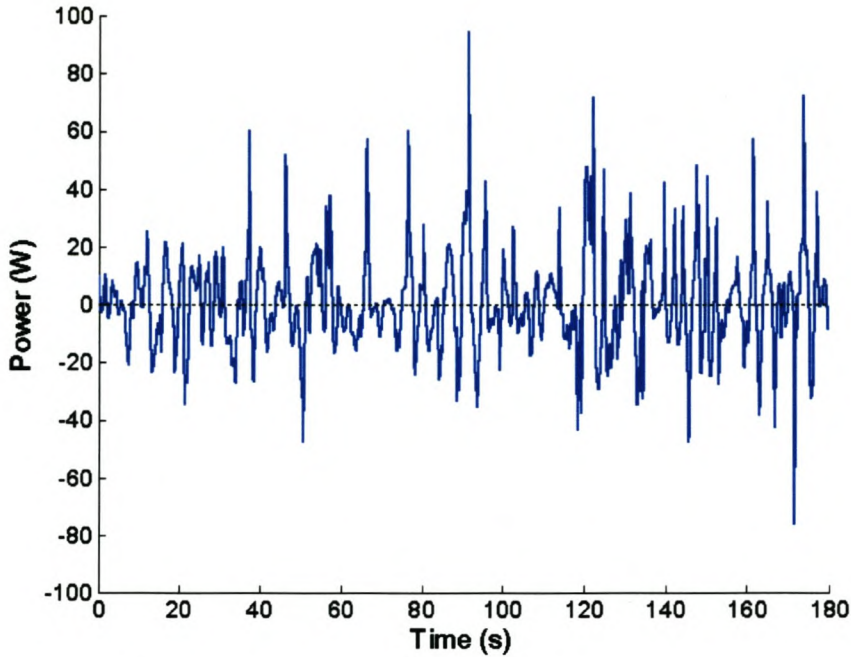


**Figure 5.10 Power difference between the calculation and anemometer methods**

Figure 5.11 shows the difference between the calculated wind speed and the actual wind speed. The slight difference can be contributed to the inertia of the mechanical system as discussed.

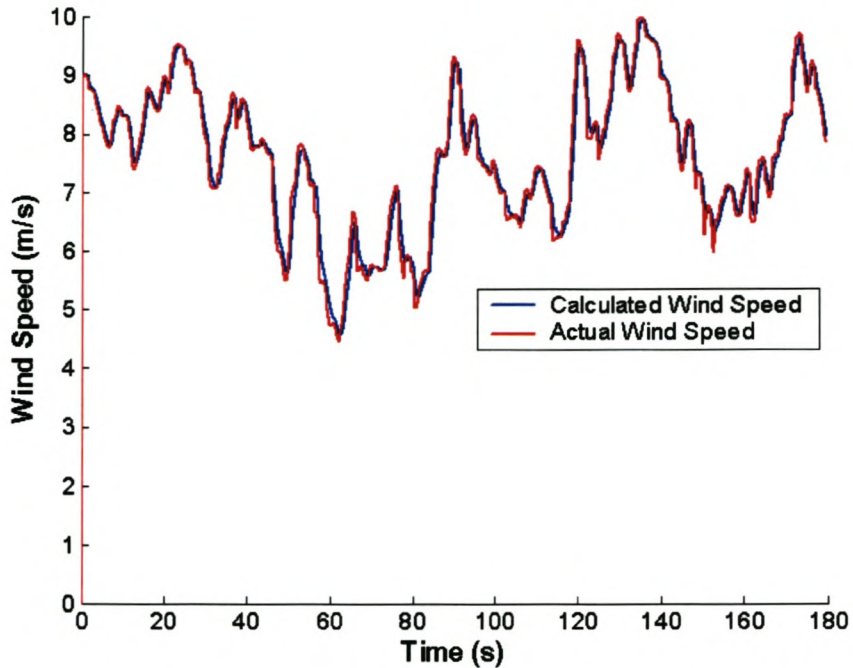


**Figure 5.11** Calculated wind speed versus real wind speed

### 5.2.3 Constant step method result

The constant step algorithm is not able to track the instantaneous change in wind speed thus the tracker was given a ‘head start’ in the simulation to enable it to start in the correct region of operation and not from zero, as would be the case in a practical situation. The algorithm was initialised with the optimal loading for approximately 6 m/s.

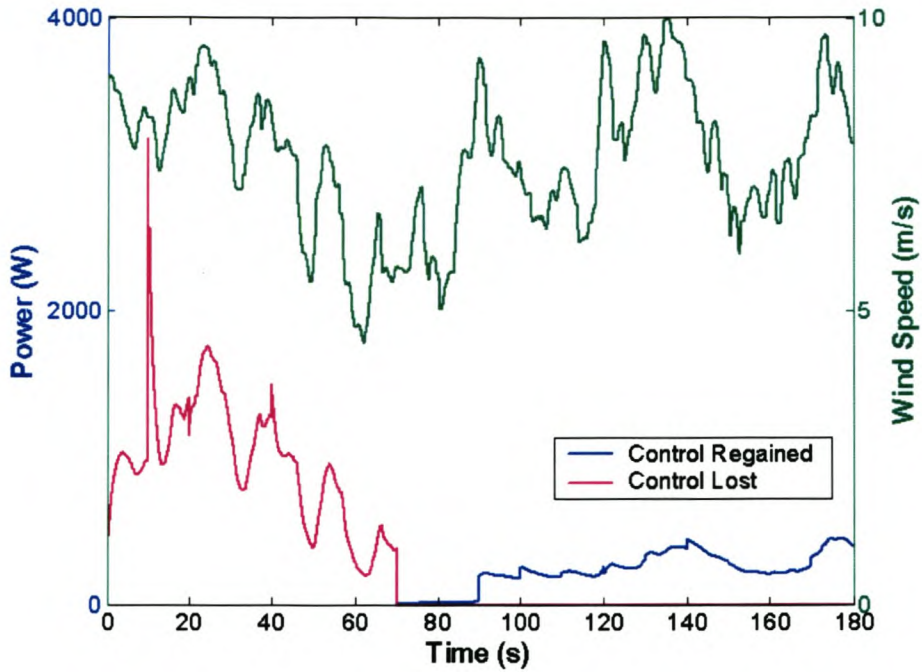


**Figure 5.12 Constant step control- lost & regained control**

Figure 5.12 represents two simulations. The ‘Control Lost’ trace is the result of the basic constant step algorithm with no protective measure for the scenario where the system runs into the unstable region. This scenario was discussed in section 4.2.1.1 where the position of the operating point meant that the decline in wind speed moved the operating point into the unstable region. As can be seen in Figure 5.12, the system loses control at approximately 70 s and never recovers. The ‘Control Regained’ trace is the system with the protective measure incorporated. After the system lost control, the protective system was enabled and the control was slowly recovered. Figure 5.13 shows the requested current for the two systems.

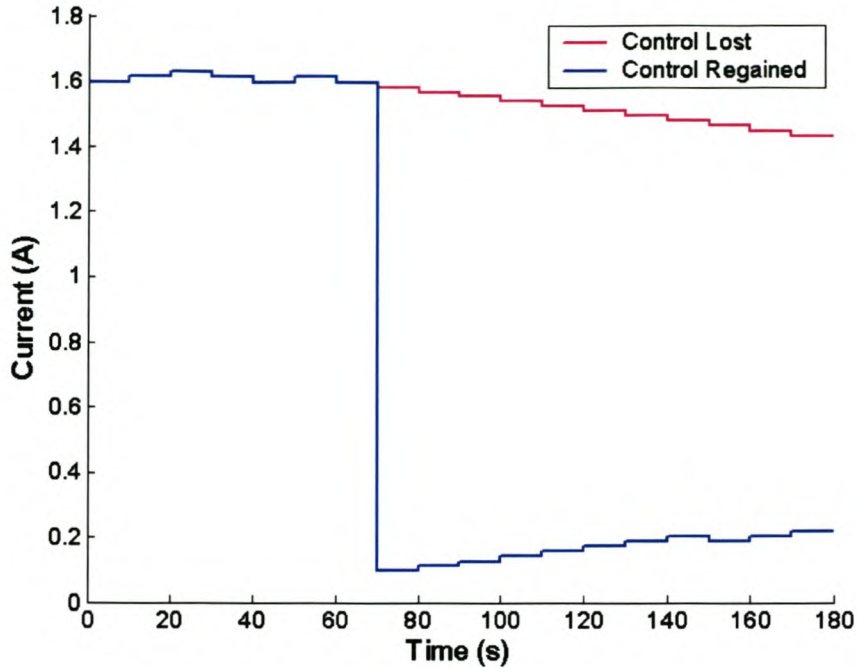


**Figure 5.13 Lost & regained control comparison of current reference**

Once the system loses control, the load is almost completely removed in order to allow the wind turbine to build up speed and then the algorithm slowly begins tracking the optimal power point once again.

#### 5.2.4 Measured results to random wind

The average power produced for each method simulated is tabulated in Table 5.2.

**Table 5.2 Average simulated power production**

Method used	Average power produced (W)
Anemometer	996.95
Calculation	997.57
Constant step (Lost Control)	373.69
Constant step (Regained Control)	513.36

As can be seen from the results, the constant step method does not perform satisfactorily. The anemometer and calculation methods show very good and very similar results, with the

calculation method performing slightly better than the anemometer method under these ideal, theoretical conditions.

### **5.3 Summary**

As can be seen from simulations, the constant step method of tracking does not work very well. The inability of the tracker to react fast enough leads to it lagging the available power to such an extent that during large drop in wind speed, the operating point falls into the unstable region of operation. Even with the protective measure incorporated, the power that the constant step method is able to produce is significantly lower than the power produced by the other two methods. Thus from the results seen in the simulations, the constant step method of tracking presented is not a viable option of tracking for a wind turbine.

The anemometer method of tracking worked very well. The trace describing the maximum available power was very similar to the resultant output power of the tracker. The slight discrepancy between the two traces has been contributed to the effect of the inertia of the system and is expected and acceptable. The perceived disadvantage with this method is that inaccuracies in the initial determination of the equation or look-up table would result in the system being permanently slightly inefficient. This is not a serious problem as discussed in section 4.2.2.1, as there is a relatively broad region in the power profiles where the power production loss is minimal.

The calculation method is favoured due to the attractiveness of it to small-scale systems and it has proved to be the pre-eminent method proposed from the simulation results. Not only does this method of tracking remove the need of an expensive anemometer, but it also shows an increase in produced power under these ideal, theoretical conditions. The disadvantage of this method is that it introduces more opportunity for error in the practical system measurements and initial setup of the system parameters needed in the wind speed calculation. As discussed in section 4.2.2.1, this is not a serious problem and fine-tuning of the calculation system would reduce the severity of this.

In order to try and implement these tracking methods on a realistic system, an analog wind turbine simulator is developed. Details of the practical system are presented in the following chapter.

## Chapter 6. Development of an Analog Wind Turbine Simulator

The algorithms proposed and computer simulated in Simplorer™ were then tested on an analog model in order for the system that was simulated to be verified. This system provided a realistic model of what was to be expected from a wind turbine and an active rectifier. This system was modelled around the actual wind turbine and the process, from the different wind speeds striking the blades to the DC current produced, was simulated. Figure 6.1 below shows the setup used. The analog model that was used consisted of two sections- a wind turbine section and a converter section.

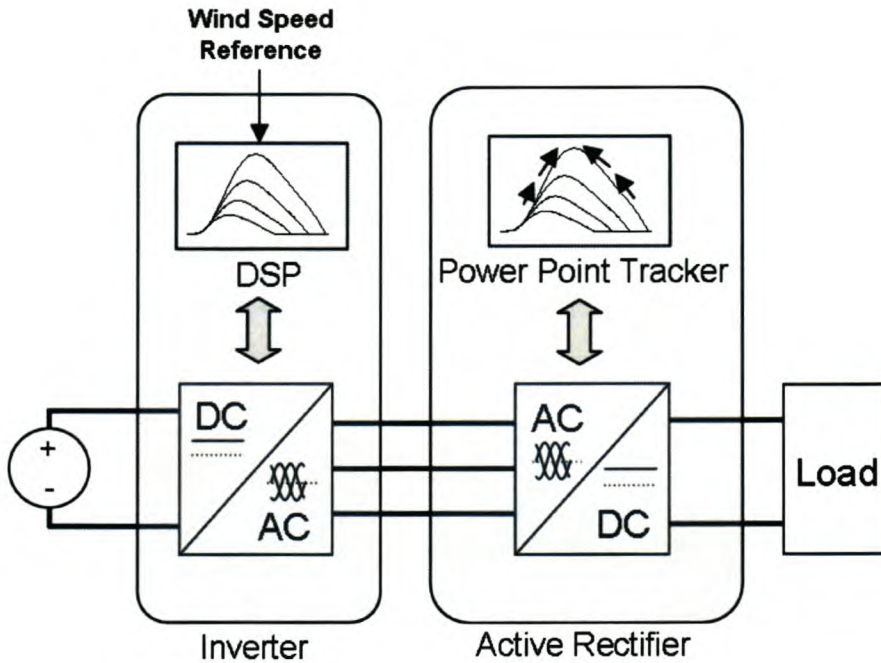


**Figure 6.1 Analog system setup**

An inverter, which switches the inputted DC to a 3-phase output, was used to electrically simulate the wind turbine so that it provided the electrical characteristics at its output, as was to be expected at the terminals of an ideal wind turbine. The effect of the internal impedances of the generator was ignored in the model due to its small effect on the overall system. This meant that the inverter was programmed to react to the loading on itself and respond to different wind speeds provided to it, as an ideal wind turbine would in the field.

Due to electrical constraints, the exact ranges of electrical characteristics expected from the wind turbine were not able to be implemented on the inverter and so the characteristics were scaled

down to accommodate for these limitations. The power characteristics were nonetheless still maintained, but the voltage and current parameters were altered. This inverter is thus a complete model of the wind turbine with the same power responses as would be produced by a wind turbine in the field.

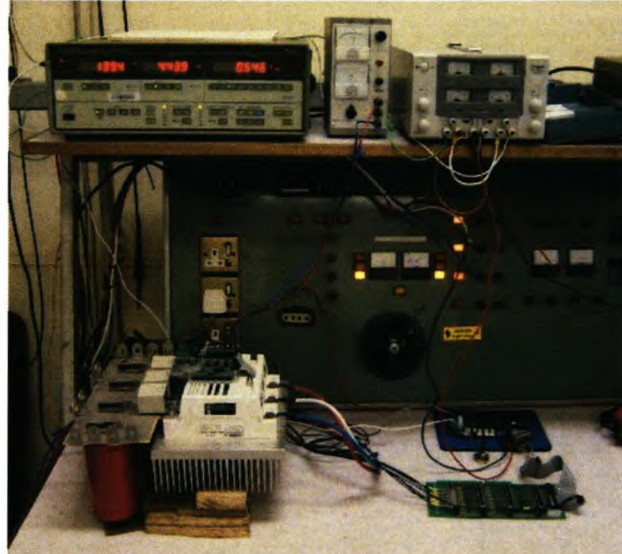


**Figure 6.2 Inverter**

The converter is the system by which the loading can be regulated. This converter was operated as an active rectifier which switches the 3-phase waveforms inputted to a DC output. The waveforms inputted to the active rectifier are evaluated and the present power point tracking method is used to alter the power flow.

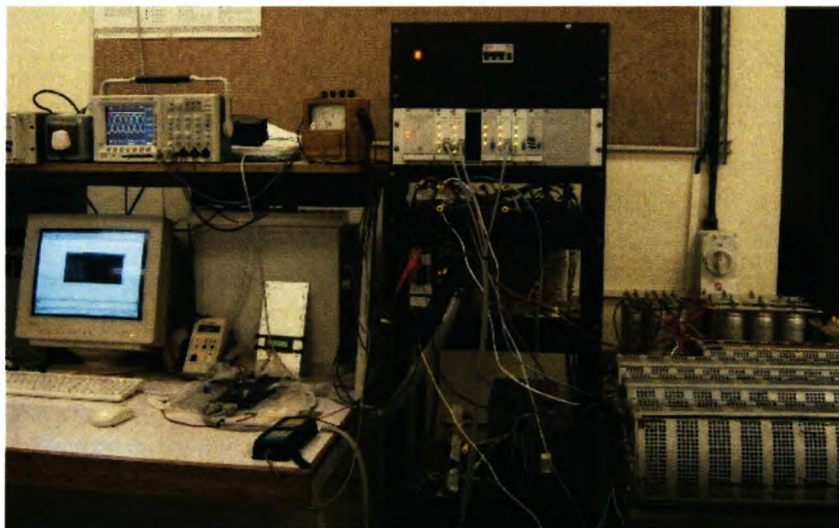


**Figure 6.3 Converter**

## **6.1 The Inverter**

The implemented inverter uses a full bridge topology implemented by a Semikron SKIIP 202 GD 061-357CTV module. The controller is a fixed point, Texas Instruments TMS320LF2407A and has a clock speed of 40 MHz and a switching frequency of 5 kHz. This DSP has the feature to enable it to directly generate the required switching signals for the semiconductor switches.

As simulated in Simplorer™, two input parameters are needed for operation, namely the present wind speed and the external loading on the system. The wind speed was predetermined and loaded into a look-up table in the DSP. Measuring the power flow out of the inverters three phases is costly and complex so the DC voltage and current into the inverter was measured.

As explained in section 3.1.2, acceleration on the wind turbines shaft is result of a difference between the torque provided by the blades and the counter torque developed by the generators windings. This acceleration is also a function of the inertia of the shaft, and is integrated to obtain a value of the rotors angular velocity or rotor speed. The amplitude and frequency of the outputted voltage of the wind turbine system is a function of the rotor speed, which is also used for the blades torque characteristics.

### **6.1.1 Inverter programming structure**

The DSP controlling the inverter was responsible for the implementation of the wind turbine characteristics. The program for this was important as the response of the inverter had to be as close as possible to the practical wind turbine.

The inverter's modulation index was linked to the frequency of the output waveforms, thus ensuring a linear relationship between the frequency and the voltage amplitude produced, as expected from the rotating machine. The modulation index was also used to limit the available output amplitude after a certain input voltage was reached. The input voltage had to be kept above this value to ensure accurate representation of the wind turbine.

The required frequency of the output waveforms is obtained from discrete integration of a torque difference multiplied by a constant. The constant represents the effect of inertia and of the sampling period of the integration and the torque difference is difference between the electrical and mechanical torque.

The electrical torque is calculated by the measured electrical power divided by the angular rotational velocity of the output waveforms. The electrical power is a product of the measured DC bus voltage that is measured using the onboard voltage measurement feature, and the

measured current flowing into the DC bus. This current measurement is measured by a Hall-Effect current sensor on the input terminals to the DC bus.

The mechanical torque is the torque that the wind turbine blades produce and is a function of the wind speed and the angular velocity of the machine. The torque profile is obtained from the wind speed under investigation. This wind speed is either pre-programmed using a look-up table or externally controlled via the user. The wind speeds that did not exactly correlate to a specific torque resulted in the torque curve being interpolated between two neighbouring curves. The exact mechanical torque value is then obtained at a specific angular velocity.

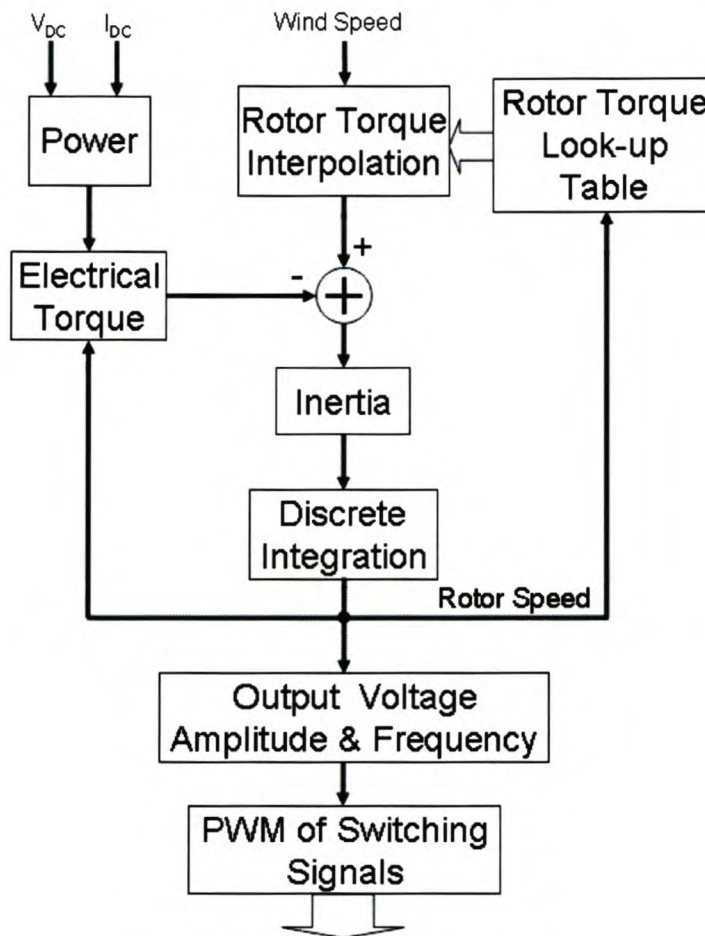


**Figure 6.4 Inverter programming flow chart**

### 6.1.2 Low-pass filter

A LC filter was included at the output of the inverter to remove the undesired harmonics from the 5 kHz switching frequency. An LC filter circuit diagram is displayed in Figure 6.5 below.

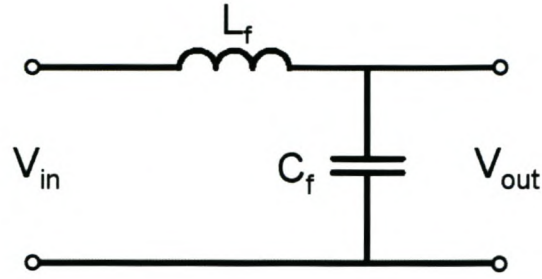


**Figure 6.5 Filter**

The Laplace transformation of this filter is [31]:

$$V_{out} = V_{in} \left( \frac{sL_f}{sL_f + \frac{1}{sC_f}} \right) \quad (6.1)$$

Simplifying (6.1) leads to:

$$\frac{V_{out}}{V_{in}} = \frac{1}{1 + s^2 L_f C_f} \quad (6.2)$$

The cut-off frequency is defined as follows:

$$\omega_c = \sqrt{\frac{1}{L_f C_f}} \quad (6.3)$$

The size of inductor  $L_f$  is  $200 \mu\text{H}$  and the capacitor  $C_f$  is  $350 \mu\text{F}$ . From (6.3), the cut-off frequency of this low pass filter is  $3780 \text{ rad/s}$  which corresponds to  $602 \text{ Hz}$ . This is above the maximum limited frequency of  $160 \text{ Hz}$  deliverable by the inverter and well below the switching frequency of  $5 \text{ kHz}$ , thus the desired signal will pass through to the load and the effects of the switching will be eliminated. A bode plot of the practical filter is represented in Figure 6.6.

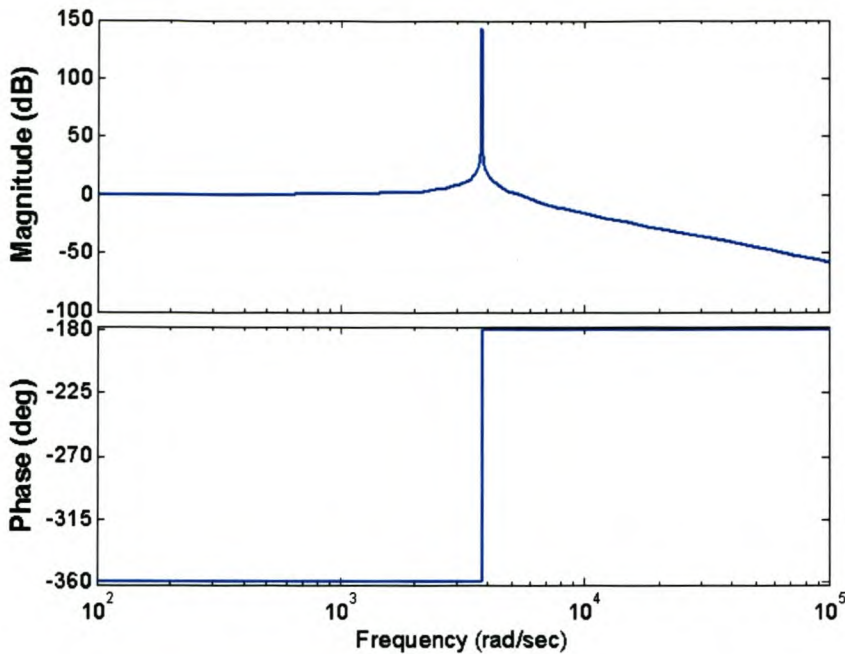


**Figure 6.6 Bode plot of the filter used**

From Figure 6.6, it can be seen that the phase of the output is undisturbed at the desired frequencies and the higher frequency components are removed.

## 6.2 The Active Rectifier

The active rectifier is the section in which the power point tracking is achieved. The different algorithms are programmed into its controller and the required loading is calculated and then executed by controlling the switching of the rectifier. The outputted DC is applied over a resistive load for the purposes of these tests but is used to charge batteries and supply different loads in the practical implementation.

The rectifier was adapted from an existing converter used for educational purposes [32]. This training tool includes a standard 6-pulse converter with three Semikron SKM 200GB 122D IGBT modules. The DC bus has six 450 V, 3.3 mF capacitors across it. The total capacity of this capacitor bank is 9.9mF and it is rated up to 900 V. This rectifier was not built for the purpose of the required conditions and so some functionalities were not optimal, but overall, the rectifier proved the validity of the different tracking algorithms.

The PEC31 Digital Signal Processor was used to control the switching signals for the rectifier. It uses a TMS 320C31 Texas Instruments processor. This 32-bit digital signal processor is a floating-point processor and can perform 40 MFLOPS. The board also has onboard analog to

digital converters. The PEC31 has its own pulse width modulation feature that enables switching of semiconductor switches. The reference signal is simply inputted to a Field Programmable Gate Array (FPGA) and the FPGA controls the top and bottom switching signals and includes the pre-determined dead time.

The current and voltage measurements were performed by the PEC31 Measurement System. The current and voltage of each phase is measured and the DC bus voltage on the output is also measured. The gains of the various measurements are set on the measurement system and the outputs are then applied to the analog to digital converters onboard the PEC31.

### 6.2.1 Active rectifier programming structure

The main program to determine the switching signals is run at 10 kHz and begins with the current and voltages measurements of the three phases and the DC bus voltage measurement. The  $\alpha\beta$  transformation is used on the voltage signals and also on the current signals to acquire representation of the three signals, which is easier to evaluate. The system is assumed to be balanced and so the  $\alpha\beta$  plane can be visualised as a dimension in which the three balanced signals can be represented by a single vector  $\Lambda$ , rotating around the  $\alpha$  and  $\beta$ -axis' origin, where the length of the vector is a linear function of the signals' amplitudes and the angular velocity of the vector is the angular velocity of the signal under investigation. The transformation provides an alpha and beta axis component. This length of this vector can then be determined by means of Pythagoras' Theorem.

$$|\Lambda| = \sqrt{\Lambda_{\alpha}^2 + \Lambda_{\beta}^2} \quad (6.4)$$

Thus if the amplitudes of the signals were constant, the length of the vector would remain constant and the vector would trace a perfect circle around the origin.

The vector lengths of the transformations are calculated and filtered slightly to remove the high frequency noise accumulated from the measurement systems. The instantaneous reactive power theory defined by [33] stipulates the following:

$$P = V \cdot I \quad (6.5)$$

Or,

$$P = v_{\alpha} i_{\alpha} + v_{\beta} i_{\beta} \quad (6.6)$$

As the voltage and current vectors are in-phase with each other, the voltage transformation's vector length and the current transformation's vector length can simply be multiplied together to acquire the inputted power which is used in the various algorithms examined.

The angular velocity of the sinusoidal signals inputted is represented by the angular velocity of the rotating vector. A simple method of determining the frequency of the voltage and current entering the rectifier is to measure the time taken for the rotating vector to complete a half cycle in the  $\alpha\beta$  plane and scale proportionally. A counter was implemented so that once the vector passed through the  $\beta$ -axis, the controller would not do multiple counts until the vector was considered to be out of the region around the  $\beta$ -axis. Once the vector is assumed to be out of the  $\beta$ -axis region, tests for the vector passing through the new  $\beta$ -axis commence. This becomes more complex because the frequency being measured varies between 0 Hz and 160 Hz (limited). The size used for evaluation of whether the vector is in the axis region is determined and the counter to ensure that the vector has left the axis region are both updated with regards to the speed and the proportional length of the rotating vector (faster and thus longer vector need a greater area in which to be evaluated as apposed to a slower vector).

Due to the desire for maximum efficiency, the controlled input current must be in-phase with the input voltage. This creates the need for three current reference signals. The simplest method is to use the input voltages as reference signals. This is achieved by scaling the  $dq$  representation of the measured voltages to unity by using the length of the vector and then transforming these values back to the  $abc$  plane, therefore creating three unitary signals synchronous with the input voltage.

Once the power point tracker algorithm for the method under consideration has calculated a required current, the unitary signals are scaled by this calculated reference current.

The current reference signals are then used as the input to an inner current control loop. This inner current control loop uses conventional predictive current control to realise the required current reference for the next sample.

The current value at the next sample that would be realised if no control was done on the system is obtained as follows:

$$i(t+1) = i(t) + \frac{\Delta t \times V_{DC}}{L} \quad (6.7)$$

where  $L$  represents the boost inductor on each phase which is required for the rectifier's operation. The change that must be implemented in the current signals to acquire the desired current reference at the next sample point is then calculated.

$$\Delta i(t+1) = i_{ref}(t+1) - i(t+1) \quad (6.8)$$

Using the current-voltage relationship of an inductor, the required voltage to realise the demanded current can then be calculated.

$$\begin{aligned} v &= L \frac{di}{dt} \\ \Rightarrow V_{ref}(t+1) &= L \frac{\Delta i(t+1)}{\Delta t} + v_{meas} \end{aligned} \quad (6.9)$$

The duty cycles required for this reference voltage are then calculated using zero state distribution and delivered to the FPGA.

The flow diagram in Figure 6.7 represents the basic structure involved with the rectifier's DSP program.

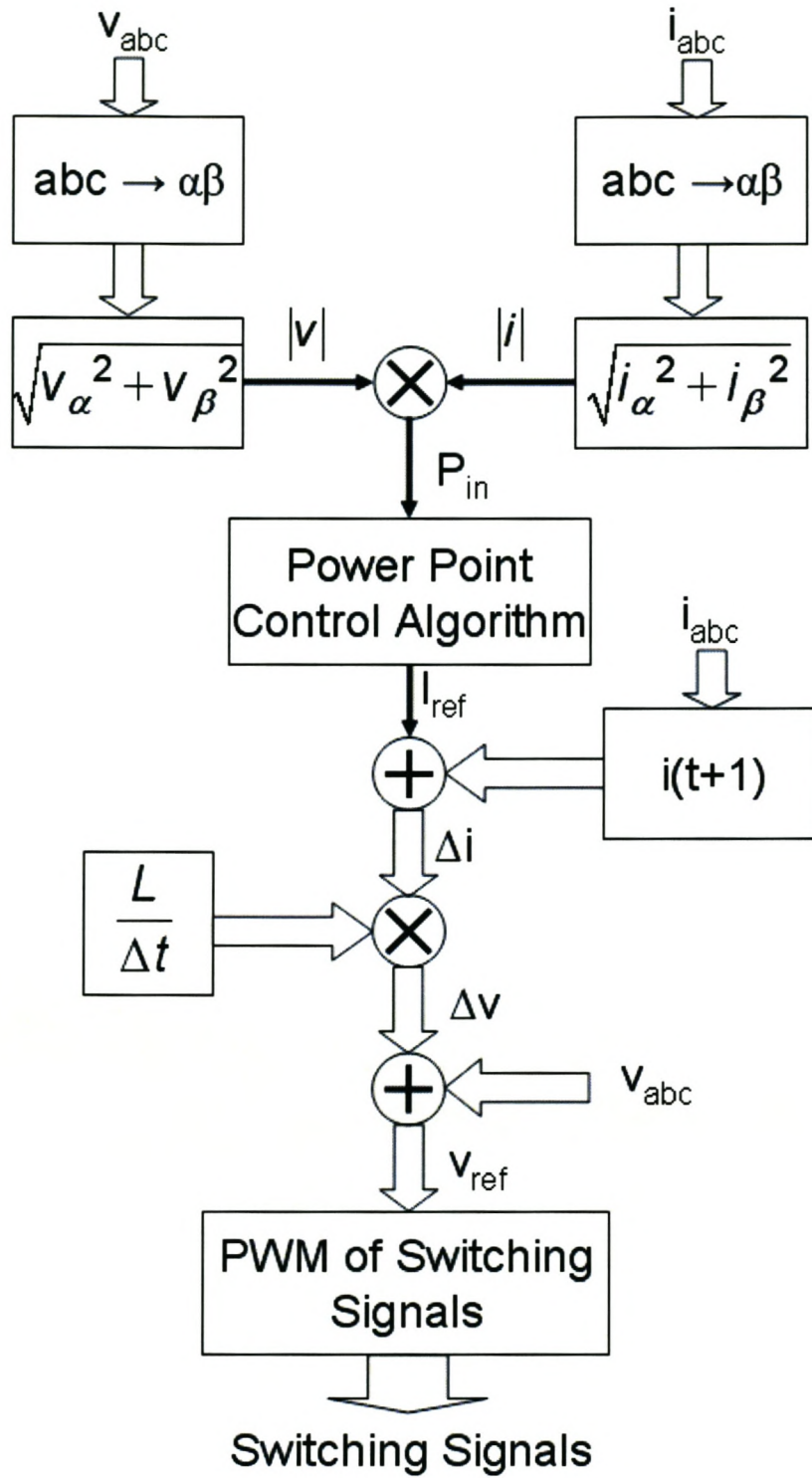


Figure 6.7 Rectifier programming flow chart

### 6.2.2 Equivalent active rectifier model

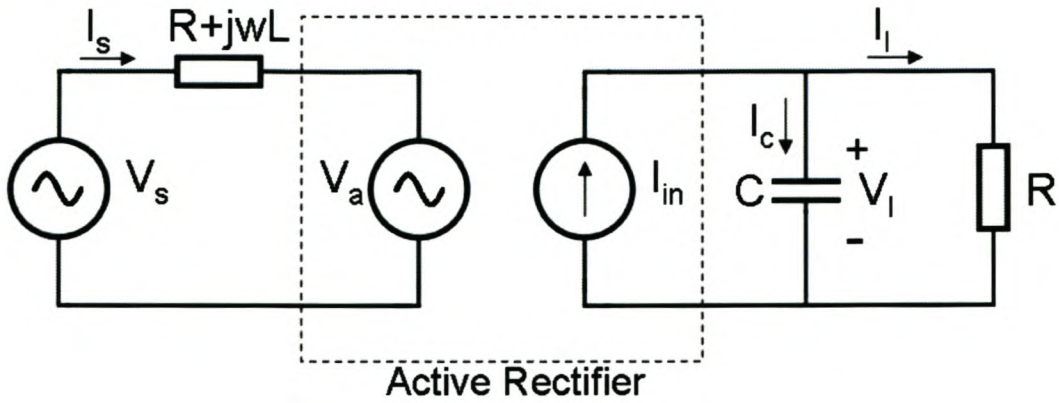


Figure 6.8 System equivalent circuit

The equivalent power circuit model of the basic AC to DC active rectifier is given by [34] and is displayed in Figure 6.8. The transfer function is given in (6.10) below.

$$\frac{V_l}{I_s} = \frac{3V_s}{V_{ref}} \frac{\frac{1}{C}}{s + \frac{1}{RC}} \quad (6.10)$$

A block diagram of the system can now be derived from (6.10) and is shown in Figure 6.9 below, where  $K_d = \frac{3V_s}{V_{ref}}$ .

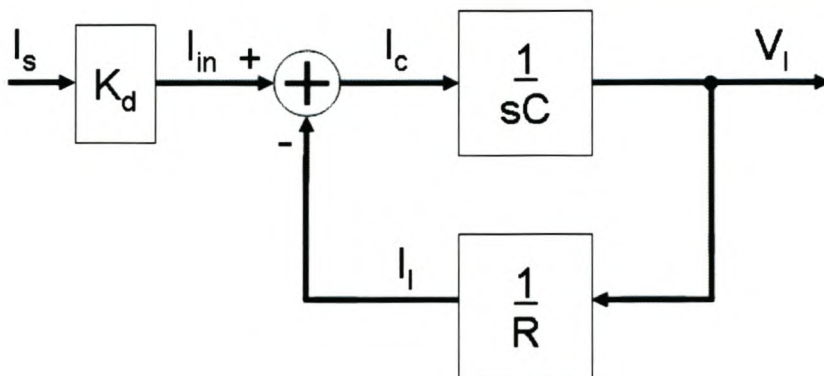


Figure 6.9 Active rectifier's dynamic model

### 6.2.3 Overall active rectifier description

The active rectifier can be seen as an active impedance on the source. By adjusting the voltage output from the active rectifier over a constant load, the power dissipated by the load can be

controlled. By considering the active rectifier to be ideal without any internal losses, the power produced by the source is controlled by the rectifier and equal to the power dissipated in the load. As explained in Chapter 4, the output characteristic of the source is determined by the loading on it.

Figure 4.14 below is a block diagram of the whole system under consideration.

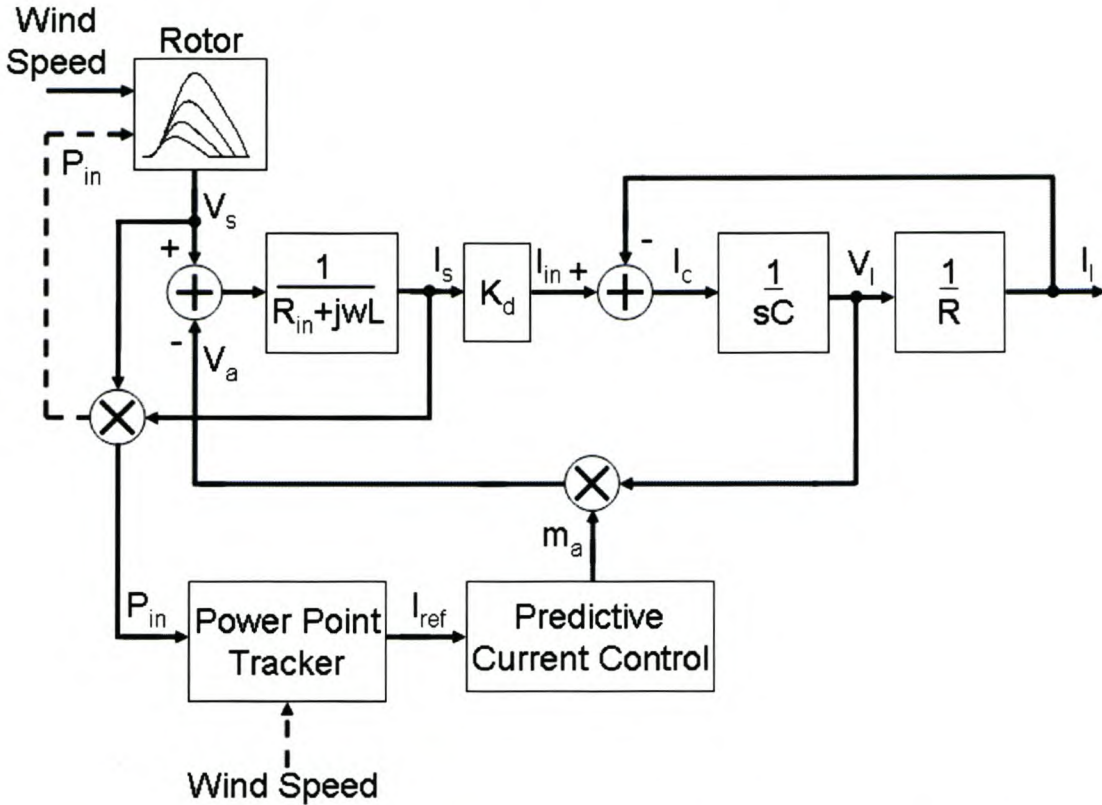


**Figure 6.10 Block diagram of the active rectifier with the wind turbine**

The wind turbine block has been simplified and involves its own block diagram as seen in Figure 4.14 with the produced power and wind speed as its inputs. The Power Point Tracker block is the system whereby the maximum power point trackers are introduced. The power entering the active rectifier is measured and analysed by this section and one of the trackers also includes a wind speed input. The result produced from the power point tracking block is a current reference signal and is processed by the predictive current control. The predictive current control regulates the modulation index which determines the switching signals of the active rectifier. The voltage source  $V_a$  is controlled by the modulation index  $m_a$  and the voltage over the load  $V_l$  by the relationship  $V_a = m_a V_l$ .

### 6.3 Initial Practical System Results

The system was implemented as explained above and simple tests were run to fine tune the different parameters. The inverter was set to deliver a response for a 5 m/s wind, then a 6 m/s wind and a 7 m/s wind speed. The active rectifier was programmed to constantly increase the loading on the inverter. The results of logged power delivered by the active rectifier are plotted in the figures below along with the power profile for that specific wind speed that was programmed into the inverter. The 'X' mark is the maximum power measured by the DSP controlling the active rectifier and the '\*' trace represents the measured power on the rectifier's DC bus at specific frequencies. The solid trace is the programmed blade power profiles.

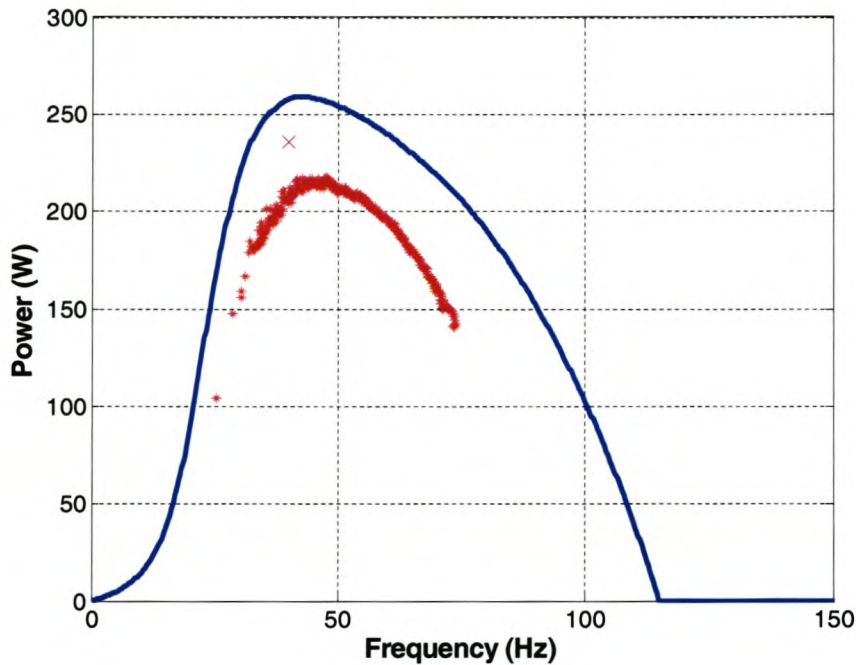
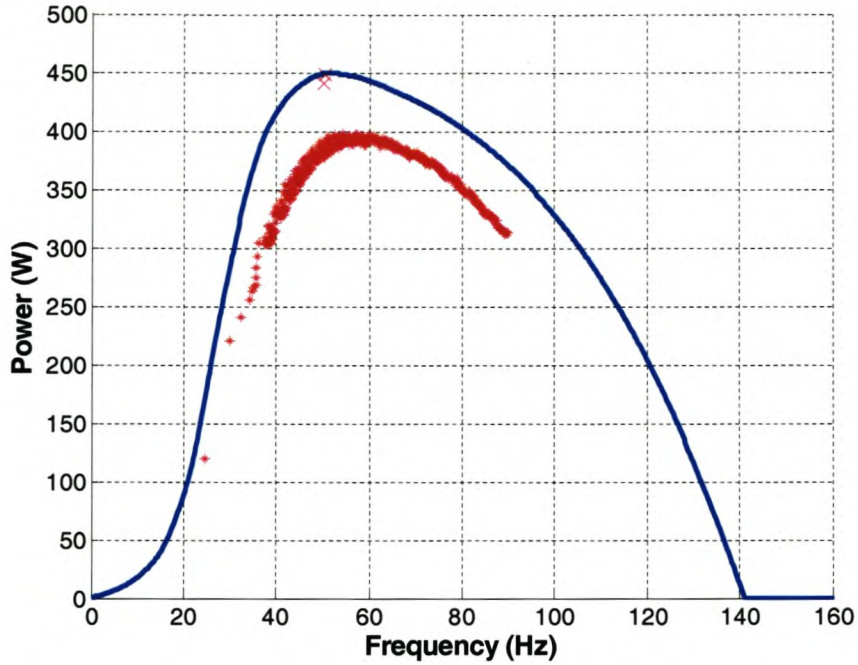
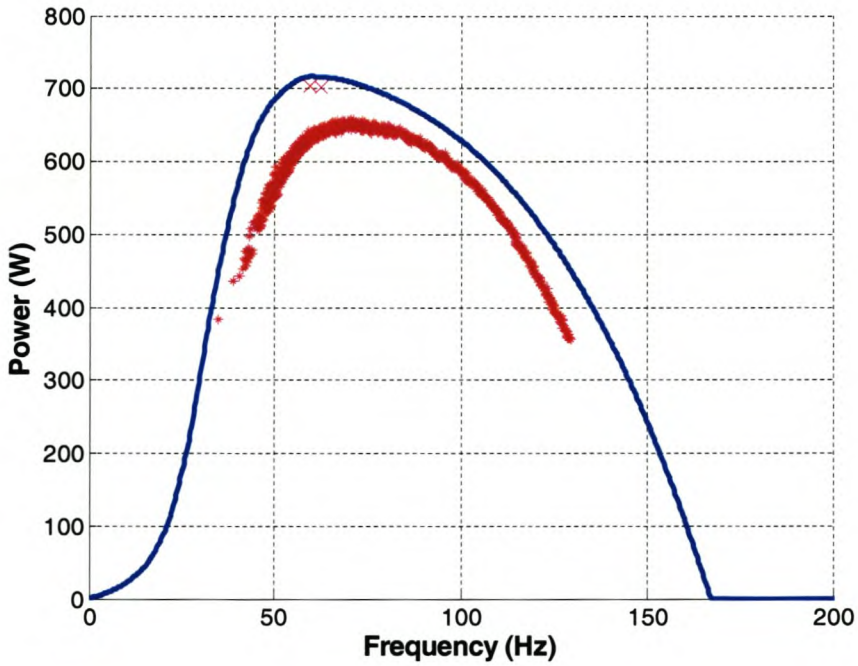


Figure 6.11 Measured and programmed power profiles for 5 m/s



**Figure 6.12 Measured and programmed power profiles for 6 m/s**



**Figure 6.13 Measured and programmed power profiles for 7 m/s**

From the figures above, it can be seen that there is a power difference between the measured output and the programmed input. This power difference is to be expected from the losses associated with the semi-conducting switches, both in the inverter and the active rectifier, and

the line losses between the inverter and active rectifier. There is a slight mismatch in the frequency range resulting in the measured profile being slightly off centre with regards to the programmed profile. This is a result of a measurement error in the inverter resulting in the frequency being calculated from the slightly incorrect power measurement. These measurement errors are to be expected and the power profiles used in the maximum power point tracking algorithms need to be tuned to compensate for them.

## **6.4 Summary**

The preferred manner to evaluate proposals for a system is to conduct tests on that specific system. Due to the complications of evaluation on an actual wind turbine such as the inconstancy of wind and the inability to reproduce the exact wind profile, an analog system was developed whereby the complete wind turbine system is replicated. The output signals generated by a wind turbine are simulated using an inverter controlled by a DSP loaded with the power profiles of a wind turbine rotor. The loading is achieved using an active rectifier as will be used on the practical system. From this analog system, it is possible to evaluate the proposed maximum power point tracking algorithms.

The simulated tracking methods results presented in Chapter 5 are compared to the analog simulated results in the following chapter.

## Chapter 7. Experimental Results

The algorithms and proposals made throughout this thesis were tested on the analog test system presented in Chapter 6. Measurements were made using Tektronix 3014B e\*Scope™ oscilloscope. Logging of the real time results over long periods was achieved between the RS232 TDS3VM Tektronix communication module in the oscilloscope and a personal computer. MATLAB® was used to communicate with the oscilloscope via the serial port and store the data returned by the oscilloscope. The specific data acquired was the values returned from the oscilloscopes ‘mean’ and ‘frequency’ measurement functions.

The power measurements were obtained by measuring the DC bus voltage and current produced by the active rectifier. The frequency measurements were taken from the input signals entering the active rectifier.

### 7.1 Practical System Parameters

The power profiles supplied by the blade designer and the number of poles and inertia used in the simulations were also used in the analog system. The effects of the internal losses of the simulated generator were disregarded for the analog system. The physical limitations of some of the components implemented in the analog system, lead to the voltage levels being scaled down, and a limiting factor being placed on the output frequency in the implementation of the source inverter. These changes do not affect the overall high level power simulations needed for the power point tracking evaluation. The machine parameters used in the analog system are tabulated in Table 7.1 below.

**Table 7.1 Analog system parameters**

<b>Parameter</b>	<b>Value</b>
Total inertia (J)	1.954 kgm <sup>2</sup>
Voltage constant (k <sub>e</sub> )	0.0746
Poles (p)	32

## 7.2 Equation Methods Results

### 7.2.1 Step Response Results

The step response of the wind speed from 5 m/s to 7 m/s was investigated. The results in Figure 7.1 and Figure 7.2 below are images captured from the oscilloscope for the anemometer method. Figure 7.1 is the systems response to a wind speed increase and Figure 7.2 is the systems response to a wind speed decrease. The red trace is the power calculated from the current and voltage traces.

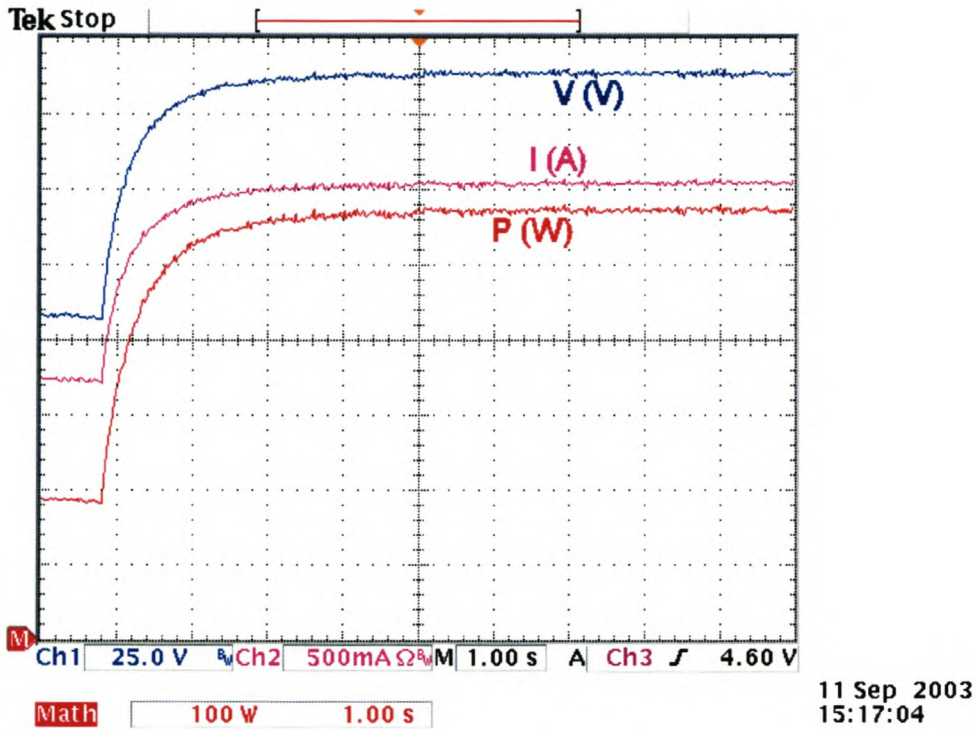
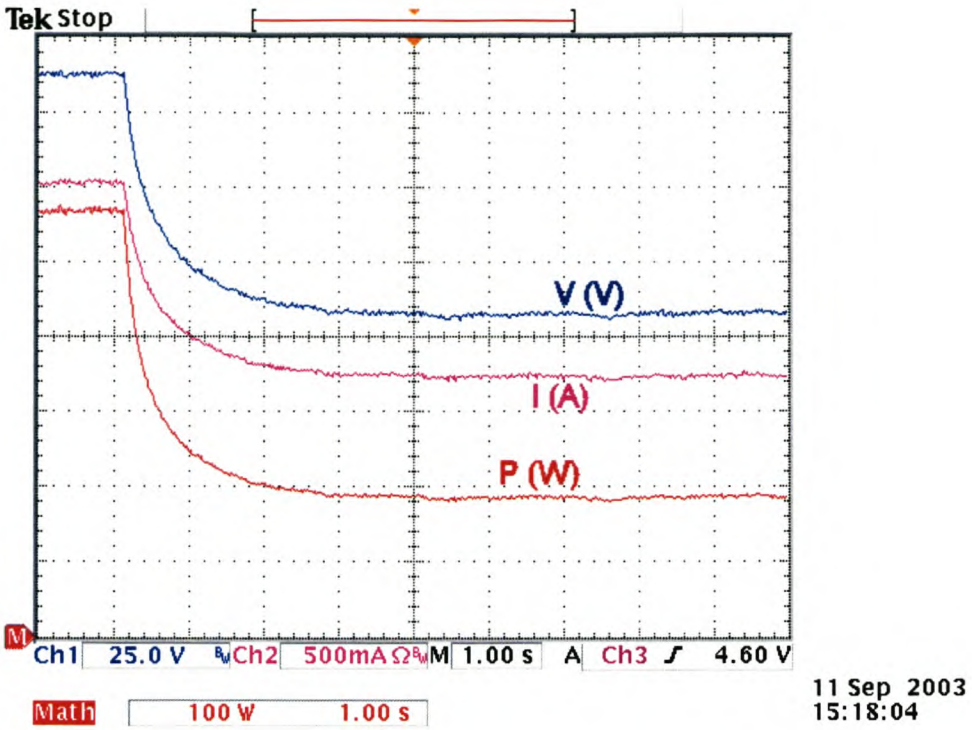
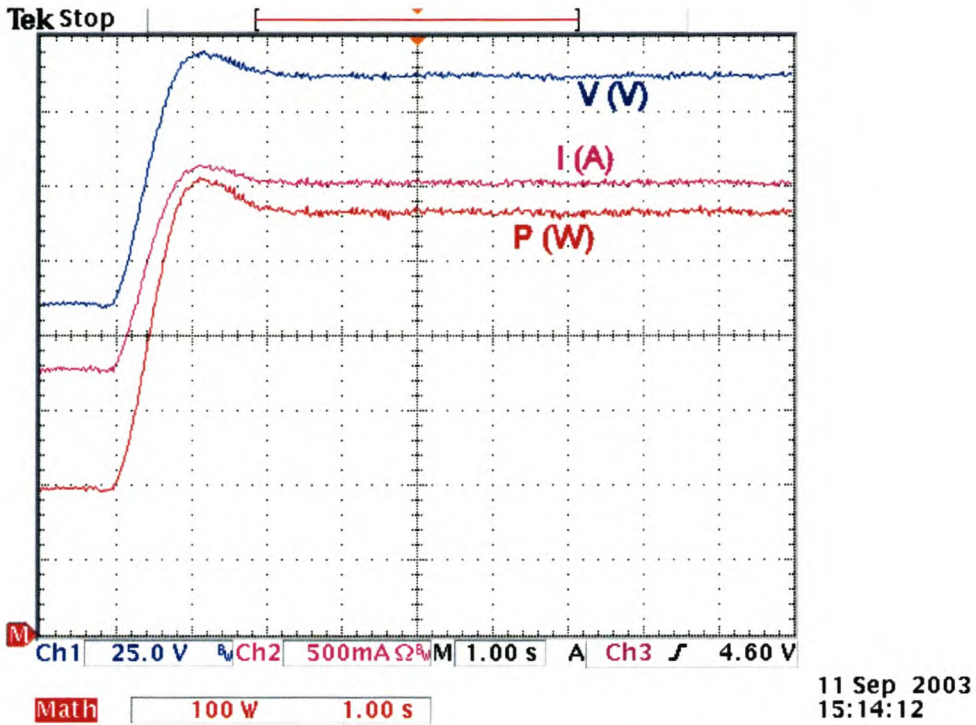


Figure 7.1 Anemometer method increasing step response



**Figure 7.2 Anemometer method decreasing step response**

Similarly to the previous figures, Figure 7.3 and Figure 7.4 are the system responses to input steps using the calculation method.



**Figure 7.3 Calculation method increasing step response**

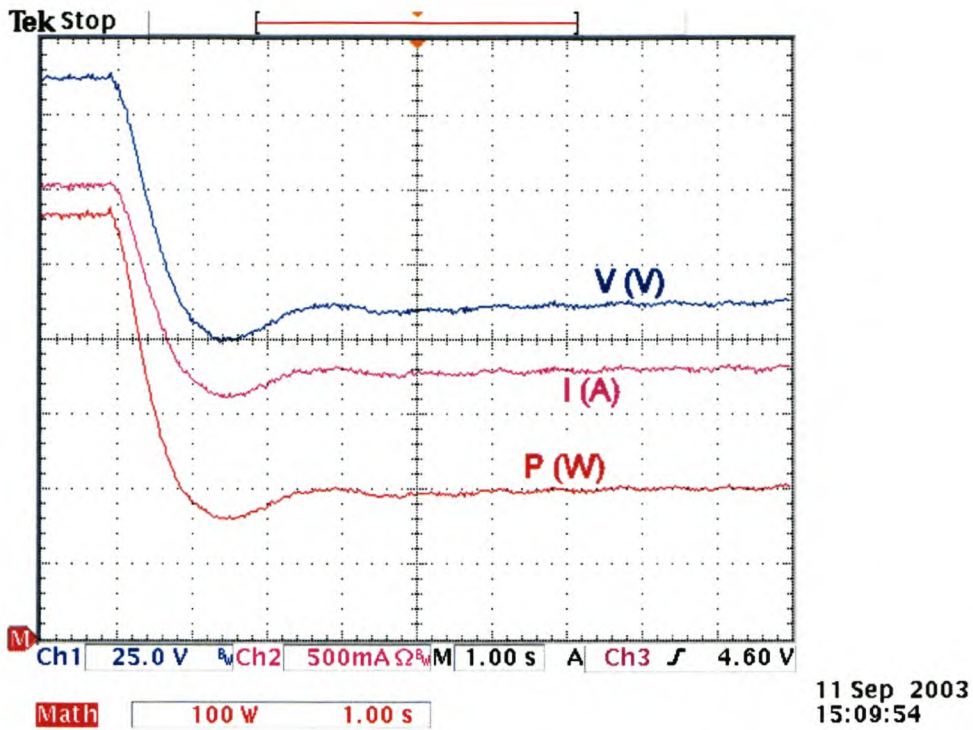


**Figure 7.4 Calculation method decreasing step response**

From the step responses in the figures above, it can be seen that the calculation method does have a faster response time than the anemometer method. The measured results of the settling times for the step responses are tabulated in Table 7.2. It must be kept in mind that the slight noise on the measured signals makes it impossible to find the precise settling times.

**Table 7.2 Settling times**

	Anemometer method		Calculation method	
	5%	2%	5%	2%
<b>Rising settling times (s)</b>	1.82 (2.309)	2.38 (3.019)	1.74 (1.805)	1.98 (2.270)
<b>Falling settling times (s)</b>	1.82 (2.499)	2.60 (3.449)	1.84 (1.909)	2.20 (2.584)

The values displayed in brackets are the simulated results found in Table 5.1. It can be seen from the results in Table 7.2 that the calculation method has an overall faster response but that the anemometer method has a faster response than originally simulated. This faster anemometer method's response time can be attributed to the reasoning proposed in section 5.1.1. The practical system is not an ideal system as simulated and the loading on the generator is unable to change instantaneously. The point 2 as seen in Figure 5.4 thus moves closer towards point 3. The

anemometer method's route taken to the new operating point as described in Figure 5.4 is thus shorter, and this can be seen by the faster response times.

### 7.2.2 Random Wind Results

The same random wind profile used in the simulations in Chapter 5 was implemented in the DSP on the active rectifier side and used to provide the wind speeds via its D/A to the inverter's A/D. The wind profile was generated in the active rectifier's DSP as it was easier to implement there and the wind speed was also required for the anemometer method. The generated wind speed value was however not used by the calculation method in any way.

The result from the anemometer method is shown in Figure 7.5 below. The instantaneous result of the maximum available power is superimposed onto the measured result to show the similarities.

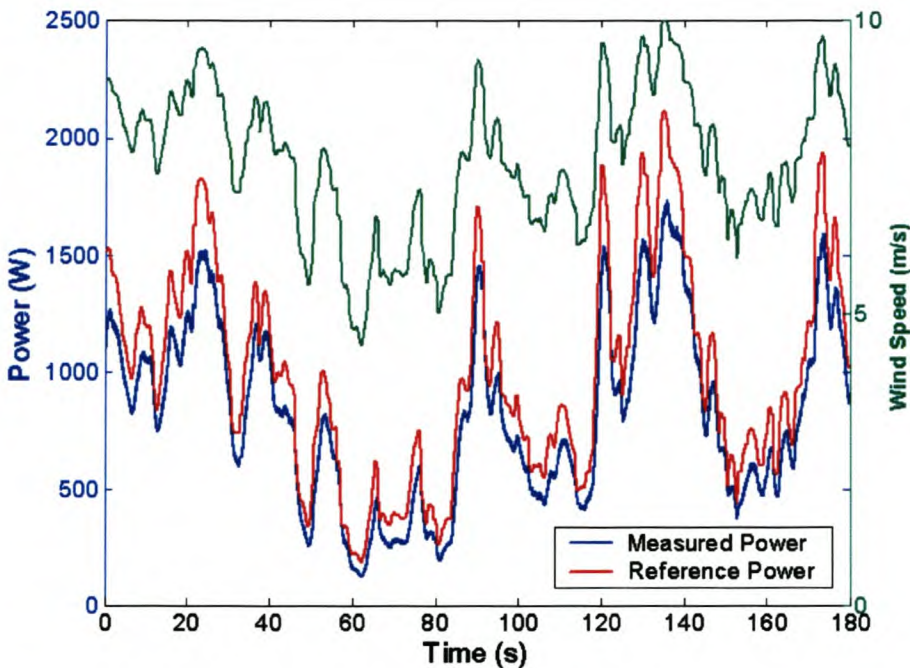


**Figure 7.5 Anemometer method**

The result of the calculation method using the same wind speed profile is shown in Figure 7.6 below. Once again, the power produced by the system is very similar to the maximum available power except for the slight difference, which can be attributed mostly to switching losses. The effects of the losses in the switches in the inverter and the active rectifier in the practical system have not been accounted for.

Also, allowance for slight discrepancies in the communication of the wind speeds between the two DSP's must be made. A slight error in the wind speed measurement was shown in section 2.2.1 to have a very large effect in the power production due to the cubic relationship between the power and wind speed. Thus, if the wind speed reference outputted to the inverter was slightly offset, the power offset would be quite noticeable.

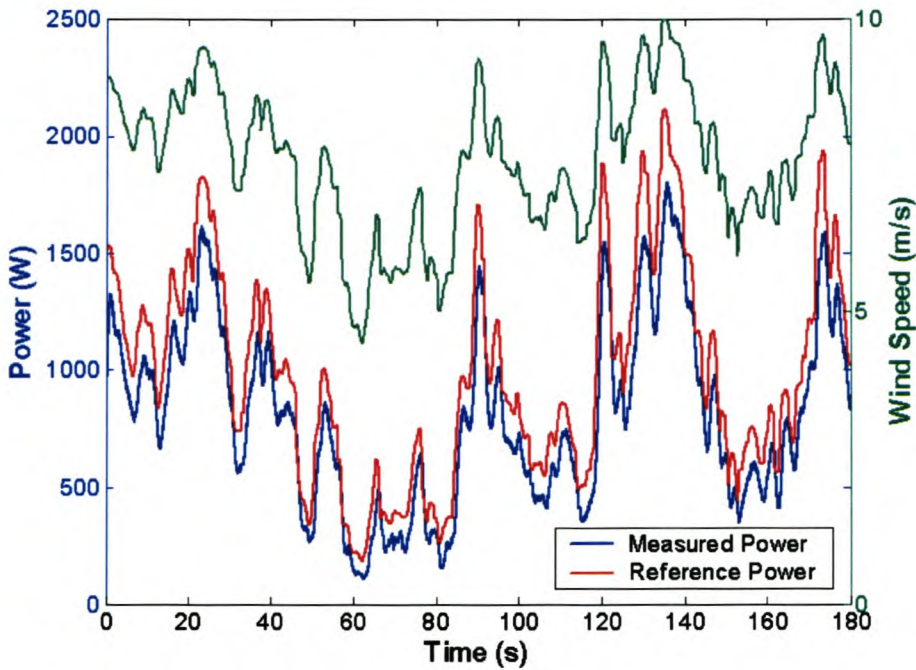


**Figure 7.6 Calculation method**

The anemometer and calculation methods are compared in Figure 7.7. As in the simulations, the results of the two methods are very similar. The difference between the practical results and the simulated results from Chapter 5, is that the practical results from the calculation method show it to produce a slightly less average power than the anemometer method which is contrary to the proclamation made in section 5.2.4.

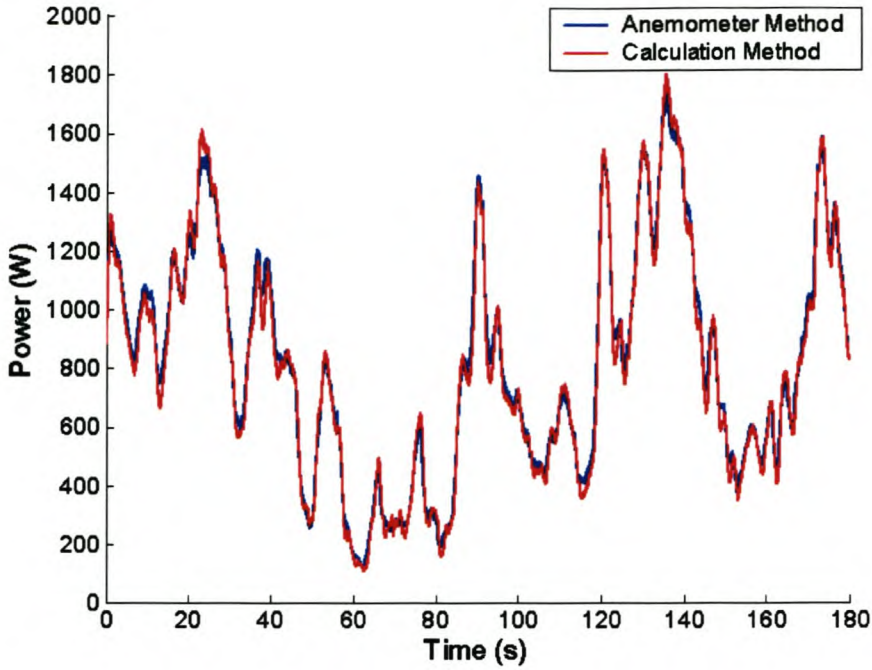


**Figure 7.7 Comparison of power from anemometer and calculation methods**

Figure 7.8 shows a comparison between the wind speed generated by the DSP and the wind speed calculated in the calculation method. The magenta trace displays the actual wind speed generated by the PEC31 and the green trace represents the calculated wind speed. As can be seen in the figure, there appears to be a constant error between the two results.

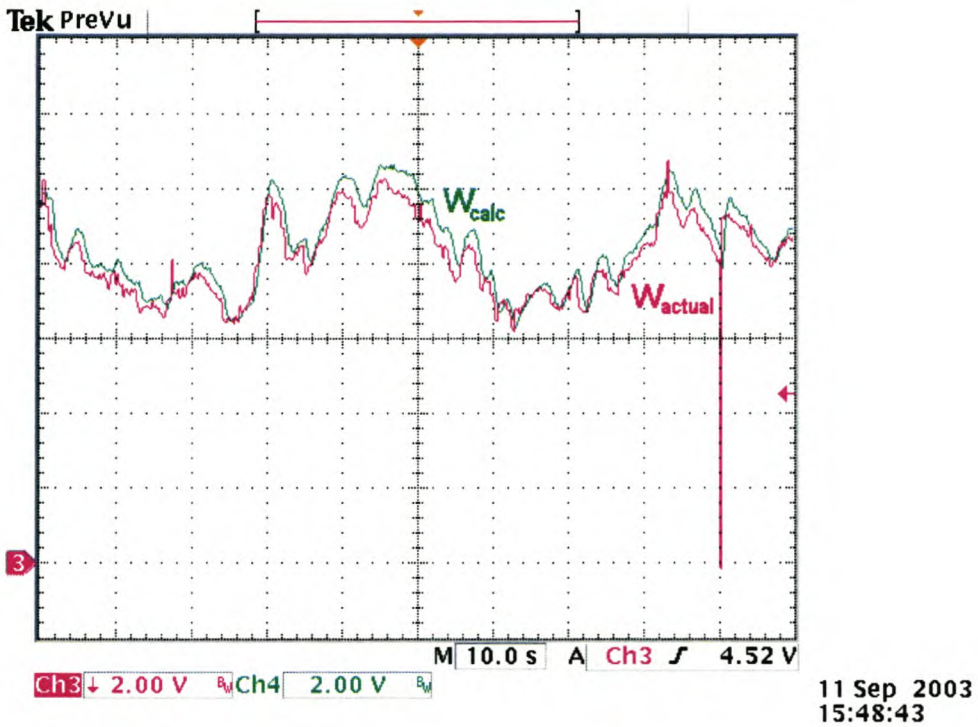


**Figure 7.8 Wind speed comparisons**

The offset error between the actual and calculated wind speeds was adjusted in the calculation method procedure and the analog system was rerun. The power produced was increased due to this adjustment and the results of all tested methods are tabulated in Table 7.3 below.

**Table 7.3 Average power production in the analog system**

<b>Method used</b>	<b>Average power (W)</b>
Anemometer	798.88
Calculation	789.56
Adjusted calculation	805.81

As can be seen from the results, once the calculation method was adjusted, it was superior as deduced in the simulations.

### **7.3 Constant Step Method Results**

In order to confirm that the constant step method is inappropriate for a wind turbine tracking method as discussed in Chapter 5, the constant step method was evaluated in the analog system. Figure 7.9 below represents the results from a random wind simulation where the red trace is the power measured and the pink trace is wind speed.

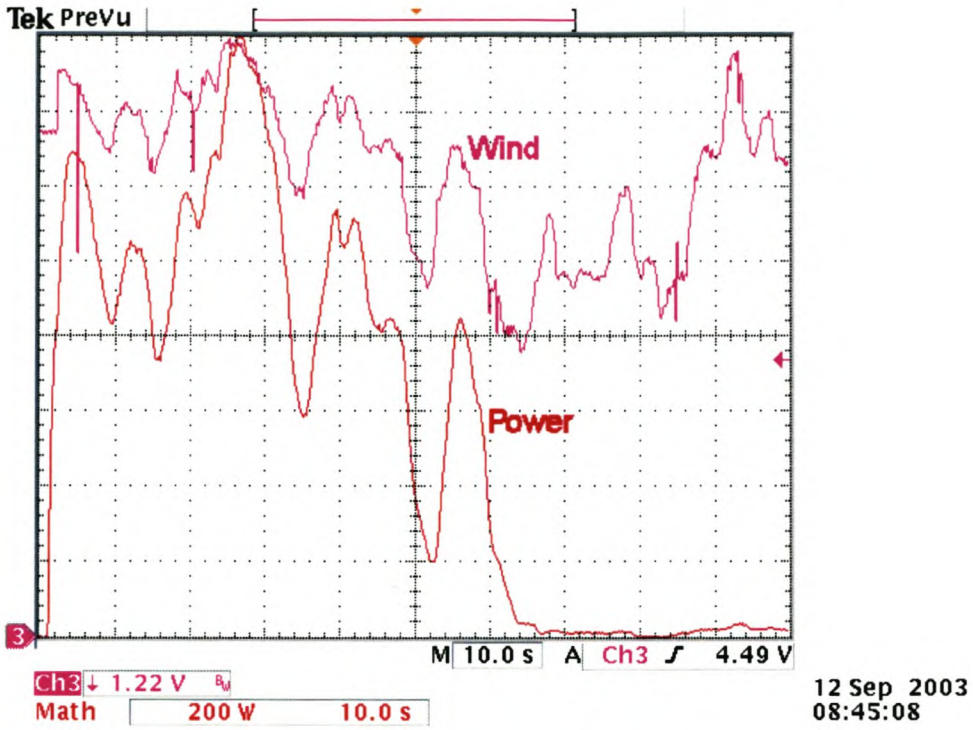


**Figure 7.9 Constant step result**

This result is very similar to the simulated response as seen in Figure 5.12. The simulated result is superimposed onto the measured result and displayed in Figure 7.10.

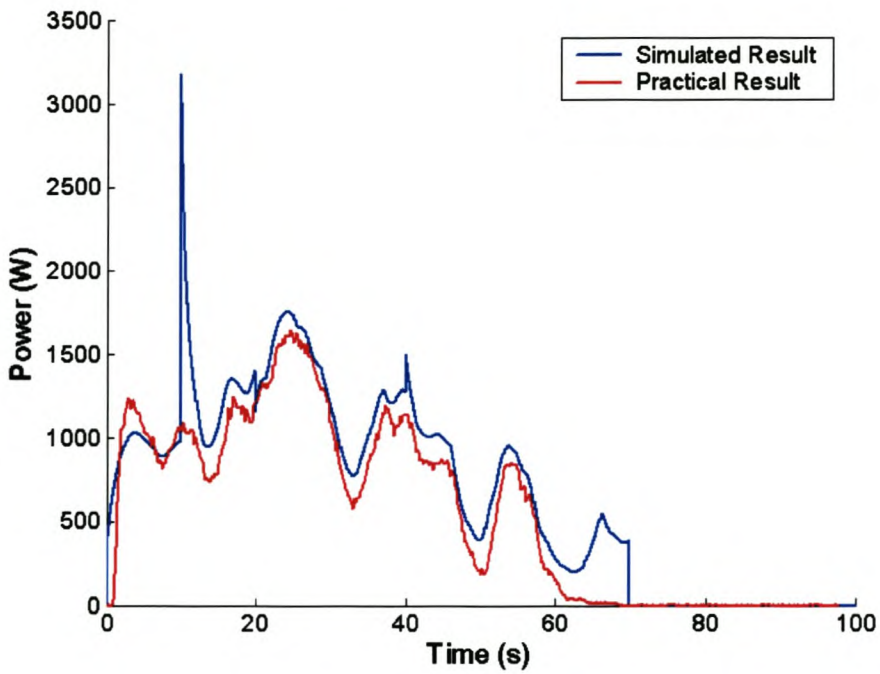


**Figure 7.10 Comparison of simulated and measured results**

It can be seen that the analog result loses control slightly earlier than the simulated result. This is due to the switching losses that were unaccounted for in the simulations, slightly altering the behaviour of the system.

## **7.4 Summary**

The results of the algorithms implemented in the analog system, confirmed the results seen in the simulations. The calculation method's settling times from the step responses, was very similar to the simulated result. The practical settling times of the anemometer method were slightly better than simulated due to the inability of the practical system to change the loading instantly as discussed in section 7.2.

The responses to the varying wind were also as expected. The results were in the same form as the simulations but for a power offset which can be attributed to switching losses and measurement error. The calculation method produced a slightly less than expected output power due to a minor offset in the wind speed calculation, but an adjustment made in the calculated wind speed corrected the output power to the expected result. Testing of the constant step method confirmed the inappropriateness of this proposed method for this application.

The authenticity of the analog system developed was validated by the similarities of the results to the simulated results.

## Chapter 8. Conclusions

### 8.1 System Conclusions

The aim of this project was to investigate methods to increase the efficiency of wind turbines for small-scale applications.

The first topic discussed was the physical placement of the wind turbine to utilize the effects of the surrounding terrain and topography for an increase in the expected wind speeds striking the wind turbine blades. Prudent understanding of the different effects of terrain and topography on the wind dynamics could result in a wind turbine experiencing twice as much wind speed at its blades. This leads to a potential eight times more power being produced by the wind turbine.

The accuracy and feasibility of using the available wind data to determine possible wind turbine site feasibility was discussed. It was concluded that an accurate anemometer at the proposed site is needed which can be correlated with neighbouring weather stations. This correlation could be used to get a more accurate indication of the expected wind. It was also shown that a higher resolution of sampled wind speed data is needed for the accurate calculation of expected power productivity of the wind turbine site.

Maximum power point trackers are methods whereby the electrical loading on the system is optimized to ensure a maximum power transfer from the available wind energy. Most small-scale wind turbines in operation do not incorporate any form of maximum power point tracker due to the additional cost of equipment and the general unawareness of them and the principals they employ. Three algorithms were proposed whereby the loading on the wind turbine could be controlled by the control of an active rectifier.

1. The *constant step* method is a widely renowned method for solar panels whereby the effect of a load change on the power output is analyzed to establish the new loading.
2. An *anemometer method* was discussed. The present wind speed is measured using an anemometer, and a predetermined optimal loading equation is used to adjust the loading accordingly.
3. A variation on the anemometer method entitled the *calculation method* was proposed, where the wind speed is calculated from the present system parameters. The anemometer method is then used to calculate the optimal loading for that calculated wind speed. The attraction of this method is that it removes the need for an expensive external

anemometer, but the disadvantage is that it introduces more opportunity for error in the system measurements. Initial setup of the system parameters is needed in the wind speed calculation and error here results in a permanent inefficiency. This disadvantage is not of great concern as the nature of the rotor's power profiles allows for a broad region of inaccuracy where the reduction of output power is minimal.

A better understanding of the wind turbine and the proposed system was obtained through simulation and experimentation of the system. An electro-mechanical model of the complete system was developed and the responses to load and wind speed changes were considered. It was discovered that the response time to a load change was very long which questioned the suitability of the constant step tracking method proposed for wind turbines.

A simulation model was created from the electro-mechanical model proposed in this thesis, in order to provide a means by which to assess the proposed algorithms. The simulated results from the constant step method were unsatisfactory, confirming the initial suspicion. The system's slow transient response meant that the tracker was unable to respond fast enough to wind variation. There was also a likelihood of the system becoming unstable and thus it is obvious that this proposed method is unsuited for use in wind turbines. The anemometer method however produced excellent results in the simulations and the power response was always very close to the maximum available power for the varying wind. The calculation method proved to be even better than the anemometer method; producing a slightly higher average power provided the correct offset was adjusted. It must be remembered that these results are from an ideal system where the exact system parameters are used.

The preferred method to evaluate the different proposed maximum power point tracking methods would be to use an actual wind turbine. This would prove difficult as the inconstancy of wind and the inability to reproduce the exact wind profile without an expensive, controlled wind tunnel. Thus an analog system was developed where the wind turbine was replicated by an inverter and an active rectifier, similar to the proposed one, was implemented for the loading. Minor enhancements on the analog system should have been made as described in section 8.2, but the overall system simulated an actual wind turbine very well for the purpose of the power point tracking algorithms evaluation.

The results from the analog system confirmed the results obtained in the computer simulations, though a slightly inferior result of the calculation method confirmed that incorrect modelling of the wind turbine system would result in a slightly lower efficiency. An adjustment made in the

calculated wind speed improved the average output power measured and it was once again superior to the anemometer method.

The analog simulation of the constant step method proved similar to the computer simulated result which confirmed that in a wind turbine system, it is an inappropriate power point tracking system.

The anemometer and calculation methods have shown to produce an output power close to the maximum available power. This leaves very little opportunity for improvement and so it can be assumed from the simulated results, that this method of tracking is almost ideal. The calculation method is slightly better than the anemometer method provided it is setup correctly, and it has the added advantage of no required anemometer. This is under exact modelling of the system and so a slightly less efficient system can be expected in practice.

The additional cost of an active rectifier and controller to the price of a wind turbine was not investigated for the purpose of thesis, but it is believed that the benefits gained from the additional power harvested will compensate for the extra cost.

## **8.2 Future Work**

### **8.2.1 Modifications on current system**

With regards to the analog model, a few improvements to the existing system can be made.

#### **8.2.1.1 Oscillation of the analog model**

A slight oscillation at a very low frequency (approximately 0.05 Hz) of the power produced by the inverter was noted during steady state operation. This slight oscillation did not affect the outcome of the algorithms tested and was insignificant to the operation of simulating a wind turbine. This oscillation could be explained by the lack of high resolution data manipulation ability in the fixed point processor. A floating point processor is thus proposed to replace the fixed point DSP in controlling the inverter.

#### **8.2.1.2 Switching losses**

The effect of the switching losses on the overall operation was not taken into account. This means that the characteristic power profiles of the wind turbine were not exactly correct at the output terminals of the inverter. Due to the incorrect power measurement being fed back to the measurement system, the lower wind speeds were not able to be tested on the analog system. This inability of the system to run these lower wind speeds was not imperative to the project as

the main aim of the analog system was to test the proposed maximum power point tracker algorithms. The algorithm's performances are not dependant on the wind speeds and success of these algorithms at the tested wind speeds imply the success at lower wind speeds as well.

In order to solve the problem of the switching losses in the inverter, the power measurement for the wind turbine simulation calculations should bypass the switches and be taken on the output of the inverter- not the input. This involves more measurements, as each phase voltage and current has to be measured, but the effect of switching losses on the system will be removed.

### **8.2.1.3 Test bed**

The effect of the losses in the electrical generator in the wind turbine process has not been investigated. Only the power profiles of the blades have been used to provide an insight into the expected signals on the output terminals of the wind turbine. The efficiency of the generator could be investigated separately and then included in the blade power profiles but the following solution would be better.

A test bed with the actual generator to be used should be constructed. This would provide an even more realistic model of the physical system to be implemented in the field. The inverter simulating the wind turbine could be used directly to control a machine to drive the generator. The machine driving the generator thus provides the effect of the wind turbine blades on the shaft. A synchronous machine would be used as the rotational velocity of the shaft can be directly controlled by the inverter's output frequency. A more complicated system using an induction motor is presented in [35].

If the power measurement needed in the wind turbine simulation algorithm were to be taken electrically from the power supplied to the machine simulating the blades, there would still be the losses associated from the internal losses of that machine. In order to provide an exact replica of the power and torque to be delivered to the shaft by the blade simulating machine, the torque between the machine and generator can be measured using a torque transducer. This measured result would be combined with the electrical frequency to provide an improved model of the effect of the blades on the generator.

Thus the model of the wind turbine system could be extended to include all the actual components of a wind turbine with the exception of the blades, which have no electro-mechanical analogue

## **8.2.2 Practical implementation**

The purpose of this thesis is to implement these proposals on a commercial wind turbine system. Two concerns are addressed with regard to this practical implementation.

### **8.2.2.1 Battery bank storage**

In order to reduce losses in the system, the wind turbine is designed to produce a high rated voltage. Due to the characteristic operation of a converter, the DC bus value of the converter will always be larger than the rms value of the AC signal. The connotation of a “small-scale” wind turbine system is that the system does not require an extremely large storage capacity and will most likely be satisfied by a few 12 V lead acid batteries. The DC output of the active rectifier will have to be reduced to accommodate the lower voltage of the lead acid batteries. A buck converter is proposed to accomplish this. This could increase the cost of the overall rectification section, but the use of a common heat sink for the rectifier and buck converter and the same DSP to control the active rectifier and the buck converter, would reduce this cost. MOSFETs would be used to reduce the switching losses.

### **8.2.2.2 Autonomous recalibration system**

Equation control in the future can be extended to include an autonomous system whereby the system continuously recalibrates the maximum power points by analyzing the power points at corresponding wind speeds. Effects of acceleration would need to be taken into account and thus only the power points measured during more constant wind periods would be of value to update the maximum power profile, unless the effect of acceleration and deceleration could be integrated into the recalibration system. Effects such as dust and dirt on the blades and ageing bearings ensure that the blade power profiles change slightly over time. The recalibration of the parameters would ensure that the system continued to perform optimally over time.

## Chapter 9. References

- [1] The Potential of Wind Energy to Reduce CO<sub>2</sub> Emissions, Available: <http://www.garradhassan.co.uk>
- [2] R.P. Mukund, "Wind and Solar Power Systems," CRC Press LLC, Boca Raton, Washington, D.C., 1999.
- [3] "Green Electricity Buyers' Guide," Available: <http://www.foecanada.org/>
- [4] "Green Power Takes Off With Choice in Electricity," Available: <http://www.eere.energy.gov/greenpower/pufweb.html>
- [5] L. Guey-Lee, "Wind Energy Developments: Incentives in Selected Countries," Available: [http://www.eia.doe.gov/cneaf/solar.renewables/rea\\_issues/html/windart.html#windenergy](http://www.eia.doe.gov/cneaf/solar.renewables/rea_issues/html/windart.html#windenergy)
- [6] "Energy Efficiency and Renewable Energy," Available: <http://www.eere.energy.gov>
- [7] The Danish Wind Industry Association, Available: <http://www.windpower.org>
- [8] Renewable Energy for Rural Electrification in the Eastern Cape, Available: <http://www.garradhassan.co.uk>
- [9] M. Rycroft, "Wind Energy as an Alternative to Solar Power in a South African Telecommunications Network," Eskom Standby Power System Conference, 2002.
- [10] I Smit, D Blake and R Smit, "Wind Turbines and Power Quality," Energize, Power Journal of the South African Institute of Electrical Engineers, pp. 31-34, June 2002.
- [11] E. Muljadi, C.P. Butterfield, "Pitch-Controlled Variable-Speed Wind Turbine Generation," *IEEE Transactions on Industry Applications*, Vol. 37, No. 1, January/February 2001, pp. 240-246.
- [12] S. Bhowmik, R. Spee, J.H.R. Enslin, "Performance optimization for doubly fed wind power generation systems," *IEEE Transactions on Industry Applications*, Vol. 35, No. 4, July/August 1999, pp. 949-958.
- [13] T. Thiringer, J. Linders, "Control by Variable Rotor Speed of a Fixed-Pitch Wind Turbine Operating in a Wide Speed Range," *IEEE Transactions on Energy Conversion*, Vol. 8, No. 3, pp. 520-526, September 1993.

- [14] T. Nakamura, S. Morimoto, M. Sanada, Y. Takeda, "Optimum Control of IPMSG for Wind Generation System," PCC, Osaka, April 2002.
- [15] A. Miller, E. Muljadi, "A Variable Speed Wind Turbine Power Control," *IEEE Transactions on Energy Conversion*, Vol. 12, No. 2, June 1997, pp. 181-186.
- [16] J.J. Bosman, "Design of the AE 1kW Wind Turbine Blade (AE-A9610)," *Aero Energy Design Report*, April, 2003.
- [17] I. Smit, private communication, Eskom, August, 2003.
- [18] B.J. Chalmers, E. Spooner, "An Axial-Flux Permanent-Magnet Generator for a Gearless Wind Energy System," *IEEE Transactions on Energy Conversion*, Vol. 14, No. 2, June 1999, pp. 251-257.
- [19] H. Keppola, R. Perälä, L. Söderlund, H. Vihriälä, "Preliminary Test Results of an Axial Flux Toroidal Stator Wind Power Generator," Available:  
[http://www.em.tut.fi/tuuliryhma/weg\\_articles/icem2000.pdf](http://www.em.tut.fi/tuuliryhma/weg_articles/icem2000.pdf)
- [20] T. Rovio, H. Vihriälä, L. Söderlund, J. Kriikka, "Axial and Radial Flux Generators in Small-Scale Wind Power Production," Available:  
[http://www.em.tut.fi/tuuliryhma/weg\\_articles/ewec2001c.pdf](http://www.em.tut.fi/tuuliryhma/weg_articles/ewec2001c.pdf)
- [21] A. Koyanagi, H. Nakamura, M. Kobayashi, Y. Suzuki, R. Shimada, "Study on Maximum Power Point Tracking of Wind Turbine Generator using a Flywheel," PCC, Osaka, April 2002.
- [22] R. Cárdenas, R. Peña, G. Asher, J. Clare, "Control Strategies for Enhanced Power Smoothing in Wind Energy Systems Using a Flywheel Driven by a Vector-Controlled Induction Machine," *IEEE Transactions on Industrial Electronics*, Vol. 48, No. 3, June 2001, pp. 625-635.
- [23] B. Sørensen, "Renewable Energy," Second Edition, Academic Press, 2000.
- [24] "Wind Speed with Height," Available:  
[www.wind.ttu.edu/education/calculating%20wind%20speed.htm](http://www.wind.ttu.edu/education/calculating%20wind%20speed.htm)
- [25] P.C. Krause, O. Wasynczuk, S.D. Sudhoff, "Analysis of Electric Machinery," First Edition, IEEE Press, 1995.

- [26] R. Wang, "Design Aspects and Optimisation of an Axial Field Permanent Magnet Machine with an Ironless Stator," Ph.D. dissertation, Department Electrical & Electronic Engineering, University of Stellenbosch, September 2002.
- [27] P.D. Fick, "Evaluation of the Constant Current Angle Controlled Reluctance Synchronous Machine Drive," M.Sc. Thesis, Department Electrical & Electronic Engineering, University of Stellenbosch, March 2002.
- [28] B.S. Borowy, Z.M. Salameh, "Dynamic Response of a Stand-Alone Wind Energy Conversion System with Battery Energy Storage to a Wind Gust," *IEEE Transactions on Energy Conversion*, Vol. 12, No. 1, March 1997, pp. 73-78.
- [29] L.M. Tolbert, T.G. Habetler, "Comparison of Time-Based Non-Active Power Definitions for Active Filtering," Available: <http://powerelec.ece.utk.edu/pubs/ciep2000.pdf>
- [30] G.F. Franklin, J.D. Powell, A. Emami-Naeini, "Feedback Control of Dynamic Systems," Third Edition, Addison Wesley, 1994.
- [31] J.W. Nilsson, S.A. Riedel, "Electric Circuits," Fifth Edition, Addison Wesley, 1996.
- [32] C.G. Gerhardt, "The Development of a STATCON Training Tool," *Elektrische Energietechnik*, Fachhochschule Dortmund, January 1999.
- [33] H. Akagi, Y. Kanazawa, A. Nabae, "Instantaneous reactive power compensators comprising switching devices without energy storage components," *IEEE Transactions on Industrial Applications*, Vol. 20, No. , pp 625-630, May/June 1984.
- [34] C. Mostert, "The Analysis, Design and Implementation of a Constant THD Current Controller for Active AC/DC Converters," M.Sc. Thesis, Department Electrical & Electronic Engineering, University of Stellenbosch, December 1997.
- [35] H. Madadi Kojabadi, L. Chang, T. Boutot, "Development of a Novel Wind Turbine Simulator for Energy Conversion Systems Using an Inverter Controlled Induction Motor," Submitted for review to *IEEE Trans. on Energy Conversion*, 2001.

# Appendix A Inverter Code

A section of the C++ code implemented in the DSP controlling the inverter is presented. This file is part of a collection of files implemented in the control of the DSP. Only this file is presented as only it deals with the implementation of the wind turbine simulation.

```

/*_ [ MD_F2407.c ] _____
Project: Optimization of Wind Energy Transfer using Wind Turbines

- function
  -Simulation of a Wind turbine using an inverter

- remarks
  -Input wind speed acquired through A/D and then superposition is used to retrieve the
  corresponding torque that the Wind Turbine would be able to provide. The P_Meas from
  the DC Bus is measured and the corresponding torque is calculated using the current
  outputted frequency. The two acquired torques' difference is integrated to produce the
  new "rotor speed" (frequency). The modulation index is proportional to the calculated
  rotor speed.

- program
  G.D. Moor
  2003/09

- original framework
  J.P.F. Mostert
  2002/11
*/

#include "F2407Regs.h"

#define _MD_F2407

void F2407_SYSTEM(void);
void F2407_IO_SETUP(void);
void F2407_ADC(void);
void F2407_TMR_PWM(void);
void F2407_LEDS(void);
void MD_Delay(void);
void F2407_WD_EN(void);
void F2407_Int(void);
void Sin_Comp(void);
void F2407_Kick_Dog(void);

/*===== Look-Up Tables =====*/

int          Sine(int);          /*Sine signal look-up table*/
unsigned int Torq_1(int);        /*Turbine torque characteristic look-up table*/
unsigned int Torq_2(int);
unsigned int Torq_3(int);
unsigned int Torq_4(int);
unsigned int Torq_5(int);
unsigned int Torq_6(int);
unsigned int Torq_7(int);
unsigned int Torq_8(int);
unsigned int Torq_9(int);
unsigned int Torq_10(int);

/*_____ MAIN PROGRAM _____*/

void main(void)
{
  F2407_SYSTEM();
  F2407_IO_SETUP();
}

```

```

F2407_ADC();
F2407_TMR_PWM();
MD_Delay();
F2407_WD_EN();
F2407_Int();
}

/* _____SYSTEM SETUP_____ */

void F2407_SYSTEM(void)
{
#define wd_DISABLE (1<<6)
#define wd_CHK      0x28

    iaWDCR   = wd_DISABLE|wd_CHK; /* Disable Watchdog */
    iaSCSR1  = 0x008C;           /* Enable EVA,EVB,A/D Clock */
}

/* _____IO SETUP_____ */

void F2407_IO_SETUP(void)
{
    iaMCRA   = 0x0FC3;           /* PWM1-PWM6, SCITXD, SCIRXD */
    iaMCRC   = 0x0001;           /* IOPE1, IOPE2 Selected */
    iaPEDATDIR = 0xF0F0;         /* IOPE4-IOPE7 = '1' */
    iaPFDATDIR = 0x1000;         /* IOPF4 Relay Off */
}

/* _____A/D SETUP_____ */

void F2407_ADC(void)
{
    iaADCTRL1 = 0x4000;           /* Reset A/D Module */
    asm (" NOP");                 /* Delay */
    iaADCTRL1 = 0x0100;           /* 3 Conversions MAX_CONn+1 */
    iaMAXCONV = 0x0002;           /* CH3 & CH2 Selected */
    iaCHSELSEQ1 = 0x0023;
}

/* _____TIMER & COMPARE SETUP_____ */

void F2407_TMR_PWM(void)
{
    /* Assume CPUCLK=40MHz

    Timer1: To Generate PWM
    Timer2: To Generate Accurate Timing

    Set to 5kHz (taking into account up/down counting mode, Period = TPRD*2).
    Set to continuous up/down mode (for PWM generation).
    Set prescale to 1 (clock divide by two).*/

    iaCOMCONA = 0x0000;           /* Put PWM Output in High Impedance State */

    iaT1PR   = 2000;              /* 40MHz/5kHz/2/2=2000 ; Up-Down Count */
    iaT2PR   = 0xFFFF;           /* 40MHz/305Hz/2 = 65536; Only Up Count */

    iaACTRA  = 0x0999;           /* PWM2,4,6 Active High. PWM1,3,5 Active Low */

    iaCMPR1  = (2000/2);          /* No Use, Gets Updated Later */
    iaCMPR2  = (2000/3);          /* No Use */
    iaCMPR3  = (2*(2000/2));      /* No Use */

    iaT1CNT  = 0xFFFFE;          /* Counter1 Starting Value */
    iaT2CNT  = 0xFFFFE;          /* Counter2 Starting Value */

    iaDBTCONA = 0x06EC;          /* Deadband Prescale x/8, Enable All Deadband Units, DB=1.2us
*/
}

```

```

    iaT2CON   = 0x1180;          /* Timer2 To Generate Accurate Delay Timing */
    iaT1CON   = 0x0942;          /* Start Timer1 and Timer2 */
}

/* _____ LED's _____ */
void F2407_LEDS(void)
{
    static int count1 = 0;
    static int count2 = 0;
    static int LED_SEQ[6] = { 0xF0E0, 0xF0D0, 0xF0B0, 0xF070, 0xF0B0, 0xF0D0 };

    if (++count2 > 80)
    {
        if (++count1 >= 6) count1 = 0;

        iaPEDATDIR = LED_SEQ[count1];
        count2 = 0;
    }
}

/* _____ DELAY _____ */
void MD_Delay(void)
{
    static int DL_Clk = 0;
    static int DL_Clk1 = 0;

    while(DL_Clk1 < 1000)
    {
        while(!(iaEVAIFRB)&(1));          /* Wait for 305Hz Timer2 Period Flag */
        iaEVAIFRB |= 1;                  /* Clear Flag */

        DL_Clk1++;
    }

    iaCOMCONA = 0x8200;                  /* Enable Compare Operation */
}

/* _____ WATCH DOG SETUP TIMER _____ */
void F2407_WD_EN(void)
{
    iaWDCR = 0x28;                      /* Enable Watchdog */
}

/* _____ INTERRUPT SETUP _____ */

void F2407_Int(void)
{
    /*
    INT1: P_Meas Drive Protection
    INT2: Timer 1 Period Interrupt
    INT3: Timer 2 Period Interrupt
    INT5: None
    INT6: None
    */

    asm (" CLRC INTM");                  /* Enable Interrupts Globally (assembler Code) */

    iaIFR   = 0xFFFF;                   /* Clear all Flags */
    iaIMR   = 0x0007;                   /* Enable Int1,2,3 */

    iaEVAIFRA = 0xFFFF;                 /* Clear all Flags */
}

```

```

iaEVAIMRA = 0x0081;          /* PDPINTA, Timer1 Period Interrupt Enable */
iaEVAIMRB = 0x0001;          /* Timer2 Period Interrupt Enable */
}

/* _____ SINE GENERATION _____ */

void Sin_Comp(void)
{
    static unsigned int    V_Meas      = 0;
    static unsigned int    I_Meas      = 0;
    static unsigned long int T_Elec     = 0;
    static unsigned long int P_Scale    = 0;
    static unsigned long int W_Torq     = 0;
    static unsigned long int P_Meas     = 0;
    static unsigned long int P_Filt     = 0;
    static unsigned long int rpm        = 156;
    static long int        T_Diff       = 0;
    static unsigned long int rpmD       = 163577856;
    static unsigned int    Ws           = 20000;
    static unsigned int    Freq         = 0;

    static float           Amp_Lim      = 0;
    static unsigned long int pnt_A      = 0;          /*3 phase counters*/
    static unsigned long int pnt_B      = (64000/3);
    static unsigned long int pnt_C      = 2*(64000/3);
    static int             Ref_A;
    static int             Ref_B;
    static int             Ref_C;
    static long int        check        = 16000;
    static int             Ampl         = 0;

    /*===== Wind Speed Input =====*/
    /** Gather Wind Speed from A/D **/
    /*3.29V input = 65472, scale to 40960, thus 10m/s = 40960*/

    Ws = ((long)iaRESULT0 * (long)40960) >> 16;          /*max = 40960, min = 0*/

    /*===== Torque Computation =====*/
    /*Torque = LowTCurve + ((HighTCurve-LowTCurve)/(WindSpeedRangeBetweenThem)*(Wind from the Lower
    curve))*/

    if (Ws < 4096)          /* 0m/s -> 1m/s */
    {
        W_Torq = 0;
    }

    if ((Ws >= 4096) & (Ws < 8192))          /* 1m/s -> 2m/s */
    {
        W_Torq = Torq_1(rpm) + (((long)(Torq_2(rpm)-Torq_1(rpm)))*(long)(Ws - 4096))>>12);
    }

    if ((Ws >= 8192) & (Ws < 12288))          /* 2m/s -> 3m/s */
    {
        W_Torq = Torq_2(rpm) + (((long)(Torq_3(rpm)-Torq_2(rpm)))*(long)(Ws - 8192))>>12);
    }

    if ((Ws >= 12288) & (Ws < 16384))          /* 3m/s -> 4m/s */
    {
        W_Torq = Torq_3(rpm) + (((long)(Torq_4(rpm)-Torq_3(rpm)))*(long)(Ws - 12288))>>12);
    }

    if ((Ws >= 16384) & (Ws < 20480))          /* 4m/s -> 5m/s */
    {
        W_Torq = Torq_4(rpm) + (((long)(Torq_5(rpm)-Torq_4(rpm)))*(long)(Ws - 16384))>>12);
    }

    if ((Ws >= 20480) & (Ws < 24576))          /* 5m/s -> 6m/s */
    {
        W_Torq = Torq_5(rpm) + (((long)(Torq_6(rpm)-Torq_5(rpm)))*(long)(Ws - 20480))>>12);
    }

    if ((Ws >= 24576) & (Ws < 28672))          /* 6m/s -> 7m/s */

```

```

{
    W_Torq = Torq_6(rpm) + (((long)(Torq_7(rpm)-Torq_6(rpm)))*(long)(Ws - 24576))>>12);
}

if ((Ws >= 28672) & (Ws < 32768)) /* 7m/s -> 8m/s */
{
    W_Torq = Torq_7(rpm) + (((long)(Torq_8(rpm)-Torq_7(rpm)))*(long)(Ws - 28672))>>12);
}

if ((Ws >= 32768) & (Ws < 36864)) /* 8m/s -> 9m/s */
{
    W_Torq = Torq_8(rpm) + (((long)(Torq_9(rpm)-Torq_8(rpm)))*(long)(Ws - 32768))>>12);
}

if ((Ws >= 36864) & (Ws < 40960)) /* 9m/s -> 10m/s */
{
    W_Torq = Torq_9(rpm) + (((long)(Torq_10(rpm)-Torq_9(rpm)))*(long)(Ws - 36864))>>12);
}

if (Ws >= 40960) /* Limited to 10m/s */
{
    W_Torq = Torq_10(rpm);
}

/*===== P_Meas Measurement =====*/

/* iaRESULT2 is now Vdc, a maximum of 303.3V = 2^16-2^5 */
/* With a 120 Ohm R, and 1000:1 CT, 13.75A = 65472, 0A= 32736, -13.75A= 0 */

V_Meas = iaRESULT2; /* (DSPvalue = 104.2 * V) */
I_Meas = iaRESULT1 - 33152; /* Remove offset (DSPvalue = 2350 * I) */
P_Meas = (V_Meas * I_Meas); /* DSP = 244870 * WATT */
P_Scale = P_Meas >> 8;
P_Filt = P_Filt + ((long)(P_Scale - P_Filt) >> 3); /*Filter slightly*/

/*===== Torque Computation =====*/

T_Elec = ((P_Filt * 611) / rpm) >> 6; /*real wr conversion, P at same scale*/
T_Elec = (T_Elec * 7354) >> 12; /*value @ 2^11 scale*/
W_Torq = (W_Torq * 9639) >> 12; /*scale table values, values @ 2^11 scale*/

/*===== Torque Difference & Inertia Integration =====*/

T_Diff = W_Torq - T_Elec; /* value @11 scale */
T_Diff = (T_Diff * 859) >> 10; /* Add inertia */
check = (T_Diff >> 1) + (rpmD >> 1); /* check for overflow */
rpmD += (T_Diff); /* Integrate */

/*===== Frequency Manipulation =====*/

if (check < 1) rpmD = 5242880; /*check for overflow*/
if (rpmD < 1) rpmD = 1; /*limit rotor speed +ve*/
if (rpmD > (314572800 * 2)) rpmD = (314572800 * 2); /*limit rotor speed*/
rpm = (long)(rpmD) >> 20; /*scale DSP rotor speed value*/
Freq = ((long)(rpmD >> 10) * 874) >> 18; /*revert to electrical frequency*/
if (Freq < 1) Freq = 1; /*Check limits*/
if (Freq > 2048) Freq = 2048; /*Check limits*/

```

```

/*===== Amplitude Computation =====*/

Amp_Lim = (30984500 / (float)(iaRESULT2)); /*Holds voltage reference, irrespective
Amp_Lim = (((float)(Freq)) / 1999) * Amp_Lim; /*calculate corresponding
Ampl = (int)(Amp_Lim); /*Convert to integer*/
if (Ampl >= 2000) Ampl = 1999; /*limit */
pnt_A += Freq; /* 64000/640=100 ; 5kHz/100=50Hz */
pnt_B += Freq;
pnt_C += Freq;

/*===== Sinusoidal Outputs =====*/

if (pnt_A >= 64000) pnt_A -= 64000; /* 2^6=64 ; 1000 Pts Sin Table */
    Ref_A = (Sine(pnt_A >> 6)); /* 64*1000=64000 */
    Ref_A = ((long)Ref_A * (long)Ampl) >> 16;
    iaCMPR1 = 1000 + (Ref_A);

if (pnt_B >= 64000) pnt_B -= 64000; /* 2^6=64 ; 1000 Pts Sin Table */
    Ref_B = (Sine(pnt_B >> 6)); /* 64*1000=64000 */
    Ref_B = ((long)Ref_B * (long)Ampl) >> 16;
    iaCMPR2 = 1000 + (Ref_B);

if (pnt_C >= 64000) pnt_C -= 64000; /* 2^6=64 ; 1000 Pts Sin Table */
    Ref_C = (Sine(pnt_C >> 6)); /* 64*1000=64000 */
    Ref_C = ((long)Ref_C * (long)Ampl) >> 16;
    iaCMPR3 = 1000 + (Ref_C);

}

/*_____KICK DOG_____*/
void F2407_Kick_Dog(void)
{
    iaWDKEY = 0x55;
    iaWDKEY = 0xAA;
}

/*_____*/

```

## Appendix B Active Rectifier Code

A section of the C++ code implemented in the DSP controlling the active rectifier is presented. This file is part of a collection of files implemented in the control of the DSP. Only this file is presented as only it deals with the implementation of the equation algorithms used for maximum power point tracking. The look-up tables used have been shortened in the presented code below.

```

/*_ [ main.c ] _____
Project: Optimization of Wind Energy Transfer using Wind Turbines

- function
  -Adjust the power flow to the DC bus, through active rectification
  -Generate random wind profiles from a look-up table

- remarks
  -This program is responsible for controlling the switching of the STATCON system
  which together control the loading on an analog simulation system of a wind turbine.
  The input currents and voltages are measured and the power and frequency of the
  signals are calculated. A current reference is determined using maximum power point
  tracking algorithms and then a conventional predictive current control method is
  used to switch the required current, thus controlling the power flow to the DC bus.

- program
  G.D. Moor
  2003/09

- original framework
  A.D. le Roux
  2000/06
_____ */

#define _C_MAIN

#include <math.h>
#include <float.h>
#include "type.h"
#include "dac8413.h"
#include "c3x.h"
#include "lcd.h"
#include "ad7891.h"
#include <stdio.h>

#define L          (900.0e-6)  /*inductor size*/
#define L_inv      (1/L)
#define S_freq     (10.0e3)   /*switching frequency*/
#define S_period   (1/S_freq)
#define KF         (1.0)      /*weight of current prediction*/
#define KP         (1.0)      /*weight of voltage increment*/

/*_____ GLOBAL VARIABLES _____*/

char    string_buffer[100];

C3X_TIMER_EVENT c3x_timer_flash;
C3X_TIMER_EVENT c3x_timer_example;
C3X_TIMER_EVENT ad7891_timer;

float theta0      = 0.0;
float freq        = 0.0;
float freqFilt    = 0.0;
float Ws          = 0.0;
float Power_in    = 0.0;
float i_ref       = 0.0;

```

```

float Wind      = 8.0;

/*===== Look-Up Tables =====*/

/*Power Profiles*/

const float p3[160] = {0.2555, 0.6094, 1.0543, .....};
const float p4[160] = {0.4313, 0.975, 1.6265, .....};
const float p5[160] = {0.682, 1.4906, 2.4224, .....};
const float p6[160] = {1.0195, 2.1656, 3.4349, .....};
const float p7[160] = {1.4438, 3, 4.664, .....};
const float p8[160] = {1.8938, 3.9, 6.0133, .....};
const float p9[160] = {2.3695, 4.8656, 7.4835, .....};
const float p10[160] = {2.9203, 5.9813, 9.1794, .....};

/*Inverted differences*/

const float inv30[160] = {3.913894325, 1.64095832, 0.948496633, .....};
const float inv43[160] = {5.688282139, 2.735229759, 1.747640685, .....};
const float inv54[160] = {3.988831272, 1.939487975, 1.256439251, .....};
const float inv65[160] = {2.962962963, 1.481481481, 0.987654321, .....};
const float inv76[160] = {2.356823003, 1.198465964, 0.81360345, .....};
const float inv87[160] = {2.222222222, 1.111111111, 0.741125028, .....};
const float inv98[160] = {2.10216523, 1.035625518, 0.680179567, .....};
const float inv109[160] = {1.815541031, 0.896298288, 0.589657409, .....};

/*Random wind profile*/

const float randwind[1440] = {8.9716, 8.9716, 8.9716, 8.9716, 8.9716, 8.9894, .....};

/*-----PROGRAM-----*/

void c_int01()
{
    static float ia_dc = 0.0;
    static float ib_dc = 0.0;
    static float ic_dc = 0.0;
    static int _state = 0;
    static float ref_va,ref_vb,ref_vc,vd_inv;
    static float da = 0.0;
    static float db = 0.0;
    static float dc = 0.0;
    static float d_min,d_max;
    static float c;
    static float d0 = 0.0;
    static float delta_ia = 0.0;
    static float delta_ib = 0.0;
    static float delta_ic = 0.0;
    static float ref_ia,ref_ib,ref_ic;
    static float invR_V,alpha_V,beta_V,unit_a,unit_b,unit_c,R_V;
    static float alpha_I,beta_I;
    static float R_I;
    static int cnt_Power = 0;
    static float PowerO = 0.0;
    static float cnt_freq = 0.0;
    static int freq_int = 0;
    static int freq_state = 0;
    static float PSum = 0.0;
    static int wind_pnt = 0;
    static int windcnt = 0;
    static int initalcnt = 0;
    static float VdFilt = 0.0;
    static float R_IFilt = 0.0;
    static float R_VFilt = 0.0;
    static float va,vb,vc,vd,ia,ib,ic,Id;

/*===== AD7891.0 => Setup & Conversion =====*/

    _c3x_timer_event_set_time( &ad7891_timer, AD7891_CONV_TIME );

```

```

    while (!_c3x_timer_event_check( &ad7891_timer ));

/** Current measurements scaled to actual current values */
ia   = -50.0*(((float)((*(VINT*)0x700000)>>20))/2047.0);
ic   = -50.0*(((float)((*(VINT*)0x700001)>>20))/2047.0);
ib   = -50.0*(((float)((*(VINT*)0x700002)>>20))/2047.0);
Id   = -50.0*(((float)((*(VINT*)0x700003)>>20))/2047.0);

/** Setup AD to acquire voltages */
*((VUINT*)0x700000) = (AD7891_CNTRL_SIGNED|AD7891_CNTRL_CONVST|AD7891_CNTRL_CH0)<<20;
*((VUINT*)0x700001) = (AD7891_CNTRL_SIGNED|AD7891_CNTRL_CONVST|AD7891_CNTRL_CH0)<<20;
*((VUINT*)0x700002) = (AD7891_CNTRL_SIGNED|AD7891_CNTRL_CONVST|AD7891_CNTRL_CH0)<<20;
*((VUINT*)0x700003) = (AD7891_CNTRL_SIGNED|AD7891_CNTRL_CONVST|AD7891_CNTRL_CH0)<<20;

_c3x_timer_event_set_time( &ad7891_timer, AD7891_CONV_TIME );
while (!_c3x_timer_event_check( &ad7891_timer ));

/** Voltage measurements scaled to actual voltage values */

va   = 5*100.18*(((float)((*(VINT*)0x700000)>>20))/2047.0)+0.0005;
vb   = 5*100.18*(((float)((*(VINT*)0x700001)>>20))/2047.0)+0.0015;
vc   = 5*100.18*(((float)((*(VINT*)0x700002)>>20))/2047.0)+0.0001;
vd   = 5*100.18*(((float)((*(VINT*)0x700003)>>20))/2047.0)-0.0024;

/** Setup AD to acquire currents in next cycle */
*((VUINT*)0x700000) = (AD7891_CNTRL_SIGNED|AD7891_CNTRL_CH2)<<20;
*((VUINT*)0x700001) = (AD7891_CNTRL_SIGNED|AD7891_CNTRL_CH2)<<20;
*((VUINT*)0x700002) = (AD7891_CNTRL_SIGNED|AD7891_CNTRL_CH2)<<20;
*((VUINT*)0x700003) = (AD7891_CNTRL_SIGNED|AD7891_CNTRL_CH2)<<20;

/*===== Alpha-Beta plane Conversion for Measured Current =====*/
/** Current */

alpha_I = 0.8165*(ia-(0.5*ib)-(0.5*ic));
beta_I  = 0.7071*(ib-ic);
R_I     = sqrt((alpha_I*alpha_I)+(beta_I*beta_I)); /*Current Vector Length (radius)*/
R_IFilt = R_IFilt + ((R_I - R_IFilt)*0.05);      /*filter current radius*/

/** Voltage */

alpha_V = 0.8165*(va-(0.5*vb)-(0.5*vc));
beta_V  = 0.7071*(vb-vc);
R_V     = sqrt((alpha_V*alpha_V)+(beta_V*beta_V)); /*Voltage Vector Length (radius)*/
R_VFilt = R_VFilt + ((R_V - R_VFilt)*0.05);      /*filter voltage radius*/

/*===== Frequency Computation =====*/

switch (freq_state) /*Select frequency range*/
{
case 0: /*from 50Hz to 160Hz*/
    if ( ++cnt_freq > 25.0) /*Allow time for vector to pass axis once freq calculated*/
    {
        if (fabs(alpha_V) < 10.0) /*Region around axis in which to trigger*/
        {
            freq = 5000.0/cnt_freq;
            cnt_freq = 0.0;
            if (freq < 70) freq_state = 1;
        }
    }
break;

case 1: /*from 25Hz to 80Hz*/
    if ( ++cnt_freq > 60.0) /*Allow time for vector to pass axis once freq calculated*/
    {
        if (fabs(alpha_V) < 5.0) /*Region around axis in which to trigger*/
        {
            freq = 5000.0/cnt_freq;
            cnt_freq = 0.0;
            if (freq < 30) freq_state = 2;
            if (freq > 72) freq_state = 0;
        }
    }
}

```

```

    }
    break;

case 2:
    if ( ++cnt_freq > 120.0)          /*from 11Hz to 40Hz*/
        /*Allow time for vector to pass axis once freq calculated*/
        {
            if (fabs(alpha_V) < 1.0)  /*Region around axis in which to trigger*/
                {
                    freq      = 5000.0/cnt_freq;
                    cnt_freq = 0.0;
                    if (freq > 32) freq_state = 1;
                }
        }
    break;
}

freqFilt = freqFilt + ((freq - freqFilt)*0.005);    /*Filter out noise*/

/*===== Unity Sinusoidal Reference signals =====*/

invR_V = 1.0/R_V;
invR_V = (invR_V>1.0) ? (1.0) : invR_V;    /*Precaution: Limit ref signal size*/

alpha_V = alpha_V*invR_V;    /*Scale to alpha-beta to unity*/
beta_V = beta_V*invR_V;

unit_a = alpha_V;    /*Ref signals in-phase with voltage*/
unit_b = (-0.5*alpha_V)+(0.886*beta_V);
unit_c = (-0.5*alpha_V)-(0.886*beta_V);

/*===== Wind Speed Calculation =====*/

cnt_Power += 1;
PSum += (R_IFilt*R_VFilt);    /*Calculate Power Sum*/

if (cnt_Power > 1000)
{
    cnt_Power = 0;    /*reset counter*/
    freq_int = freqFilt;    /*save present frequency value*/
    if (freq_int > 159) freq_int = 159;    /*limit max frequency value for look-up table*/
    if (freq_int < 1) freq_int = 1;    /*limit min frequency value for look-up table*/
    Power_in = PSum*0.001;    /*Take average Power over interval*/
    PSum = 0;
}

/** Wind Speed Determination **/

PowerO = Power_in - 0.0;    /*fine tuning power for look-up table*/
freq_int += 0;    /*fine tuning frequency for look-up table*/

if ((PowerO < p3[freq_int]))    /* 0m/s -> 3m/s */
{
    Ws = PowerO*inv30[freq_int];
}

if ((PowerO >= p3[freq_int]) && (PowerO < p4[freq_int]))    /* 3m/s -> 4m/s */
{
    Ws = 3.0 + ((PowerO-p3[freq_int])*inv43[freq_int]);
}

if ((PowerO >= p4[freq_int]) && (PowerO < p5[freq_int]))    /* 4m/s -> 5m/s */
{
    Ws = 4.0 + ((PowerO-p4[freq_int])*inv54[freq_int]);
}

if ((PowerO >= p5[freq_int]) && (PowerO < p6[freq_int]))    /* 5m/s -> 6m/s */
{
    Ws = 5.0 + ((PowerO-p5[freq_int])*inv65[freq_int]);
}

if ((PowerO >= p6[freq_int]) && (PowerO < p7[freq_int]))    /* 6m/s -> 7m/s */
{
    Ws = 6.0 + ((PowerO-p6[freq_int])*inv76[freq_int]);
}

```

```

}

if ((PowerO >= p7[freq_int]) && (PowerO < p8[freq_int])) /* 7m/s -> 8m/s */
{
    Ws = 7.0 + ((PowerO-p7[freq_int])*inv87[freq_int]);
}

if ((PowerO >= p8[freq_int]) && (PowerO < p9[freq_int])) /* 8m/s -> 9m/s */
{
    Ws = 8.0 + ((PowerO-p8[freq_int])*inv98[freq_int]);
}

if (PowerO >= p9[freq_int]) /* 9m/s -> */
{
    Ws = 9.0 + ((PowerO-p9[freq_int])*inv109[freq_int]);
}
Ws -= 0.1;
}

/*===== Random Wind Profile Generation =====*/

/*This section generates a random wind profile from a lookup table. This reference is used for
the equation method of tracking and to provide a wind profile to the inverter simulating the
wind turbine via an external connection from the D/A. This wind value is not used in any
other algorithms*/

if (++initalcnt > 50000) /*delay initial random wind generation*/
{
    initalcnt = 50005; /*Delay only at Startup*/
    if (++wndcnt > 1250) /*wait for 0.125s before inc pointer*/
    {
        windcnt = 0;
        wind_pnt += 1; /*inc pointer*/
        wind_pnt = (wind_pnt>1440) ? (1) : wind_pnt; /*reset pointer of random wind profile*/
        Wind = randwind[wind_pnt]; /*find new wind speed from look-up table*/
    }
}
_dac8413_update_v( &spec31_dac8413, 0, -Wind); /*Analog output wind speed*/

/*===== Optimal Current Reference Calculations =====*/

/* The two equation methods are presented below. The method not used must be commented out as the
Calculation Method in this case */

/** Anemometer Control: pre-determined optimal current equation **/

i_ref = (0.331*Wind*Wind) + (0.8881*Wind) - 5.8857;

/** Calculation Control: pre-determined optimal current equation **/

/* i_ref = (0.331*Ws*Ws) + (0.8881*Ws) - 5.8857;

i_ref = (i_ref > 50.0) ? (50.0) : i_ref; /*Precaution: limit reference currents*/
i_ref = (i_ref < 0.0) ? (0.0) : i_ref;

/*===== Inner Current Loop =====*/

VdFilt = VdFilt + ((vd - VdFilt)*0.001); /*Filter DC bus measurement*/

ref_ia = i_ref*unit_a; /*adjust new current references*/
ref_ib = i_ref*unit_b; /*onto unitary 3 phase waves*/
ref_ic = i_ref*unit_c;

/* current dc offset */
ia -=
ia_dc += 10e-6* (ia-ia_dc); /*filter out ac component*/
ib -=
ib_dc += 10e-6* (ib-ib_dc); /*so that only dc offset is left over*/
ic -=
ic_dc += 10e-6* (ic-ic_dc);

```

```

/* current prediction */
d0      = (0.33333)*(da+db+dc);           /*average of duty cycles*/

ia      -= KP * S_period* L_inv * VdFilt * (da-d0);
ib      -= KP * S_period* L_inv * VdFilt * (db-d0);
ic      -= KP * S_period* L_inv * VdFilt * (dc-d0);

/* calculate new error */
delta_ia = -ref_ia+ia;
delta_ib = -ref_ib+ib;
delta_ic = -ref_ic+ic;

/* calculate voltage change needed for new current */
ref_va  = 1.0* (KF* (S_freq *L)* delta_ia) +1.0* va;
ref_vb  = 1.0* (KF* (S_freq *L)* delta_ib) +1.0* vb;
ref_vc  = 1.0* (KF* (S_freq *L)* delta_ic) +1.0* vc;

/* AD: voltage control */

/* calculate 1/vd without dividing by zero */
vd_inv  = (VdFilt<1.0) ? (1.0) : (1.0)/(VdFilt);

/* calculate normalized duty cycles */
da      = vd_inv * ref_va;
db      = vd_inv * ref_vb;
dc      = vd_inv * ref_vc;

/* get min & max */
d_min  = da;
d_min  = (db>d_min) ? (d_min) : db;
d_min  = (dc>d_min) ? (d_min) : dc;
d_max  = da;
d_max  = (db<d_max) ? (d_max) : db;
d_max  = (dc<d_max) ? (d_max) : dc;

/* setup zero-state distribution */
d0     = -0.5*(d_max + d_min);
da     += d0;
db     += d0;
dc     += d0;

/* limit duty cycles */
c      = d_max - d_min;
c      = (c<1.0) ? (1.0) : (c);
c      = (1.0) / (c);
da     = c*da;
db     = c*db;
dc     = c*dc;

*((VUINT*)0x700088) = 0x1111;           /*set watchdog timer*/

switch (_state)
{
case 0:
*((VUINT*)0x700216) = 1250 - (int)(da*2499.0);
*((VUINT*)0x700217) = 2500;
*((VUINT*)0x700212) = 1250 - (int)(db*2499.0);
*((VUINT*)0x700213) = 2500;
*((VUINT*)0x700210) = 1250 - (int)(dc*2499.0);
*((VUINT*)0x700211) = 2500;
    if ( VdFilt > (450.0))           /*halt system if DC bus gets too large*/
    {
        while (1)
        {
        }
    }
*((VUINT*)0x700200) = 0x0213;
_state = 1;
break;

case 1:
*((VUINT*)0x700216) = 0;
*((VUINT*)0x700217) = 1250 + (int)(da*2499.0);
*((VUINT*)0x700212) = 0;
*((VUINT*)0x700213) = 1250 + (int)(db*2499.0);
*((VUINT*)0x700210) = 0;
*((VUINT*)0x700211) = 1250 + (int)(dc*2499.0);

```

```

        *((VUINT*)0x700200) = 0x0213;
        _state = 0;
    break;
}

}

/* _____ MAIN PROGRAM _____ */

void main()
{
    /* run at 1 wait-state */
    *p_c3x_reg_pbc = (1<<11) | (3<<3) | (1<<5);

    /* start c3x timer 0 */
    p_c3x_timer[0]->period = 0xffffffff;
    p_c3x_timer[0]->control = C3X_TIMER_CONTROL_GO
        | C3X_TIMER_CONTROL_nHLD
        | C3X_TIMER_CONTROL_CLKSRC;

    _c3x_timer_event( &c3x_timer_example, 0 );
    _c3x_timer_event_set_time( &c3x_timer_example, 1.0 );
    _c3x_timer_event( &c3x_timer_flash, 0 );
    _c3x_timer_event_set_time( &c3x_timer_flash, 0.0 );
    _c3x_timer_event( &ad7891_timer, 0 );

    lcd_init();

    /* set up PWM */
    *((VUINT*)0x700200) = 0x0000; /* control */
    *((VUINT*)0x700201) = 2500-1; /* ramp = 10kHz */
    *((VUINT*)0x700202) = 0; /* event */
    *((VUINT*)0x700203) = 25; /* blanking */
    *((VUINT*)0x700204) = 3; /* watch dog */
    *((VUINT*)0x700205) = 0x00|0x00|0x00; /* error polarity */
    *((VUINT*)0x700206) = 0x00|0x00|0x00; /* error mask */
    *((VUINT*)0x700200) = 0x021B; /* control */

    asm(" ldi 0000000000000000b,IF");
    asm(" ldi 0000000000000010b,IE");
    asm(" or 0010000000000000b,ST");

    while (1)
    {
        /* _LED_ */
        *((VUINT*)0x700023) = (theta0>0?0x1:0x0);

        if (_c3x_timer_event_check( &c3x_timer_flash ))
        {
        }

        /* _poll for end of 1kHz cycle_ */
        while (!_c3x_timer_event_check( &c3x_timer_example ));
        _c3x_timer_event_setp_time( &c3x_timer_example, 2.0e-3 );

        lcd_goto(0,0);
        sprintf(string_buffer, "Ws=%4.2f", Ws); /*Display Calculated Wind Speed*/
        lcd_prints_ex(string_buffer);

        lcd_goto(8,0);
        sprintf(string_buffer, "P=%5.1f", Power_in); /*Display Measured Power*/
        lcd_prints_ex(string_buffer);

        lcd_goto(0,1);
        sprintf(string_buffer, "Ref=%5.2f", i_ref); /*Display Requested Loading Current*/
        lcd_prints_ex(string_buffer);

        lcd_fill_ex( ' ' );
        lcd_ex();
    }
}

/* _____ */

```